DESIGN AND ANALYSIS OF A SEMI-SUBMERSIBLE FLOATING WIND TURBINE WITH FOCUS ON STRUCTURAL RESPONSE REDUCTION

Graduation Project presented by

FELIPE EDUARDO VITTORI

For obtaining the degree of Master of Science in Offshore and Dredging Engineering from Delft University Technology and Master of Science in Technology-Wind Energy from the Norwegian University of Science and Technology.

July 2015

European Wind Energy Master (EWEM)

European Wind Energy Master – EWEM

Offshore Specialization Track

The undersigned hereby certify that they have read and recommend to the European Wind Energy Master - EWEM for acceptance a thesis entitled "**Design and Analysis of a Semi-Submersible Floating Wind Turbine with Focus on Structural Response Reduction**" by **Felipe Eduardo Vittori** in partial fulfillment of the requirements for the degree of **Master of Science**.

Date: 17/07/2015

Supervisor: Prof. Dr.Ir. Torgeir Moan, NTNU

Supervisor: Prof. Dr. Ir. Andrei Metrikine, TU Delft

Reader: Prof. Adjunct Dr. Ir. Zhen Gao, NTNU

CONFIDENTIALITY STATEMENT

The undersigned hereby agrees to prevent unauthorized use or dissemination of any information stated on this document to any third party, except specifically authorized by all the undersigned herein during the following two (2) years from the agreement date.

Agreement date: 17/07/2015

_____

Prof. Dr.Ir. Torgeir Moan, NTNU

_____

Prof. Dr. Ir. Andrei Metrikine, TU Delft

_____

Prof. Adjunct Dr. Ir. Zhen Gao, NTNU

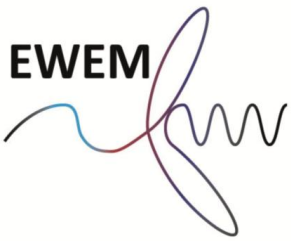

THESIS OUTLINE

MSC THESIS IN MARINE TECHNOLOGY

SPRING 2015

FOR

STUD.TECHN. Felipe Vittori

Design and Analysis of Semi-submersible Floating Wind Turbines with focus on Structural Response Reduction

Background:

Semi-submersible floaters have been proposed for offshore wind power utilization. Most of the proposed concepts have three columns with a wind turbine on one side column or four columns with a wind turbine on the central column. The columns are connected either by braces (as in WindFloat, OC4-Semi), or by pontoons (as in VolturnUS, Dr.techn. Olav Olsen's concept). Different arrangements of columns and pontoons (or braces) have been considered in these concepts.

At CeSOS, NTNU, a braceless semi-submersible for 5MW wind turbine, called CSC and similar to Dr.techn. Olav Olsen's concept, has been designed. The semi-submersible consists of one central column supporting the wind turbine and three side columns connected at the bottom to the central column by three pontoons. There will be no braces considered in this concept. The semi-submersible will be made of steel with a proper distribution of water ballast. The submerged pontoons provide sufficient buoyancy and increase the added mass so that the natural periods of vertical motion modes (such as heave, pitch and roll) are larger than the periods of main waves. However, the side columns are not connected at the top to the central column. They are cantilevered vertical columns for which the wave loads on them might induce large stresses at the column-pontoon connection as well as at the cross-sections of fully submerged pontoons.

It is therefore beneficial to connect the side columns to the central columns additionally by heavy beams at the top, to reduce the wave load effects on the pontoons. The purpose of this thesis is to propose new designs for structural connections between the columns

in the semi-submersible floater, and to illustrate the advantage of the new design by comparing dynamic structural responses of the new floating wind turbine in turbulent wind and irregular waves with those of the original CSC concept.

The MSc candidate will be provided with the design principle and the design information of an old 5MW semi-submersible wind turbine from Chenyu Luan. The candidate will also be guided to use the necessary software (DNV SESAM-GeniE and HydroD) in order to establish numerical models and to perform numerical simulations for dynamic response analysis for floating wind turbines.

Assignment:

The following tasks should be addressed in the thesis work:

1. Literature review on design of semi-submersible floaters for offshore wind turbines. Summarize the main features on braceless semi-subs (with pontoons) and semi-subs with brace connections. Focus on design requirements for stability, hydrodynamic performance as well as structural responses with respect to ULS.
2. Based on the CSC semi-sub data (the design data as well as the data of wave-induced responses (stresses in the cross-sections of the pontoons)), design the required dimension for the heavy beams on the top of the columns and adjust the water ballast to achieve the same draft.
3. Establish a numerical model of the new design in the DNV SESAM package GeniE and HydroD. Estimate the stability curve and the natural periods for rigid-body motions of the whole system. Perform hydrodynamic analysis and compare the frequency-domain motion responses of the original design and the new design in waves. Identify the advantage of the new design in view of motion responses.
4. Establish a beam model in DNV SESAM for the new design, obtain the structural responses in the heavy beams and in the pontoons and compare those obtained for the original CSC model.
5. Report and conclude on the investigation.
6. Conclude the work and give recommendations for future work.
7. Write the MSc thesis report.

In the thesis the candidate shall present his personal contribution to the resolution of problem within the scope of the thesis work.

Theories and conclusions should be based on mathematical derivations and/or logic reasoning identifying the various steps in the deduction.

The candidate should utilize the existing possibilities for obtaining relevant literature.

The thesis should be organized in a rational manner to give a clear exposition of results, assessments, and conclusions. The text should be brief and to the point, with a clear language. Telegraphic language should be avoided.

The thesis shall contain the following elements: A text defining the scope, preface, list of contents, summary, main body of thesis, conclusions with recommendations for further work, list of symbols and acronyms, reference and (optional) appendices. All figures, tables and equations shall be numerated.

The supervisor may require that the candidate, in an early stage of the work, present a written plan for the completion of the work. The plan should include a budget for the use of computer and laboratory resources that will be charged to the department. Overruns shall be reported to the supervisor.

The original contribution of the candidate and material taken from other sources shall be clearly defined. Work from other sources shall be properly referenced using an acknowledged referencing system.

The thesis shall be submitted in two copies as well as an electronic copy on a CD:

- Signed by the candidate
- The text defining the scope included
- In bound volume(s)
- Drawings and/or computer prints which cannot be bound should be organized in a separate folder.

Supervisors:

Professor Torgeir Moan

Professor Andrei Metrikine

Adjunct Professor Zhen Gao

Deadline for thesis report: 17.07.2015

SUMMARY

Floating structures as spar, semi-submersibles and TLP have been proposed for offshore wind turbines for deep waters $(> 60m)$ according to the report of Arapogianni, Moccia, Williams, & Phillips (2011), where bottom fixed sub-structures are technically and economically not feasible. Several floating concepts have been designed and just some of them were deployed as Hywind (Statoil, 2015) and WindFloat (Roddier, Cermelli, Aubault, & Weinstein, 2010), but still they are prototypes that require further improvements in order to achieve it techno-economic feasibility.

At the Centre for Ships and Ocean Structures (CeSOS) NTNU a braceless concept was developed for deep waters called CSC. This floater consists on one central column supporting the wind turbine and three side columns connected each of them at the bottom to the central one through pontoons. These cantilever columns might induce large dynamic stress at the connection section on the pontoon as well on the cross section closer the central column.

The project objective is to propose a structural connection between the central and outer columns at the top avoiding wave loads and check its stress reduction on the pontoon.

The design methodology involves a stability analysis using numerical tool from Det Norske Veritas (DNV) Genie and HydroD. The wind turbine from the National Renewable Laboratories (NREL) in E.E.U.U. of 5MW was employed to estimate the loads and workability of the floater. The hydrodynamics analysis is going to be done in frequency domain based just in wave loads.

Through the hydrodynamic loads the stresses are estimated assuming rigid body behavior. It estimation are done by Euler-Bernoulli theory and via Finite Element Method using beams and shell elements.

The results show that the upper beams reduce significantly the dynamic axial stress on the pontoon, increasing the floater strength. The FEM using beam elements is a simple and reliable numeric approach to obtain global loads and the stress distribution on the structure. The FEM shell mode could predict the stress for the simplest case but it requires more computational effort in order to set up the mesh model and achieve satisfactory results.

The Euler-Bernoulli method under predict the stress on the pontoons as the whole structure of pontoon-brace does not fulfill the beam theory assumptions.

ACKNOWLEDGMENT

I would like to thank Professor Torgeir Moan from NTNU and Professor Andrei Metrikine from TU Delft for their support and coordination for the completion of the European Wind Energy Master.

I would like to give special thanks to Professor Zhen Gao and Ph.D. Candidate Chenyu Luan for its continues guidance and its will to help me when I required to surpass the obstacle and orientate me to achieve the best results.

Also, I want to acknowledge all the EWEM folks that during the program shared their time and friendship, especially Irma, Lisa, Gonzalo, Niels, Ralph and Roel, with whom I worked closely in the offshore specialization. It was a very pleasure knows all of you.

Finally, I want to give thanks to the Erasmus Mundus Education and Culture DG for its economic support by being awarded with the Erasmus Mundus scholarship for the completion of the master course.

Trondheim, Norway 17 of July 2015

Felipe Vittori

TABLE OF CONTENT

CONFIDENTIALITY STATEMENT iii

THESIS OUTLINE iv

SUMMARY vii

ACKNOWLEDGEMENT viii

TABLE OF CONTENT ix

LIST OF SYMBOL 1

LIST OF FIGURES 3

LIST OF TABLES 5

CHAPTER 1 INTRODUCTION 6

1.1. General Objective 8

1.1.1. Specific Objectives 8

1.2 Method 8

1.3 Thesis Overview 9

CHAPTER 2 LITERATURE REVIEW 10

2.1. Hydrostatic 12

2.2. NREL 5 MW wind turbine 15

2.3. Hydrodynamics 17

2.4. Stress analysis 20

2.5. Numeric tool 20

CHAPTER 3 CSC FLOATING OFFSHORE WIND TURBINE 25

3.1. Structural definition 25

CHAPTER 4 STABILITY ANALYSIS 30

CHAPTER 5 HYDRODYNAMICS 34

5.1. Natural periods 34

5.1.1. Simulation set up 34

5.2 Response Amplitude Operator Force 35

5.3 RAO motion 38

5.3.1. Response spectrum for heeling motion 40
5.4 RAO cross section load 41
CHAPTER 6 STRESS ANALYSIS 44
6.1 Euler-Bernoulli stress 44
6.2 Finite Element Method 49
6.2.1. FEM beam check 49
6.2.2. FEM shell check 56
6.3 FEM on critical wave incidence 62
6.3.1. FEM beam 62
6.3.2. FEM shell 65
6.3.3. Ultimate Limit State 67
CHAPTER 7 CONCLUSIONS 69
7.1 Recommendations 70
REFERENCES 71
APPENDIX A 74
APPENDIX B 86

LIST OF SYMBOLS

M_R	Righting moment [L.F]
ρ	Water density [M/L^3]
g	Gravity acceleration [L/T^2]
∇	Displaced water volume [L^3]
$\overline{GN_\varphi}$	Metacentric height [L]
φ	Heeling angle [deg or rad]
I_T	Transversal water plane moment of inertia [L^4]
$\overline{B_0G}$	Weight stability [L]
A_0	Cross sectional area of piercing body [L^2]
a	Length of the vessel center line and the column [L]
$\overline{GZ_\varphi}$	Righting arm [L]
FOWT	Floating offshore wind turbine
DNV	Det Norsk Veritas
RAO	Response amplitude operator or transfer function [-]
DoF	Degree of freedom
L	Length unit
T	Time unit
M	Mass unit
F	Force unit
CSC	CeSOS Semi-submersible Concept
CeSOS	Centre for Ships and Ocean Structures
D_{ext}	External diameter of tower cross section [L]
h	Height of the tower section [L]
$m_{i,j}$	Mass matrix of FOWT [M]
$\ddot{\boldsymbol{x}}_j$	Acceleration vector for rigid body DoF's [L/T^2 or rad/T^2]
$\dot{\boldsymbol{x}}_j$	Velocity vector for rigid body DoF's [L/T or rad/T]
$\boldsymbol{x}_j$	Position vector for rigid body DoF's [L or rad]
$\boldsymbol{F}_{i_h}$	Hydromechanical force vector [F]
$\boldsymbol{F}_{i_w}, \boldsymbol{\mathcal{F}}_{w_i}$	Wave force vector [F]
$\boldsymbol{F}_{i_E}$	External force vector [F]
ω_e	Excitation wave frequency [rad/T]
$a_{i,j}(\omega_e)$	Added (or hydrodynamic) mass matrix [M]
$b_{i,j}(\omega_e)$	Potential damping matrix [F.T/L]
$c_{i,j}$	Restoring coefficient matrix [F/L]
t, τ	Time [T]
T_j	Natural period for each DoF [T]
$A_{i,j}$	Infinite-frequency added mass matrix [M]
$\boldsymbol{K}$	Retardation function matrix
$\boldsymbol{X}_j$	Response amplitude vector [L or rad]
ζ_a	Wave amplitude [L]
$\boldsymbol{R}_j$	Response function
$\boldsymbol{S}_w$	Wave spectrum [L^2.T]
F_M	Morison force [F]
D	Diameter of the slender body [L]
C_m	Inertia coefficient [-]

C_D	Drag coefficient
$\dot{u}$	Wave acceleration [L/T^2]
u	Wave velocity [L/T]
u_A	Wave velocity amplitude [L/T]
$\phi(x,z,t)$	First order wave velocity potential
H	Wave height [L]
k	Wave number
c	Wave speed [L/T^2]
σ_{Pi}^{RAO}	RAO axial stress [F/L^2/L]
Pi	Critical stress point at pontoon cross section
A_C	Cross section area of the pontoon or/and upper beam [L^2]
F_x	Wave force on the "x" direction [F]
M_y, M_z	Wave moment in the "y" and "z" direction respectively [F.L]
I_y, I_z	Bending moment of inertia respect "y" and "z" cross section axis [L^4]
$\boldsymbol{R}$	Wave loading vector [F]
$\boldsymbol{K}$	Discretized structure stiffness matrix [F/L]
$\boldsymbol{r}$	Node displacements [L]
ξ	Damping ratio
$q_j^{RAO}(x_b)$	Differential sectional load at floater cross section [F]
$I_{j(\ddot{x}_j,m)}$	Differential sectional inertial load [F]
$R_{j(c_{i,j},x_j)}$	Differential sectional restoring load [F]
$E_{j,waves}$	Differential sectional wave load [F]
$D_{j(\ddot{x}_j,\dot{x}_j,m_a,b_{i,j})}$	Differential sectional hydrodynamic load [F]
$Q_j(x)$	Integrated sectional load [F]
$\overline{Dis}(x_b)$	Distant between cross section reference point and FOWT center of gravity [L]
$M_j(x)$	Integrated sectional moment [F.L]

LIST OF FIGURES

Figure 2.1 Floating platform classification (Butterfield, Musial, Jonkman, Sclavounos, & Wayman, 2005) *10*
Figure 2.2 Notation for estimation of water plane moment of inertia (Clauss, Lehmann, & Östergaard, 2012) *13*
Figure 2.3 Typical stabilities curves (Clauss, Lehmann, & Östergaard, 2012) *14*
Figure 2.4 Genie NREL 5MW turbine and tower model *16*
Figure 2.5 Aerodynamic characteristics of the NREL 5MW turbine (Jonkman, Butterfield, Musial, & Scott, 2009) *17*
Figure 2.6 a) Critical stress point on CSC. b) Critical stress point in the new CSC. *21*
Figure 2.7 Straight beam element with two nodes. (DNV, 2010) *22*
Figure 2.8 Shell element (DNV, 2010) *23*
Figure 3.1 CSC hull dimensions, upper view, dimensions in meters [m] *25*
Figure 3.2 CSC hull dimensions, side view, dimensions in meters [m] *26*
Figure 3.3 New CSC hull dimensions, upper view, dimensions in meters [m] *27*
Figure 3.4 New CSC hull dimensions, side view, dimensions in meters [m] *27*
Figure 4.1 Genie model of a) CSC and b) New CSC. *30*
Figure 4.2 Righting moment curve for the CSC. *31*
Figure 4.3 Righting moment curve for the new CSC. *32*
Figure 5.1 Excitation wave incoming direction. *35*
Figure 5.2 RAO force in the heave direction for the CSC. *35*
Figure 5.3 RAO force in the heave direction for the new CSC. *36*
Figure 5.4 RAO Moment in the sway direction for the CSC. *37*
Figure 5.5 RAO Moment in the sway direction for the new CSC. *37*
Figure 5.6 RAO heave motion for the new CSC *38*
Figure 5.7 RAO pitch motion for the a) original and b) new CSC. *39*
Figure 5.8 RAO roll motion for the a) original and b) new CSC. *39*
Figure 5.9 STD Pitch for a) CSC new and b) CSC under ULS *40*
Figure 5.10 RAO "x" force on section 1 at 4m from the centre of the CSC. *42*
Figure 5.11 RAO "x" force on new CSC at a) section 1 and b) section 5 at 37m from the unit centre. *42*
Figure 5.12 RAO "z" moment at section 1 on a) CSC and b) new CSC. *43*
Figure 5.13 RAO "y" moment at section 1 on a) new CSC and b) CSC. *43*
Figure 5.14 RAO My for 60° of wave incidence for a) new CSC and b) CSC *44*
Figure 5.15 RAO Mz for 120° of wave incidence for a) new CSC and b) CSC *44*
Figure 6.1 RAO axial stress at point P2 from cross section 1 for a) CSC and b) new CSC45
Figure 6.2 RAO axial stress at point P2 from cross section 5 for a) CSC and b) new CSC46
Figure 6.3 Stress decomposition for P2at section 1, wave direction 60° for a) CSC and b) new CSC *47*
Figure 6.4 STD of axial stress at section 1, P2 for CSC as a function of the wave direction and design load case *47*
Figure 6.5 STD of axial stress at section 1, P2 for new CSC as a function of the wave direction and design load case *48*

Figure 6.6 a) Beam model for the CSC design. b) The segment lengths on the pontoons are 1,5m and for the columns is 1m. c) Simplified beam structure of the CSC floater with the location of the support. *50*
Figure 6.7 a) RAO Fx and b) RAO My obtained from HydroD (E-B) and Sestra (FEM) for the CSC for 0° wave direction at section 4 ..... *51*
Figure 6.8 Force comparison between the total RAO Fz on the center of gravity and the vertical component of the support reactions. *51*
Figure 6.9 Force comparison in "x" direction and relative difference between the FOWT force and the reaction. *52*
Figure 6.10 RAO axial stress from E-B and FEM-beam at section 1 for the CSC design .. *52*
Figure 6.11 Cross section My and Fx at section 4 for 0° at new CSC *53*
Figure 6.12 Difference between the magnitude of the reaction force in x direction respect the external Fx load on the new CSC *54*
Figure 6.13 RAO axial stress from E-B and FEM-beam at section 4 for the new CSC *55*
Figure 6.14 RAO axial stress contribution from Fx and My to the total stress at section 4 for P2 at the pontoon of the new CSC *56*
Figure 6.15 a) FEM shell model of the CSC. b) Close up at the structured mesh on the pontoon. c) Support location *57*
Figure 6.16 Support reaction forces and relative differences respect the Fz of the FOWT for the FEM shell CSC *57*
Figure 6.17 RAO axial stress for different mesh size at section 1 of the CSC *58*
Figure 6.18 RAO axial stress from FEM shell for the CSC design at P2 ..... *59*
Figure 6.19 Support reaction force difference in "z" direction respect the total Fz force on the CoG of the new CSC *60*
Figure 6.20 RAO axial stress from FEM shell at section 4 for new CSC design *60*
Figure 6.21 RAO axial stress decomposition by forces at section 4 on P2 at the pontoon of the new CSC *61*
Figure 6.22 RAO axial stress comparison between FEM results at section 4 of the pontoon *62*
Figure 6.23 RAO axial stress at section 4 for 130°, using FEM beams for both semi-submersibles *63*
Figure 6.24 Stress decomposition for new CSC at section 4 ..... *64*
Figure 6.25 RAO axial stress at section 4 for 140°, using FEM beams *64*
Figure 6.26 RAO axial stress at section 4, wave direction 130°, using FEM shell elements *65*
Figure 6.27 Differences between the reaction forces respect the total force in "z" direction at the CSC center of gravity *66*
Figure 6.28 RAO axial stress at section 4, wave direction 140°, using FEM shell elements *67*
Figure 6.29 STD axial dynamic stress on the pontoon for the new and original CSC at section 4 for 130° *67*
Figure 6.30 STD axial dynamic stress on the pontoon for the new and original CSC at section 4 for 140° *68*

LIST OF TABLES

Table 2.1 Heeling angle at rated speed [deg] *14*
Table 2.2 Mechanical properties of the tower *15*
Table 2.3 Turbine mechanical properties. Reference system located at the tower base. *15*
Table 2.4 Natural period for FOWT [s] *19*
Table 3.1 Structural properties for both CSC *29*
Table 4.1 Stability results of CSC *33*
Table 4.2 Stability results of new CSC *33*
Table 5.1 Natural period and angular frequencies *34*
Table 6.1 Dynamic stress reduction respect the original CSC based on E-B *48*
Table 6.2 Dynamic stress reduction between original and new CSC from FEM-beams *68*

CHAPTER 1 INTRODUCTION

Floating structures for offshore wind turbines has been a technical design challenge in the wind energy industry because it is subjected to complex interaction between the aerodynamics effects of the wind turbine and the hydrodynamics loads from the sea. Despite of this, floating foundations is an attractive concept solution due to the wind resource is abundant at long distances from shore where the water depth is larger than 20m (Butterfield, Musial, Jonkman, Sclavounos, & Wayman, 2005) and bottom founded foundations can be technically and/or economically not feasible. Additionally, remote locations outside from the visual range are preferable to develop wind farms as they have more public acceptance.

Nowadays, with the volatile energy prices, the energy demand and the public opinion against the visual impact of offshore wind farms (Musial & Ram, 2010) floating structures for wind turbines (FOWT) is becoming a recent development trend in the wind power industry. Also, because FOWT can offer important advantage respect bottom founded foundation based a low installation, maintenance and removal cost.

Other authors like Bulder et al. (2003) shows the techno-economics advantage of use FOWT from intermediate water deeps of 50m into deeper waters. They express that the installation cost can be reduced importantly as the platform can be built with the wind turbine in a harbor and then towed to its operational location. In this way the cost associated with manpower work is lower as they are the most part of the project time onshore and their work is not dependant of the weather condition that can delay the project schedule. This is common during the bottom founded installation as the hammering or drilling ships have to work in some weather windows.

There is a large successful experience in the technical design of floating units from oil and gas industry. However, in the case of wind turbine sector this methods and tools should aim to a enough robust floater design to hold the environmental loads but with an optimal material employment to be economically feasible because current offshore wind farms involve several numbers of turbines (Horn Rev 1, 80 turbines, (Horns Rev 1)) that would require a floater each, thus the unit cost is an important target to be reduced.

In the last decade there have been some floaters designs still under development like the GustosMSC Tri-Floater (Huijs, Mikx, Savenije, & de Ridder, 2013), the tri-floater from Lefebre and Collu (2012), the Olav Olsen concrete floater (Dr.techn. Olav Olsen AS, 2015). In some cases the floaters have been built for full scale experimentation as the WindFloat in Portugal (Roddier, Cermelli, Aubault, & Weinstein, 2010), the VolturnUS in E.E.U.U. (Viselli, Goupee, & Dagher, 2014), the Hywind in Norway (Statoil, 2015) and the V-shape semi-submersible floater from the Fukushima Forward project (Fukushima Offshore Wind Consortium) in Japan. Al this commissioned FOWT's are deployed just for gathering information and experience for further development, thus are not for full scale wind exploitation.

Most of the existing design concepts are floaters with three or four columns with a wind turbine located on one side or in the central column; there is also a spar concept with a large draft that make it applicable for water deep larger than 100m.

According Butterfield et al. (2005) there is not optimum platform design but from all the design varieties of offshore structures, the research and development will narrow it into some efficient platforms design for some site conditions. The cost/benefit relation shall be dependant of the location because the water deep will be a very important parameter during the design phase.

At the Centre for Ships and Ocean Structures (CeSOS) of NTNU, a braceless semi-submersible wind turbine has been designed and called CeSOS Semi-submersible Concept (CSC). The semi-submersible consists of one central column supporting the wind turbine and three side columns connected at the bottom to the central column by three pontoons. The semi-submersible will be made of steel with a proper distribution of water ballast.

This semi-submersible offers the advantage of reducing the number of welding connections, improving the floater reliability as it is less sensitive to fatigue and corrosion hot-spot, also easy the fabrication process. However, previous studies from Luan et al. (2014) shows that wave loads are generating large stresses on the pontoons, close to the central column. The reason for this can be associated that the pontoons cross section cannot offers enough inertia to hold the dynamics loads plus the structural reaction from the outer columns that are like cantilever respect the pontoon.

Based on this, the thesis project is oriented on a structural assessment of the CSC semi-submersible in order to check that a structural connection between the outer and central columns by means of heavy beams can reduce the stress loading by the waves on the pontoons. The project will be done by numeric means using the DNV SESAM software package which allows calculate the hydrodynamic loads and then transfer it to the structural model for finite element analysis or extract the cross sectional loads and estimate the stresses analytically.

The structural design of the CSC will not take into account detail such as stiffeners and bulkheads. The structural assessment is going to be carried out from a global design perspective with proper simplifications. The analysis will take into account the wind and wave loads separately.

The results of this project can lead to a re-design of the CSC with the upper heavy beams, keeping the hydrodynamic characteristics of the original design as the floater structure below the water line was not modified, but with a different mass distribution. The new CSC would require more steel but this can be considered as part of a design trade off because the floater would have more resistant, offering a larger life time than the original design.

The CSC has already good hydrodynamic characteristics as it natural periods are outside the wave frequency and previous studies from Luan et al. (2014) suggest that the platform

has lower accelerations and motion amplitudes than other floating solutions. Improvements on the CSC could make it close to achieve a technical feasibility for experimental test on basins. Of course more research work on model is required but this can contribute to the final CSC design version.

1.1. General Objective

The main objective of this thesis project is to compare the dynamics structural response between the original and new CSC concept design with new structural connection between the columns.

1.1.1. Specific Objectives

- Perform a literature review focused on design requirements on stability, hydrodynamic characteristics, main features of braceless semi-sub, semi-sub with brace connections and structural responses respect ultimate limit state (ULS) design.
- Produce an initial design of the heavy beams based on the CSC semi-sub data adjusting the water ballast to keep the same draft.
- Establish the numerical models of the new design in DNV SESAM package Genie and HydroD. Perform hydrodynamic analysis and compare the frequency-domain motion responses of the original design and the new design in waves.
- Estimate using beam theory the structural response on the pontoons and heavy beams of the new CSC. Compare these results with the original CSC model.
- Establish a finite element model on DNV SESAM and compare these structural response with previous results based on beam theory between CSC designs.

1.2. Method

In order to complete, the presented objectives in the thesis project the following methodology will be applied to the conceptual design of CSC semi submersible for an offshore wind turbine.

- Perform a literature review related with
    - Design requirements on stability.
    - Fundamental equation and principles about hydrodynamic characteristics of floating structures.
    - Gather the relevant information about the NREL 5MW (Jonkman, Butterfield, Musial, & Scott, 2009) wind turbine.
    - Structural connection used in other designs and mechanical modeling.
- Generate the new design of the CSC maintaining the original draft.
    - Define the geometry and mass properties of the new CSC floater in Genie.
    - Adapt the NREL 5MW wind turbine to the new design.
    - Generate a stability analysis in HydroD for different heeling moment directions for both CSC.
    - Calculate the hydromechanics characteristics like natural period in heave, roll and pitch motion in frequency domain.

- Generates a panel model for both CSC in HydroD to apply first order potential wave theory and viscous effect from Morison equation in frequency domain analysis. No wind effect is considered in the study.
    - Obtain the relevant Response Amplitude Operators (RAO) forces and motion respect the centre of gravity (CG) of each CSC.
    - Obtain the sectional loads at different cross section of the pontoon
- Estimate the axial stress at different cross sections assuming beam theory employing the sectional loads using Matlab.
    - Determine the wave directions that produce the largest stresses applying an Ultimate Limit State (ULS) check.
- Creates a new structural model for Finite Element Method (FEM) study based on beam and shell elements in DNV Genie.
    - Check that both FEM models have the same hydrodynamic characteristics that previous structural model for both CSC.
    - Run a static linear analysis based on hydrodynamic loads on DNV Sestra.
- Discussion and summary of results.

1.3. Thesis Overview

The following chapter presents a referential theory review of the concepts and model that were employing during the thesis project as well as a review of some papers with relevant information for the project. Chapter 3 shows the design of both CSC and its mechanical properties. The Chapter 4 the stability analysis is explained presenting the intact stability curves for the FOWT's. In Chapter 5 the hydrodynamic results are analyzed and compared between both CSC. Chapter 6 contains the results from the comparison between the stress obtained from beam theory and FEM calculation. Finally, Chapter 7 presents the conclusions and recommendations for future work.

CHAPTER 2 LITERATURE REVIEW

This chapter presents a theory review of the concepts and models applied during the projects about a floating structure. Additionally, relevant information for the study from previous works is presented as well.

Floating offshore wind turbines (FOWT) can be classified according Butterfield et al. (2005) into three main categories based on it static stability principle. Ballast, Mooring Lines and Buoyancy stabilized. For each floater it restoring capacity comes from the contribution of buoyancy (hydrostatic), ballast (weight) and mooring system. Figure 2.1 illustrate these categories.

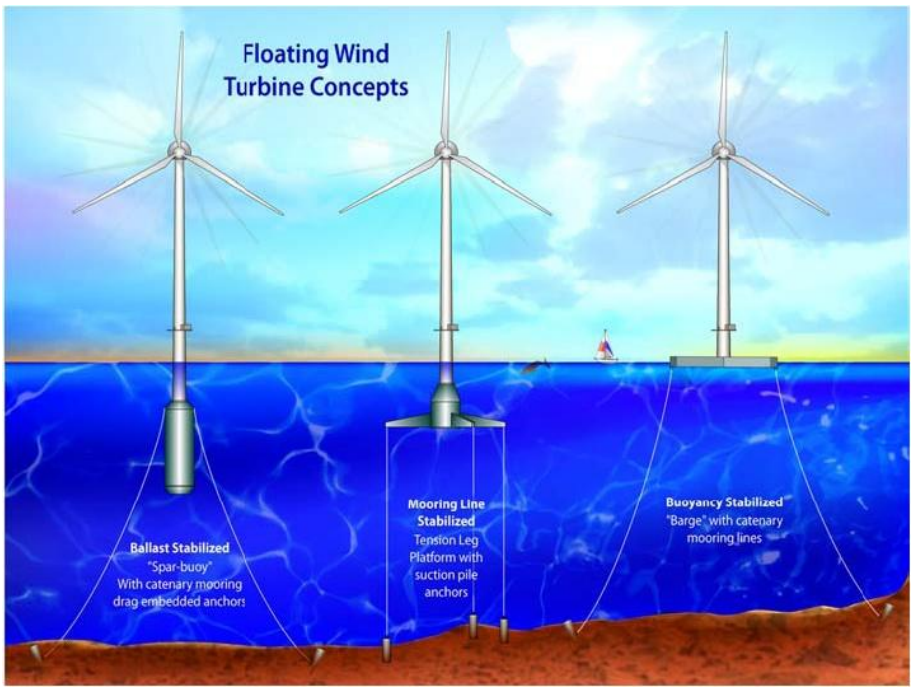

Figure 2.1 Floating platform classification (Butterfield, Musial, Jonkman, Sclavounos, & Wayman, 2005)

The ballast type floater like the spar achieve mostly its restoring capacity for pitch (and roll) from ballasting thus large draft with a considerable mass at it ends give its restoring moments against external forces. The most important restoring characteristics of the mooring lines system like tension leg platforms (TLP) rely totally on its mooring system and the buoyancy stabilized like a barge achieve its restoring capacities via water plane area moment.

From this basic concepts the buoyancy stabilized floater is the less cost efficient as it would require according to Boulder et al. (2003) very large dimension and still its restoring capacities and natural periods cannot fulfill general stability and motion requirements.

The other two basic concepts are technically more attractive leading to further studies like Karimirad and Moan (2012) that studied to expand the employment of spar type into

moderate waters deeps and Ramachandran et al. (2014) whose propose a 3-D numerical dynamic model for a TLP including wave and wind loads with its respective structural response.

All this stabilization principles might also be combined in order to achieve an improved floater behavior like the tri-floater that is basically constructed by columns linked by truss or pipe beams. This offers the advantage of having a considerable second moment of inertia with a small water plane area. It is possible to find many research and example of this design like the WindFloat from Roddier et al. (2010), the GustoMSC Tri-Floater of Huijs et al. (2013) and the Tri-Floater from Lefebvre and Collu (2012).

Other important floater that comes as a result of the combination of the mentioned stability principles is the semi-submersible. This platform was successfully adopted in the oil and gas industry and because this there is large information available regarding its dynamic behavior on the seas. The semi submersible has some structure submerged called pontoons that provide sufficient buoyancy and stability, also with the appropriate dimensions can give a large heave natural period outside the sea wave spectrum. More details about this floater can be found in works from Lefebvre and Collu (2012), the Viselli et al. (2014) VolturnUS and the CSC from Luan et al. (2014).

During floater design another important factor taken into account is the manufacture and reliability. Some existing designs uses truss as structural connection like the WindFloat because it has lower costs but it may creates a fatigue sensitive spot at the welding seams that affect the reliability. In the other hand, there are braceless concepts like the VolturnUS that employ heavy beams in order to reduce the fatigue sensitive connection but this involves a higher cost in manufacture.

Considering all this floater characteristics the design process of any floating structure for wind turbine is complex as there are many variables involved from different source like aerodynamics, hydrostatic, hydrodynamics, mooring lines, control systems and structural response. Moreover, there are important non linear effects in the interaction between the sea and the structure.

There is not a unique design methodology, also it depend of the design stage and requirements. A design methodology for a floating concept structure can be found in (Huijs, Mikx, Savenije, & de Ridder, 2013). This involves several steps and some loops in order to correct or refine the initial model to be functional. The authors indicate that all previous mentioned factors should be modeled simultaneously. However, this would lead a time domain simulations that are time consuming and not practical for an iterative design process. Therefore, a simplified analysis is possible first, a static analysis taking into account just static wind loads should be done, here the floating stability and it static inclination is assessed. This allows adjusting dimensions, mass distribution and water ballast.

Then, a frequency domain diffraction method analysis is applied to obtain the structure motion and wave loads. This hydrodynamic results can be used into the structure for a

finite element analysis and asses the strength of the hull. Additionally, is possible to check is the mooring system is appropriate or not. During these stage is possible to redesign, modifying and improve in relative quick design loops.

Finally, a time domain simulation with fully coupled system can be carried out with a floater design that should be close to a final design. The results from this approach should match with the prediction form the frequency domain analysis. After the floater fulfill the design requirements then is possible to pass to the experimental model test.

Lefebvre and Collu (2012) also followed a simplified design methodology similar to the last one but without perform the time domain simulations, instead they propose to set up a floater model and perform experimental test to compare its numerical results.

In this, project due to the CSC design still in conceptual stage a simplified methodology like the one previously described will be follow. Because this, it is important to take into account the following principles and concepts to be able of perform properly the structural assessment on the CSC. The first principle to be presented will be hydrostatic as it's the first floater characteristic to be studied.

2.1. Hydrostatic

A floating structure for offshore wind turbine should have positive stability. This occurs when its metacenter is located above its center of gravity, for any heeled position. The metacenter is defined as the intersection point between the action line of the buoyancy force and the buoyancy force at zero heeled angles, as can be review in Clauss, Lehmann, & Östergaard (2012) and Journée & Massie (2001). This condition guarantee that a righting moment would be produced between the buoyancy and mass forces on the semi submersible and will take it from a heeled to its initial neutral position.

The righting moment is dependant of the displaced water volume and the metacentric height as equation 2.1 reveals

$$M_R = \rho g \nabla \cdot \overline{GN_\varphi} \cdot sin(\varphi) \tag{2.1}$$

The heeling angle is φ and the metacentric height is obtained considering just the geometry and mass of a floating structure with equation 2.2

$$\overline{GN_\varphi} = \frac{I_T}{\nabla}\left(1 + \frac{tan^2(\varphi)}{2}\right) - \overline{B_0G} \tag{2.2}$$

The distance $\overline{B_0G}$ from the metacentric equation is called weight stability (Clauss, Lehmann, & Östergaard, 2012) and is the initial distance between the buoyancy centroid and the gravity center for the neutral position of the semi submersible.

I_T is the transversal water plane moment of inertia of the not heeled water plane and is defined for floaters with n surface piercing cylindrical columns as

$$I_T = n \cdot A_0 \left(a^2 + \frac{A_0}{4\pi} \right) \quad \textbf{(2.3)}$$

Where a is the distance from the column respect the centerline of the semi submersible and A_0 is the circular cross-sectional area. For caisson type of semi submersible equation 2.3 becomes

$$I_T = n \cdot A_0 \left(\frac{{R_S}^2}{2} + \frac{A_0}{4\pi} \right) \quad \textbf{(2.4)}$$

Where R_S is the radial distance of the columns respect the vessel center as it's showed in Figure 2.2.

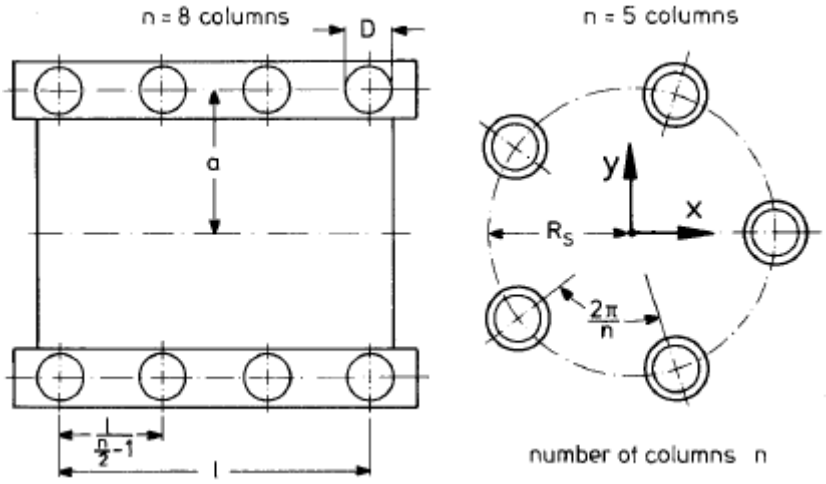

Figure 2.2 Notation for estimation of water plane moment of inertia (Clauss, Lehmann, & Östergaard, 2012)

From these equations is possible to notice that most of the static contribution to the static stability comes from the large spacing of between the columns respect the center of the semi submersible.

The righting arm or level arm $\left(\overline{GZ_\varphi} = \overline{GN_\varphi} \cdot sin(\varphi) \right)$ is more used than the metacentric height $\overline{GN_\varphi}$ and for practical applications is commonly presented a curve that is function of heeling angles and is named stability curve or GZ-curve. There are also curves based on the righting moment M_R where is possible to identify the equilibrium angle when an external moment is applied and counterbalanced by the righting moment, Figure 2.3 present an example of stability curve for different floating structures.

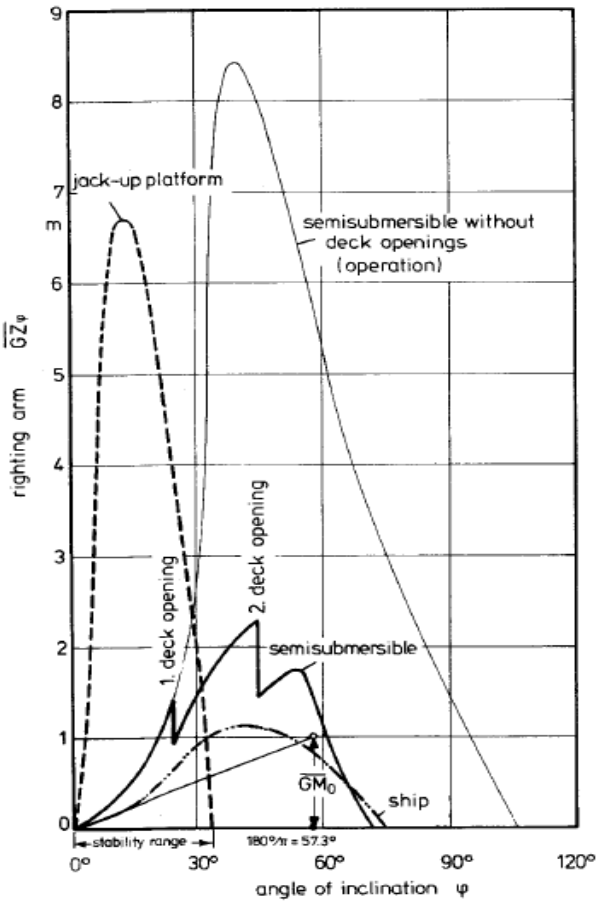

Figure 2.3 Typical stabilities curves (Clauss, Lehmann, & Östergaard, 2012)

For FOWT the stability curve is presented with an external heeling moment obtained from the maximum thrust force of the turbine at rated speed. An important characteristic is the interception point that indicates the floater inclination due to the external load. There is not a design criterion like the oil and gas industry about a heeling angle range that the platform should experience, but from previous studies is possible to have a referential value.

Table 2.1 present the heeling angles for different FOWT, it is possible to notice that the heeling angle is below 15°. Authors like Lefebvre and Collu (2012) [Tri-Floater] perfomred a stablity trade off between different floating concepts and their target was to be below 10°, this parameter was also followed by Huijs, de Bruijn, & Savenije (2014) [GustoMSC tri-floater] and Roddier et al. (2010) [Windfloat].

Table 2.1 Heeling angle at rated speed [deg]

Tri-Floater (Lefebvre & Collu, 2012)	GustoMSC tri-floater (Huijs, Mikx, Savenije, & de Ridder, 2013)	Windfloat (Roddier, Cermelli, Aubault, & Weinstein, 2010)
9	7.4	15

For the stability analysis, the wind loads are not going to be calculated for the maximum force at rated wind speed from the 5MW NREL wind turbine. This turbine is used as referential benchmarking for design and test new concepts for the wind energy industry.

Technical data from this onshore wind turbine is available from Jonkman, Butterfield, Musial, & Scott (2009). The 5MW NREL wind turbine will be adapted to the new floater keeping the same hub height but from the still water level. In the next section, relevant aspect of the wind turbine for the thesis project will be explained.

2.2. NREL 5 MW wind turbine

The 5MW National Renewable Energy Laboratory (NREL) wind turbine is used for the semisubmersible analysis. This wind turbine was developed in the E.E.U.U. to be reference and support concept studies in offshore and land based wind turbines.

For this study, the most important specifications are the tower properties and the mass distribution of the turbine blades due to the aerodynamic effect are not going to be modeled. The tower geometrical aspect is adapted to the floater, because the available data is referenced on a land based wind turbine. The hub height respect the ground was maintained but respect the still water level. This means that the tower height has to be modified in order to be adapted to the floater. The tower height is 67.6m instead of 87.6m from the original one. The tower is made of steel with a density of 7850 kg/m^3, Table 2.2 present the tower properties of the tower.

Table 2.2 Mechanical properties of the tower

Sections	h [m]	Thickness [m]	D_{ext} [m]
1	0	0.027	6.50
2	6.76	0.026	6.24
3	13.52	0.025	5.97
4	20.28	0.025	5.71
5	27.04	0.024	5.45
6	33.8	0.023	5.19
7	40.56	0.022	4.92
8	47.32	0.021	4.66
9	54.08	0.021	4.40
10	60.84	0.020	4.13
11	67.6	0.019	3.87

The turbine is going to be modeled as a point masses distribution. Five concentrated masses will represent the three blades, nacelle and turbine hub. Table 2.3 shows the respective masses.

Table 2.3 Turbine mechanical properties. Reference system located at the tower base.

Component	Mass [kg]	Center of mass		
		x [m]	y [m]	z [m]
Nacelle	240000	1.9	0	89.35
Blade	17740	20.48m along the blade from hub		
Hub	56780	-5.02	0	90

The tower is modeled in Genie though beam elements; each beam will represent a section from Table 2.2. The beams that connect each blade mass are designed without mass. Figure 2.4 present the NREL 5MW tower and turbine modeled in Genie.

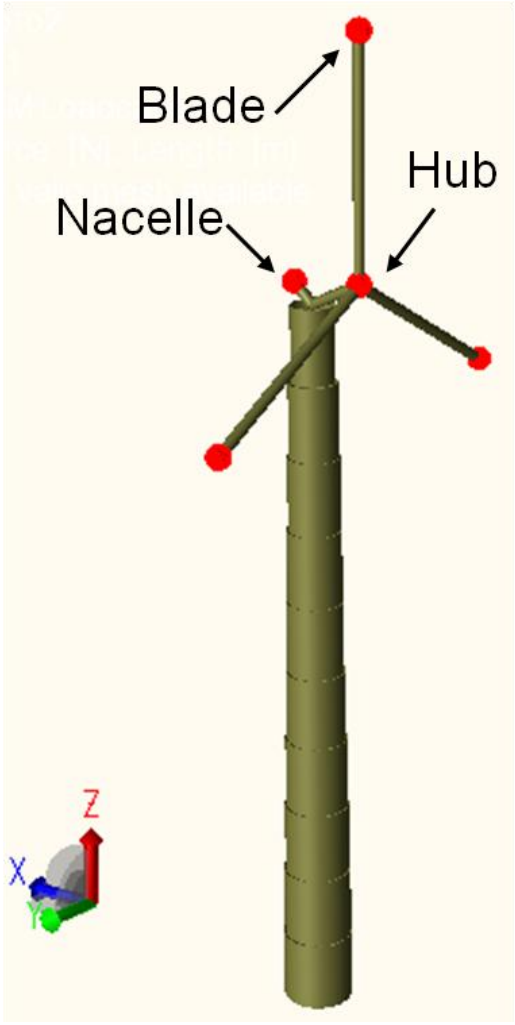

Figure 2.4 Genie NREL 5MW turbine and tower model

Due to the stability study is going to be done using the maxima thrust force produced by this turbine at rated speed and the turbine dynamics is not simulated a constant force will be applied to observe the rotation and displacement of the entire semi submersible. Figure 2.5 shows that the maximum thrust experienced by this turbine at rated wind speed is equal to 800kN.

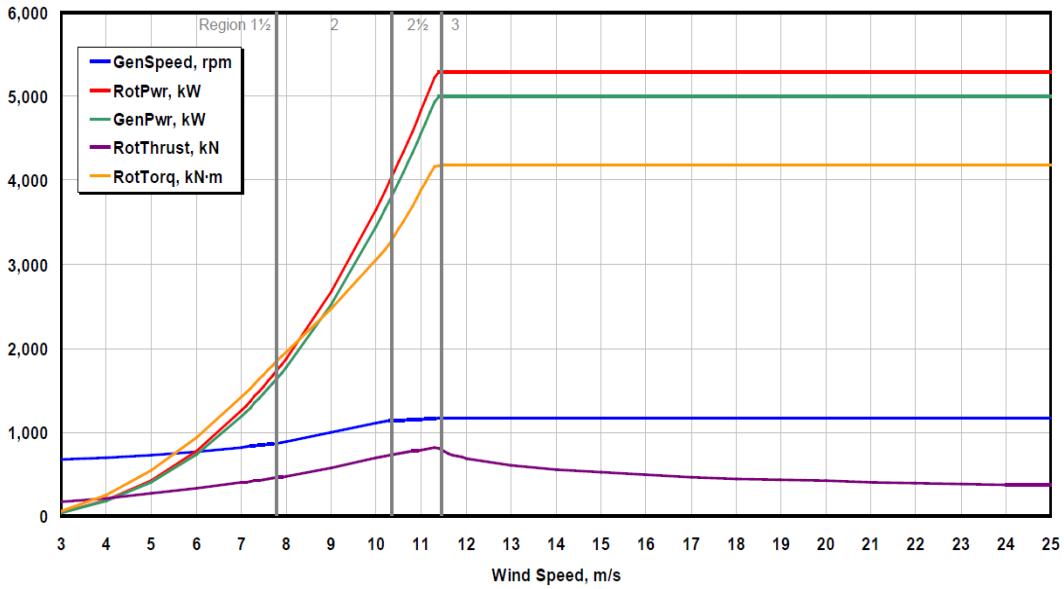

Figure 2.5 Aerodynamic characteristics of the NREL 5MW turbine (Jonkman, Butterfield, Musial, & Scott, 2009)

After define the hydromechanical properties of the semisubmersible is possible to estimate its hydrodynamics behavior.

2.3. Hydrodynamics

In order to obtain the FOWT motions behavior and loads it is possible to model it as a linear dynamic system. The rigid body equation of motions respect to an absolute coordinate system located at the center of gravity of the structure follows from Newton's second law gives equation 2.5.

$$m_{i,j}\ddot{\boldsymbol{x}}_j = \boldsymbol{F}_{i_h} + \boldsymbol{F}_{i_w} + \boldsymbol{F}_{i_E} \tag{2.5}$$

Where $m_{i,j}$ correspond to the total mass distribution over the floating structure degrees of freedom and $\ddot{\boldsymbol{x}}_j$ is the acceleration of each degree of freedom (DoF). The right hand correspond to the external forces, $\boldsymbol{F}_{i_h}$ are the hydromechanical force and moment from originated by the harmonic oscillation of the floater on undisturbed fluid, this force is also called radiation force. $\boldsymbol{F}_{i_w}$ are the exciting wave forces produced by incoming waves on the restrained platform. $\boldsymbol{F}_{i_E}$ are any other external forces like hydrostatic loads, mooring system and wind loads.

Expanding the term from the hydromechanical term is possible to re-write equation 2.5 into 2.6 which is more commonly found in the literature (Benitz, Lackner, & Schmidt, 2015) as the equation of motion for floating structures

$$\left(m_{i,j} + a_{i,j}(\omega_e)\right)\ddot{\boldsymbol{x}}_j(\omega_e, t) + b_{i,j}(\omega_e)\dot{\boldsymbol{x}}_j(\omega_e, t) + c_{i,j}\boldsymbol{x}_j(\omega_e, t) = \boldsymbol{F}_{i_w} + \boldsymbol{F}_{i_E} \tag{2.6}$$

In general this equation represents a harmonic motion model composed by and inertial, damping and restoring terms.

The restoring coefficient $c_{i,j}$ that correspond to surge$[c_{1,1}]$, yaw$[c_{6,6}]$, and sway$[c_{2,2}]$ degree of freedom depend of the mooring system meanwhile for heave $[c_{3,3}]$, pitch $[c_{5,5}]$ and roll $[c_{4,4}]$ the floating structure has its own restoring capacity. This means that if an external force is applied into any of the last DoF the platform will return by its own to its initial position. Equations 2.7 and 2.8 shows the restoring coefficients where is possible to notice that just depend of the FOWT buoyancy and metacentric height.

$$C_{3,3} = \rho g A_{WL} \quad \textbf{(2.7)}$$

$$C_{4,4} = C_{5,5} = \rho g \nabla \overline{GN_{\varphi}} \quad \textbf{(2.8)}$$

Another characteristic from equation 2.6 that defines the behavior of the FOWT is the undamped natural period or eigenperiod (eigenfrequency) defined in equation 2.9.

$$T_j = 2\pi \left(\frac{m_{i,j} + a_{i,j}(\omega_e)}{c_{i,j}} \right)^{0.5} \quad \textbf{(2.9)}$$

The natural period depend not only of the system mass and the restoring coefficient but also of the potential added mass term $a_{i,j}(\omega_e)$ that is a function of the frequency because it depends of the fluid displaced by the moving platform.

One option to solve equation 2.6 in time domain simultaneously with it potential coefficients is manipulate it into Cumming Equation 2.10 (Journée & Massie, 2001)

$$\left(m_{i,j} + A_{i,j}\right)\ddot{\boldsymbol{x}}_j(t) + \int_{-\infty}^{t} \boldsymbol{K}(t-\tau)\dot{\boldsymbol{x}}_j(\tau)d\tau + c_{i,j}\boldsymbol{x}_j(t) = \boldsymbol{F_{ext}}\left(\boldsymbol{x}_j, \ddot{\boldsymbol{x}}_j, t\right) \quad \textbf{(2.10)}$$

However, the solution of the convolution integral is computationally expensive since it has to be evaluated numerically iteratively (Borg & Collu, 2015). A more practical and fast approach since there is only wave loads in this study is solve the equation of motion in the frequency domain as it is presented in equation 2.11.

$$-\omega_e^2 \left(m_{i,j} + a_{i,j}(\omega_e)\right)\boldsymbol{X}_j(\omega_e) + \boldsymbol{i}\omega_e b_{i,j}(\omega_e)\boldsymbol{X}_j(\omega_e) + c_{i,j}\boldsymbol{X}_j(\omega_e) = \boldsymbol{\mathcal{F}}_{w_i}(\omega_e) \quad \textbf{(2.11)}$$

This approach requires the linearization of all the system therefore is not possible to capture non-linear and transient effects. However as indicates Benitz et al. (2015), Huis et al. (2013) and Lefebvre & Collu (2012) the results from the frequency domain method are useful as it can establish the natural period and predict with acceptable accuracy the wave loads.

The natural periods are an important floater parameter because it should be outside of the sea wave frequency spectrum. If not large motion due to resonance can occur producing also large accelerations that can affect the component at the nacelle like the gearbox and can induce large stress on the structure. Table 2.4 presents the natural period for some FOWT concepts that can be used for referential purposes.

Table 2.4 Natural period for FOWT [s]

	Trif-Floater (Lefebvre & Collu, 2012)	GustoMSC Tri-Floater (Huijs, de Ridder, & Savenije, 2014)	VolturnUS (Viselli, Goupee, & Dagher, 2014)
Heave	21	16	24
Pitch	22.5	31	18
Roll	23		

For the North Sea the wave period range can be defined between 5s and 20s (Lefebvre & Collu, 2012). The limit range can change depend of the turbine location and DNV standard suggest to consider this range from 5s to 25s, for this project the hydrodynamic results will be analyzed from 3s until 40s.

From equation 2.11 is possible to obtain the transfer function or the Response Amplitude Operator (RAO). This allows relating an input wave spectrum from irregular waves and generates as output the motion response of the floater in frequency domain following equation 2.12.

$$|RAO(\omega_e)|^2 = \left|\frac{\boldsymbol{X}_j(\omega_e)}{\zeta_a(\omega_e)}\right|^2 = \frac{\boldsymbol{R}_j(\omega_e)}{\boldsymbol{S}_w(\omega_e)} \tag{2.12}$$

For the structural assessment is important to consider viscous effect on the FOWT due to drag forces, this can be done by adding into the equation of motion (2.11) a damping term that comes from the Morison equation (2.13) considering relative motion between the floater and the waves.

$$F_M(t) = \frac{\pi}{4}\rho D^2(C_m(\dot{u} - \ddot{x}) + \dot{u}) + \frac{1}{2}\rho C_D D(u - \dot{x})|u - \dot{x}| \tag{2.13}$$

However, equation 2.13 is not going to be solved complete but as the CSC semi-submersible is going to be modeled in frequency domain by panel method using equation 2.11, only the non linear term of the drag force is linearized and changed into equation 2.14.

$$(u - \dot{x})|u - \dot{x}| = \frac{8}{3\pi}u_A(u - \dot{x}) \tag{2.14}$$

The term u_A correspond to the amplitude of the wave velocity. Just the drag term for Morison equation is considered as a damping term into equation 2.11.

Finally, to solve the equation of motion 2.11 a boundary integral equation method based on linear order potential theory is applied. This is known as Panel Method and is already programmed into the code WAMIT that is integrated to the software DNV HydroD. This solver uses the velocity potential defined in equation 2.15 all over the submerged surface of the platform. More detailed explanation about the method can be found in Benitzet al. (2015) and in the WAMIT manual (WAMIT, Inc.).

$$\phi(x,z,t) = \frac{gH}{2kc}\frac{cosh\big(k(x-ct)\big)}{cosh(kh)}sin\big(k(x-ct)\big) \quad \textbf{(2.15)}$$

In first order potential wave theory the water surface is modeled with equation 2.16 and $\boldsymbol{k}$ is the wave number that is calculated through the dispersion relation 2.17.

$$\zeta(x,z,t) = \frac{H}{2}cos(kx - \omega_e t) \quad \textbf{(2.16)}$$

$$\omega_e^2 = g\ k\ tanh(kh) \quad \textbf{(2.17)}$$

After the hydrodynamic model is solve in frequency domain is possible to obtain the sectional loads on the floater, then is possible to estimate the stresses as it is described in the following section or the hydrodynamic loads can be transferred to a finite element model to obtain the stress.

It is important remark that this project is focus on the dynamics loads produced by the waves, leaving the constant loads from hydrostatic for further studies.

2.4. Stress analysis

In this project two approaches are applied to obtain the axial stresses on the pontoon, one based on Euler-Bernoulli theory and the second based on finite element method that will be briefly described later.

The Euler-Bernoulli theory is based on the assumption that the cross section face of a beam turns around a neutral axis maintaining it face plain and perpendicular. This assumption implies that the longitudinal strains vary linearly across the beam. This approach was applied by Luan et al. (2014) for the CSC following the axial stress equation 2.16.

$$\sigma_{Pi}^{RAO} = \pm\frac{F_x}{A_C} \pm \frac{M_y \cdot z}{I_y} \pm \frac{M_z \cdot y}{I_z} \quad \textbf{(2.16)}$$

The RAO axial stress is because the wave loads F_x, M_y and M_z are RAO solution from the frequency domain analysis. These loads are obtained by integrating the inertial and wave loads at some desired cross section of the pontoon and the Pi term is to indicate the location of the RAO stress according the points in Figure 2.6 a) and the coordinate reference system.

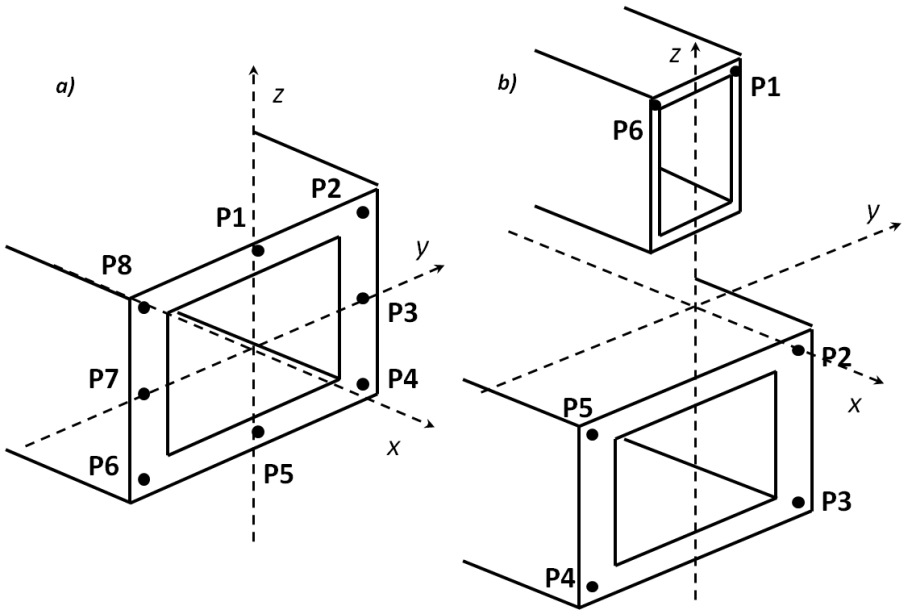

Figure 2.6 a) Critical stress point on CSC. b) Critical stress point in the new CSC.

For the new CSC, maybe the stress approach is not applicable as the cross section is going to be composed by the pontoon and the upper beam as it is show in Figure 2.6 b).

For the CSC in Figure 2.6 a) the pontoon is totally submerged and is subjected to the action of wave loads. It neutral axis goes through the gravity centre of the pontoon cross section, instead for the new CSC the wave loads are just affecting the pontoon as the upper beam is above the still water line (SWL). Assuming rigid body motion of the floater is possible that the load distribution on the cross section it's not linear for some load cases violating the assumption of the Euler-Bernoulli stress equation.

Because this reasons is important to have a second approach to compare the estimated stresses on the pontoon. This method is based on a Finite Element Method (FEM) that is based on the discretization of a structure (continuum) into smaller parts or elements like beams with an assigned mass and structural property in such way that keeps the same global mechanics features of the entire structure. Depending the type of element selected it will have a number of DoF that would let the structure be deformed accordingly by external loads and offers a more accurate load and stress distribution.

In this project the Finite Element Method will be done under the assumption of Quasi-Static Equilibrium where the changes of the floater structure are so slow that it response can be considered statically to the external loads.

The FEM approach is going to be applied on a static analysis based on the displacement method (Langen & Sigbjörnsson, 2014). The static analysis is based on the numeric solution of a set of linear algebraic equilibrium equations that produce the unknown displacement on equation 2.17.

$$\boldsymbol{R = K \cdot r} \tag{2.17}$$

Where $\boldsymbol{R}$ in this case is the wave loading, $\boldsymbol{K}$ is the stiffness matrix of the discretized structure and $\boldsymbol{r}$ is the unknown node displacement.

As was mentioned before the stiffness matrix and it size depend of the type of element. For this research two type elements will be used, beam and shell elements.

Beam element is widely used (Roddier, Cermelli, Aubault, & Weinstein, 2010), (Lefebvre & Collu, 2012) and offer acceptable results for stress analysis in conceptual design stage according Borg and Collu (2015). When a structure is discretized by beam elements like the one on Figure 2.7 is possible to obtain displacement, forces and stress, each beam element has 12 DoF on its nodes at the end of the element.

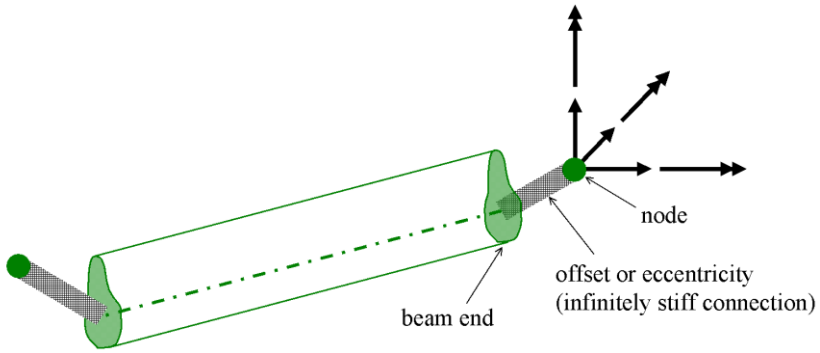

Figure 2.7 Straight beam element with two nodes. (DNV, 2010)

A more detailed result can be achieved by modeling the floater with shell elements. This can give a stress distribution in the cross section of the pontoon that beam element cannot. Figure 2.8 present a shell element with four nodes and 24 DoF, the thickness of the element is taken from the structural model created in Genie.

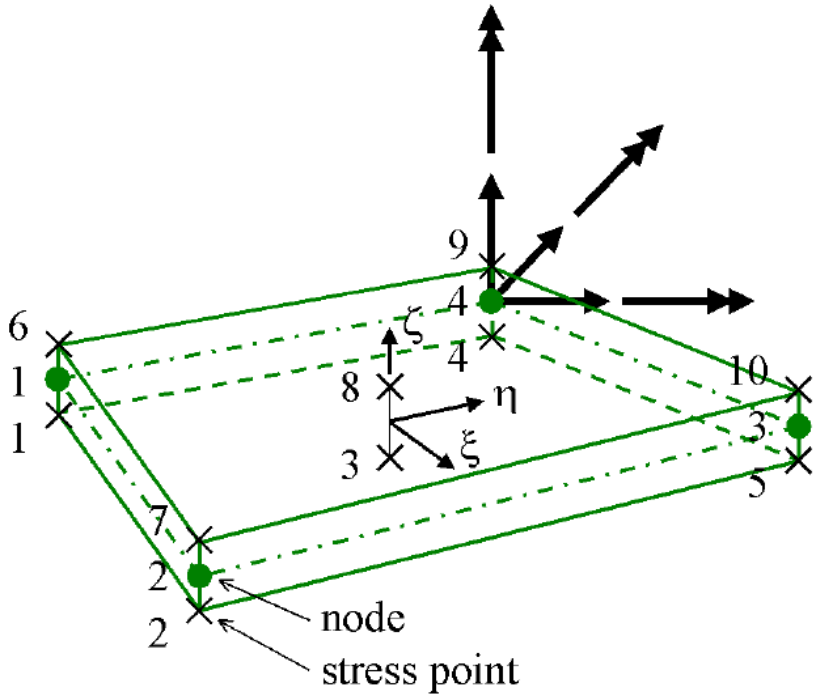

Figure 2.8 Shell element (DNV, 2010)

Due to each shell elements has more DoF the system of equations for the static analysis will increase, leading to a more computational expensive solution than from a beam element discretization. Of course it depend of the size and number of element employed during the discretization process.

All this hydrodynamics principle and numeric tools are integrated in the commercial software DNV SESAM, the next section will explain the relevant software module for the thesis.

2.5. Numeric tool

The DNV SESAM software is going to be the main tool for the study of the floating offshore wind turbine during this thesis project. Matlab software is also employed to calculate the stresses on the pontoon. DNV SESAM has several modules for each type of analysis, for the study the more important are the Genie, HydroD, Postresp, Sestra and Xtract.

• **Genie** is the module dedicated to design structural geometry specifying the material properties, beam inertia and cross section. This module can transform the geometry into a finite element model for a stress analysis or a panel model for a hydrodynamic study.

• **HydroD** is employed to do frequency domain and time domain analysis of floating or bottom founded structures. It takes as input the panel model or a Morison model generated previously in Genie. This module can produce the wave load on a structure and calculate the response motion like the RAO's. The wave loads and motions are computed using Wadam code.

• **Postresp** is an interactive graphic postprocessor for general responses from HydroD. It can read and present transfer function in the frequency domain or a time series from a time domain simulation.

• **Sestra** is the program for linear static and dynamic structural analysis within the SESAM program system. It is used for the displacement based finite element method.

• **Xtract** is a visualization module that offers several options for processing, displaying and animating results from static structural analysis. The module present general stress decompose into membrane and bending parts, principal stress and von Mises stress.

CHAPTER 3 CSC FLOATING OFFSHORE WIND TURBINE

The first stage of this project is to design a new version of the CSC that has better structural strength particularly at its pontoon cross section. This chapter presents the new CSC design and its structural characteristics.

3.1. Structural definition

The CSC semi-submersible was designed for support a horizontal axis wind turbine. The 5MW NREL wind turbine data was employed for the hull analysis. This FOWT is composed by four columns, one central to support the wind turbine and the other columns are for give large transversal water plane inertia that is traduced in stability as can be checked in section of hydrostatic in chapter 2. Additionally, the platform has three pontoons oriented radially from the central column until the outer columns. These submerged elements provide buoyancy and large heave natural period (Clauss, Lehmann, & Östergaard, 2012). Figure 3.1and Figure 3.2 shows the CSC hull dimensions.

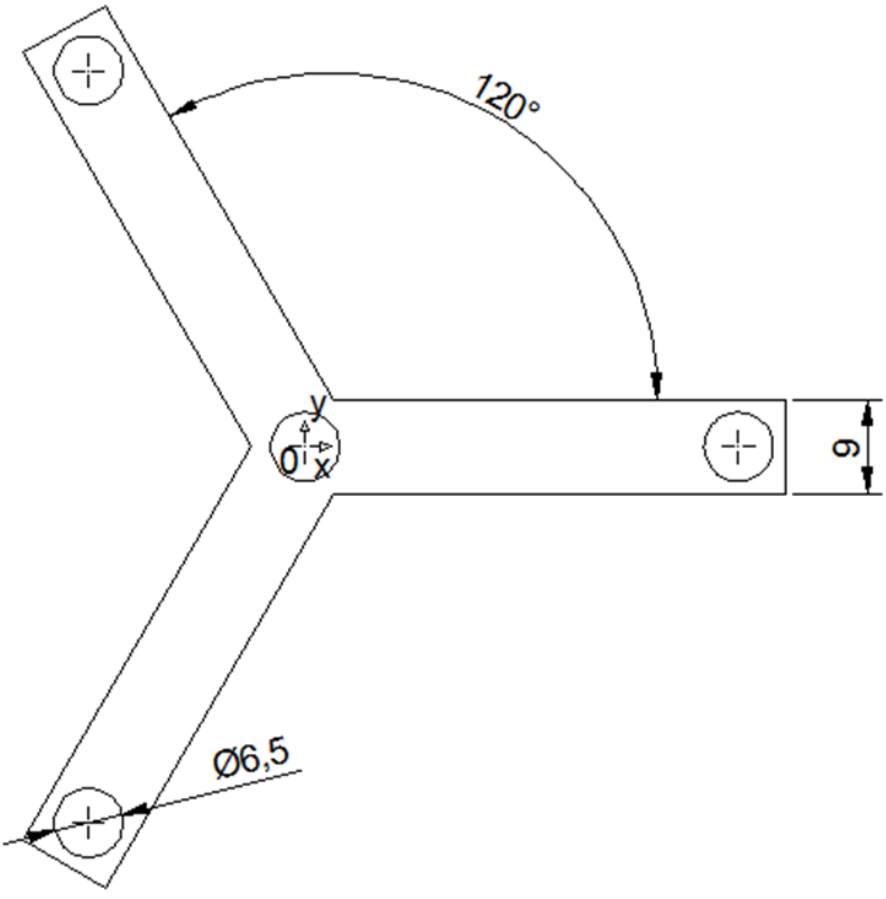

Figure 3.1 CSC hull dimensions, upper view, dimensions in meters [m]

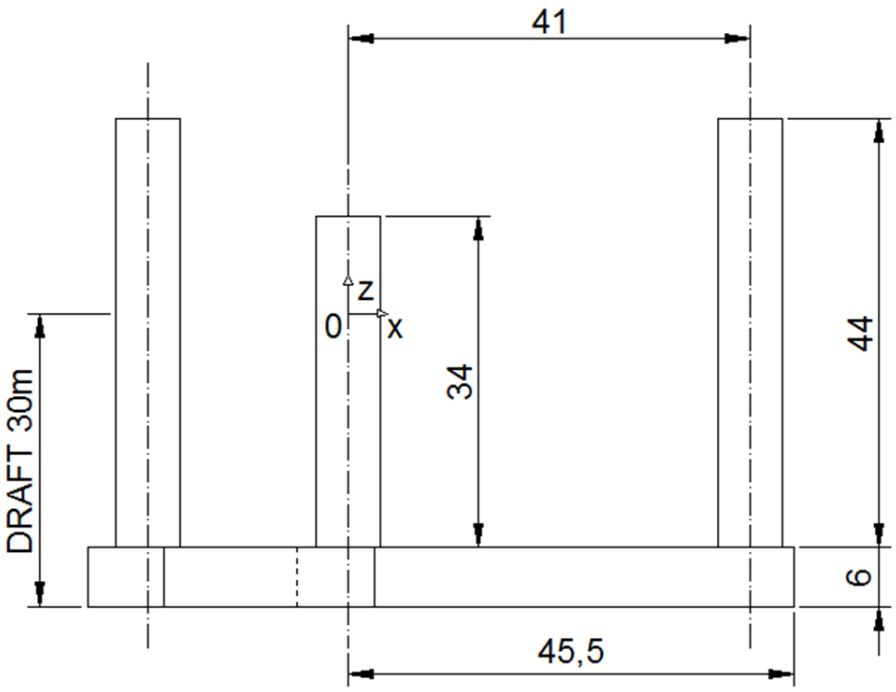

Figure 3.2 CSC hull dimensions, side view, dimensions in meters [m]

The pontoons are going to be totally filled with water ballast and also the outer columns at its bottom, the central column is considered totally empty.

Previous studies suggest that there are large stresses by dynamic loads at the cross section of the pontoon close to the central column. In order to enhance the structural strength of the CSC heavy beams are placed above the SWL radially connecting the outer columns and the central columns. This may reduce the mentioned stress generated by the outer columns as it are not transmitting totally the reaction load to the pontoon only, but can be redirected to the central column.

The upper beam could increase the strength of the pontoon as it is not like a cantilever beam instead is part of a closed loop that should be more resistant to the external loads. Figure 3.3 and Figure 3.4 present the drawing of the new hull CSC design.

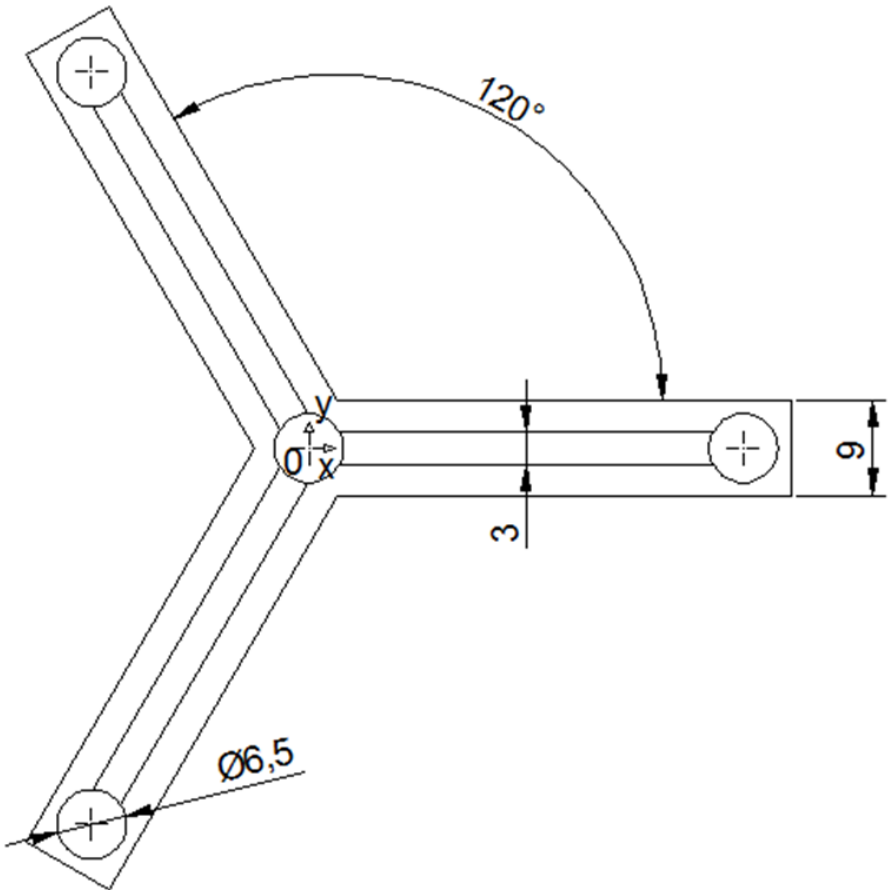

Figure 3.3 New CSC hull dimensions, upper view, dimensions in meters [m]

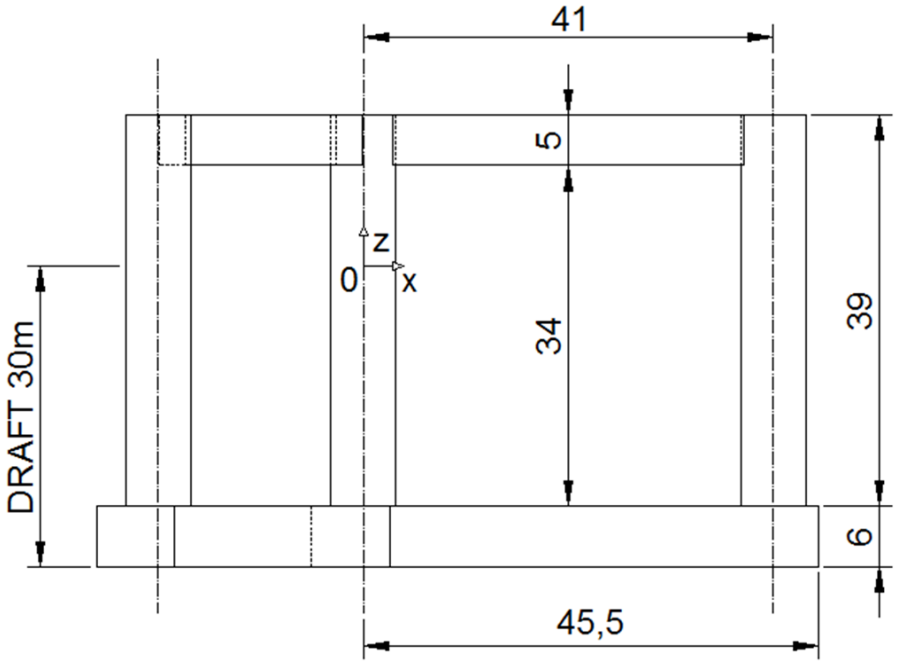

Figure 3.4 New CSC hull dimensions, side view, dimensions in meters [m]

Others FOWT designs like tri-floaters (Lefebvre & Collu, 2012), (Butterfield, Musial, Jonkman, Sclavounos, & Wayman, 2005) uses trusses or smaller beams to connect its columns but this gives as drawback more welding lines that are sensitive to fatigue damage

and corrosion. However, CSC follows the tendency of braceless concepts like the Tri-Floater (Huijs, Mikx, Savenije, & de Ridder, 2013) and VolturnUS (Viselli, Goupee, & Dagher, 2014) that use of fewer heavy beams for structural connection. Due to the large wave and wind loads expected the beam cross section should be large enough to provide good resistance. Even that in the literature review was seen circular cross sections beams and pontoon was seen as most common and cost efficient due to its dimensions. But these smaller beams are part of a structure that requires several of them to get strength and stiffness. Increasing the construction cost.

A simple rectangular cross section shape will be the starting design point. Inspired in concepts like the VolturnUS and the GustoMSC, this beam shape has large bending inertia and is expected to hold the structural stress in such way that can be reduced in size in further projects.

As was seen in others design the air gap between the still water line and the base of the tower oscillates between 10m (Roddier, Cermelli, Aubault, & Weinstein, 2010) and 12m (Huijs, Mikx, Savenije, & de Ridder, 2013) for the new CSC the air gap is increased to 15m, reducing the chances of water to strike the tower bottom. However the air gap between the SWL and the lower section of the heavy beam is maintained in 10m.

Considering reduces material and avoiding the shift of the floater center of gravity the outer columns are reduced in length from 44m to 39m. Is important remark that the "Y" configuration allows to maintain floater symmetry avoids the need of use water ballast pumps as the WindFloat (Roddier, Cermelli, Aubault, & Weinstein, 2010) to make it stable for normal operation. Also, offer the same performance respect any wind, wave and current headings.

The hull is modeled with structural steel with a density of 7850 kg/m^3, Young's modulus 2.1e11 Pa, yield stress of 375 MPa, Poisson ratio of 0.3 and structural damping ratio of 1%. For this conceptual stage there is going to be defined an equivalent thickness of 0.03m for the entire hull; this estimation is derived from oil and gas experience where the steel weight represents 20% of the total displacement (Luan et al. 2014). This parameter allows obtaining the internal loads for a global analysis.

Due to the structural modification, the water ballast is reduced in order to maintain the same draft. This floater is conceived to be used in deep waters (>60m, (Benitz, Lackner, & Schmidt, 2015)). Table 3.1 shows the structural properties for both CSC.

Table 3.1 Structural properties for both CSC

	CSC	New-CSC
Steel Mass [ton]	1755	2094
Water Ballast [ton]	8001	7765
C.G. structure [m]	-16.15	-13.8
C.G. FOWT [m]	-19.01	-18.19
Total displacement [ton]	10577	
Metacentric height at zero heeling [m]	4.67	3.85
Inertia $I_{xx}=I_{yy}$ [kg*m^2]	1.390E+10	1.368E+10
Inertia I_{zz} [kg*m^2]	8.261E+09	7.940E+09

The center of gravity is based on the coordinate "z" in the reference system located at the SWL for both floaters, check Figure 3.2 and Figure 3.4.The total effect of adding the heavy beams and removing water ballast is reflected in the reduction of the inertia on the new CSC. As a drawback in the new design the center of gravity of the hull is shifted upwards reducing its stability capabilities, this also is reflected in the reduction of the metacentric height and from equation 2.2 the level arm for the restoring moment is also decreased.

CHAPTER 4 STABILITY ANALYSIS

The stability analysis offers the basic and most important information of a floating structure that is it capability to keep an upright position in the highest wind speed or severe wave condition. For a FOWT the wind force produces the largest moment on the platform due to the trust force of the turbine combined with the tower height. In this chapter is presented a comparative stability results between the CSC and it new version.

The CSC designs presented in the last chapter are generated in the software Genie, the turbine is going to be modeled as was described in chapter 2 according Jonkman et al. (2009). Figure 4.1 a) and b) present the models.

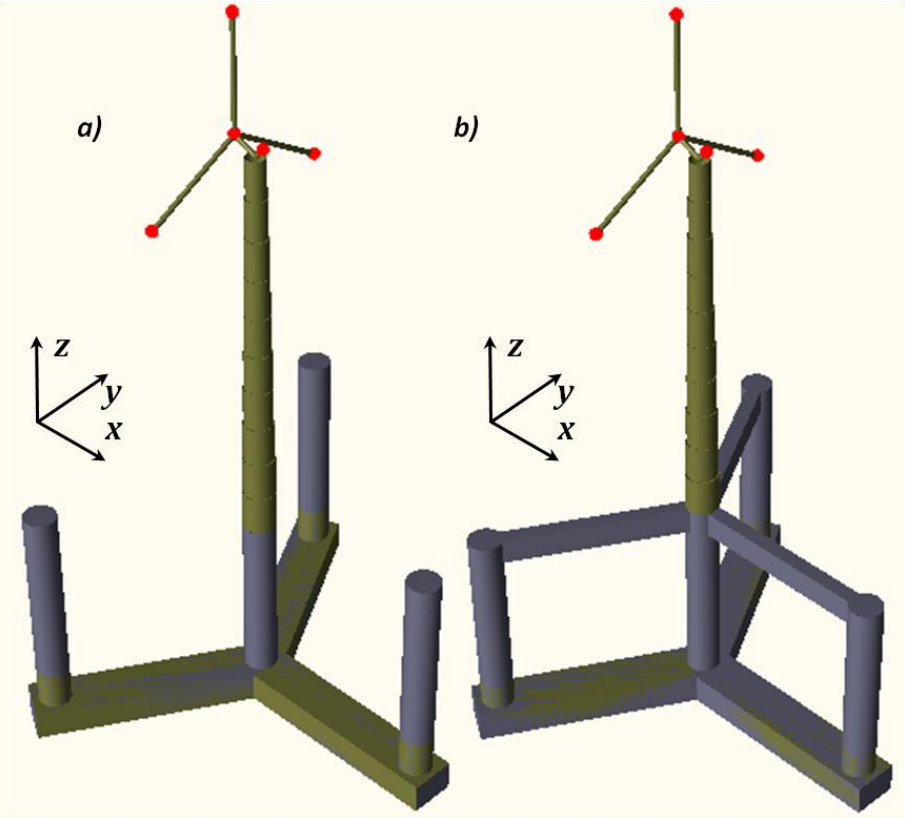

Figure 4.1 Genie model of a) CSC and b) New CSC.

For the new CSC the tower length is smaller because the heavy beams connection to the central column is part of the floater structure. The water ballast is distributed in the same way for both floaters excepting that the water in the outer column in the CSC reach a height of 7,7m from column bottom and in the new CSC this height is reduced at 5,3m.

The analysis is set up for a range angles that goes from -60° to 60° assuming intact condition of the floating unit in operation condition where there is a constant design moment of 72 MNm (Jonkman, 2006).

Even that the hull is considered to have axial symmetric along the axis “z”, in Figure 4.1 the wind force is going to be applied from 0°(along “x” axis) to 90°(parallel to “y” axis)

each 15° respect to ensure a more descriptive stability study. These calculations are performed in HydroD by defining a wet surface and a mesh, which does not require a sensitivity analysis, a coarse one with rectangular element of 1m is employed. The 75° and 90° are applied in order to check symmetry. In both CSC it matches with their respective symmetry angles.

Figure 4.2 presents the positive side of the righting moment curve for the CSC. The interception angle between the semi-submersible curve and the wind turbine moment is around 8° that is a lower value considering other FOWT design.

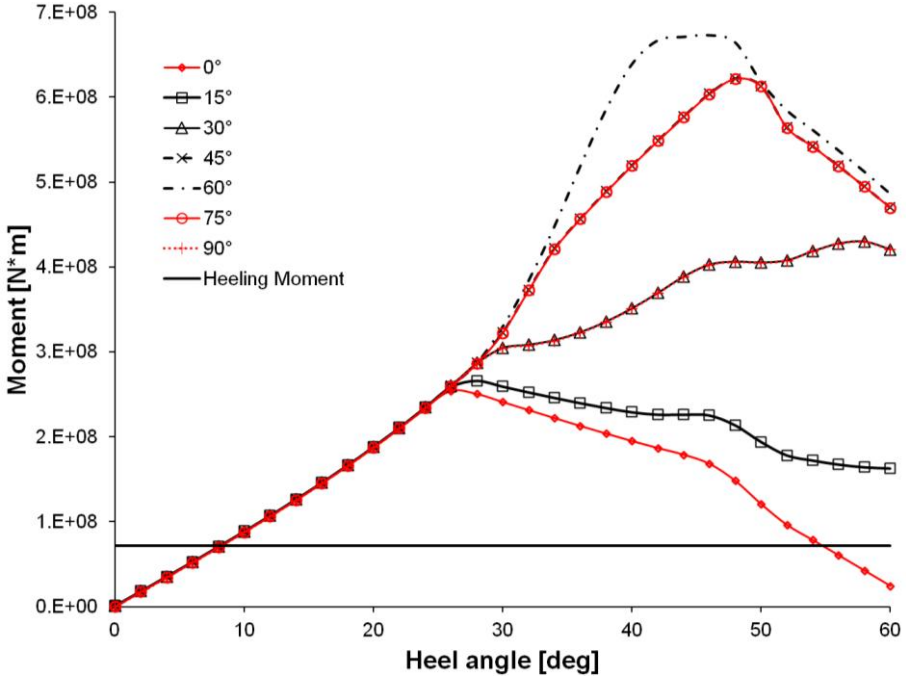

Figure 4.2 Righting moment curve for the CSC.

The inclination during operation is not defined by any international design code currently, but intuitively the target is reduced it. An inclination of 8° means that the hub is displaced 12m respect it neutral position (0°). Due to the center of gravity is shifted on the new CSC the righting moment curves have changed as it is showed in Figure 4.3.

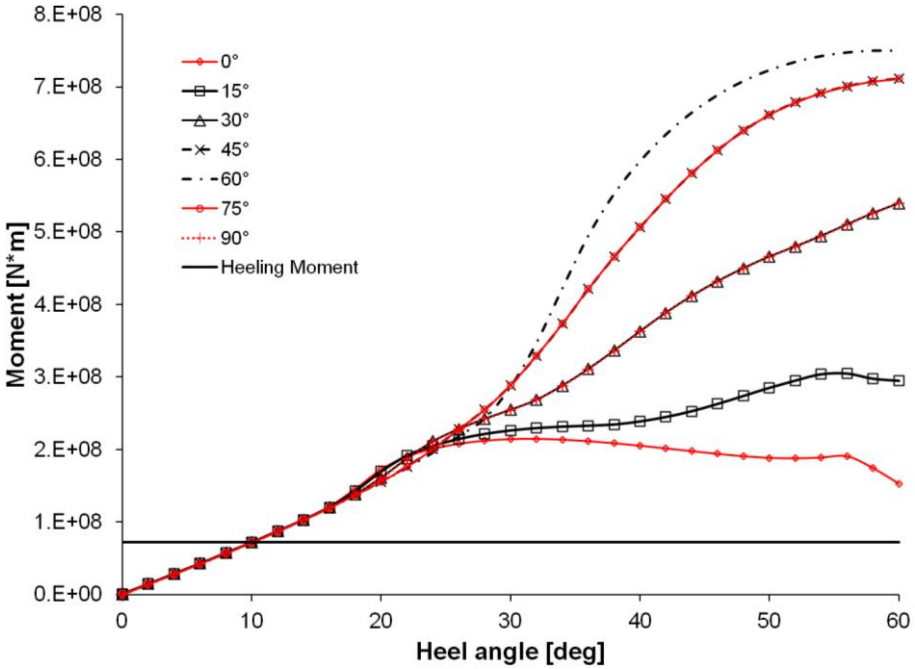

Figure 4.3 Righting moment curve for the new CSC.

The new CSC intercepts the wind moment curve at 10° that can be considered as a drawback in the design. However, the restoring moment curves are larger than original CSC due to new buoyancy added by the upper braces. This can be an important contribution to the stability of the floater as it is giving an additional buoyancy reserve in case the floater faces larger heeling angles due to wave and wind loads.

For both CSC the wind direction that produces the largest righting moment is 60°. This is because the semisubmersible is sinking two of the outer columns producing a large buoyancy force. Instead at 0° wind direction the CSC is submerging just one column generating the lowest buoyancy force. The rest of the wind directions are combination of this and produce intermediates magnitudes of righting moment's curves as it is shown in Figure 4.2 and Figure 4.3.

Both stability analyses fulfils the Offshore standard DNV-OS-J103 (DET NORSKE VERITAS AS, 2013) about column-stabilized structures for FOWT where the area of the righting moment curve is greater the wind heeling moment curve in more than 130% for all wind directions. Another standard that is meets is that the stability curve is positive for the entire test angle range. Table 4.1 and Table 4.2 present the intercepting angle point and the values for the standard requirement for the original and new CSC FOWT.

Table 4.1 Stability results of CSC

Wind direction [deg]	Start angle (H/R interception) [deg]	End Angle [deg]	Righting moment area [N*m]	Heeling moment area [N*m]	Relation DNV [%]
90	8.27	60	266081483	65005835.1	309
75	8.23	60	339811754	65056100.6	422
60	8.2	60	365782685	65093799.7	462
45	8.16	60	340293134	65144065.2	422
30	8.15	60	267056379	65156631.6	310
15	8.13	60	179284842	65181764.3	175
0	8.13	54.7	142340472	58521587.9	143

Table 4.2 Stability results of new CSC

Wind direction [deg]	Start angle (H/R interception) [deg]	End Angle [deg]	Righting moment area [N*m]	Heeling moment area [N*m]	Relation DNV [%]
90	9.98	60	158288311	62856986	152
75	9.99	60	193774654	62844419	208
60	9.99	60	271020445	62844419	331
45	10	60	351129330	62831853	459
30	10	60	135404286	37699112	259
15	10	60	351044843	62831853	459
0	10.1	60	270642326	62706189	332

The stability analyses usually present as well the level arm or righting arm curve $\left(\overline{GZ_{\varphi}}\right)$ as a function of the heel angle. These results are proportional to righting moment curve results presented previously. However, these curves are presented in the Appendix A in Figure A 1 and Figure A 2, for the original and new CSC design.

The stability results have showed that the new CSC offers acceptable restoring capacities against the wind load if it's compared with the original design. The restoring moments is increased for larger heels angles due to the new buoyancy given by the upper heavy beam. This can balance the new heeling angle of 10° and the fact that the floater has it center of gravity in a new upper position.

CHAPTER 5 HYDRODYNAMICS

In this chapter is discussed the motion and the hydrodynamics wave loads of both CSC in order to check any change on the hydrodynamics characteristics of the original design due to the new mass distribution. The presented results are obtained from frequency domain simulations in HydroD.

5.1. Natural periods

The natural periods of the floater are an important parameter that defines the dynamics behavior of the platform. To obtain these values is needed to solve equation 2.9 that is dependant of the frequency dependant added mass using panel method (WAMIT, Inc.). Table 5.1 presents the natural periods for both CSC for heave, pitch and surge.

Table 5.1 Natural period and angular frequencies

	CSC	New CSC
Heave [s] ([rad/s])	25.57 (0.25)	25.61 (0.25)
Pitch [s] ([rad/s])	35.47 (0.18)	38.84 (0.16)
Roll [s] ([rad/s])	35.47 (0.18)	38.84 (0.16)

This natural period can be considered acceptable as they are outside of the wave spectrum as it's recommended by the DNV standard for floating wind turbines DNV-OS-J103 (DET NORSKE VERITAS AS, 2013) in it section 2.1.3 which considers the wave energy spectrum between 5s and 25s. Additionally, there is a noticeable difference (39%) between the periods of heave and pitch for the CSC that avoid coupled vibration.

The structural modification does not produce a significant change in the natural period of the CSC. The small increase in the eigenperiods is in the case of heave because the modification of the semi-submersible mass following equation 2.9. In the case of pitch and roll the reason is due to the reduction in metacentric height (Table 3.1) that also reduces the restoring coefficient (eq. 2.8).

The new CSC maintain the same eigenfrequencies that it original design.

5.1.1. Simulation set up

To solve equation 2.11 the DNV HydroD software is employed. Selecting the option Composite Model is possible to solve the equation of motion of the FOWT considering first order potential wave theory and viscous effect from Morison term. Table B 1 in the Appendix B shows a table with the wave frequencies given as input. Per each frequency an RAO is calculated resulting in a curve of these discretized values.

In the case of viscous term Table B 2 in the Appendix B present the drag coefficient used in order to obtain the appropriate viscous force without creating numeric deviation of wave forces. Figure 5.1 shows the wave direction used per each frequency respect the semi-submersible.

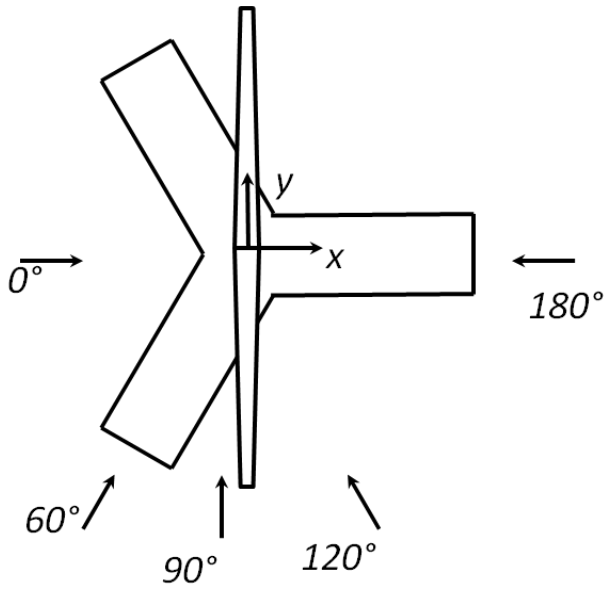

Figure 5.1 Excitation wave incoming direction.

5.2. Response Amplitude Operator Force

The RAO as showed in equation 2.12 is a function that depend of the excitation frequency but also from the wave direction. In this case the response amplitude operator is based on a wave input and an output force. The floater will have different response forces that are depending of the direction from where the excitation wave is coming. Figure 5.2 and Figure 5.3 present the RAO force in heave direction applied at the CSC center of gravity for the original CSC and the new CSC, respectively.

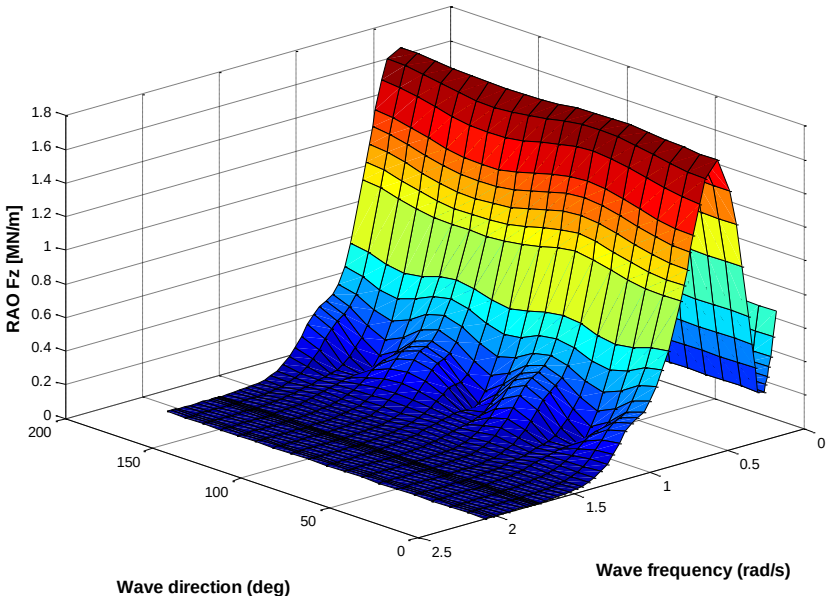

Figure 5.2 RAO force in the heave direction for the CSC.

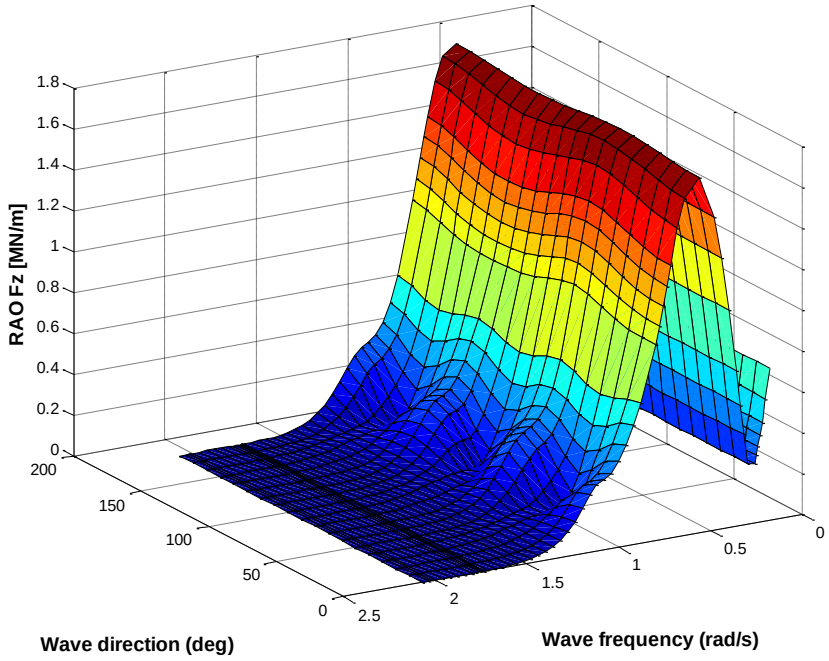

Figure 5.3 RAO force in the heave direction for the new CSC.

From both figures is possible affirm that the RAO forces are unchanged for the new CSC. This as a consequence of maintains the same draft and wet surface of the semi-submersible. Additionally, the surfaces show that this "z" RAO force is independent of the wave direction, this is an expected characteristic in this response because the FOWT was designed to be symmetric respect the vertical axis respect the incoming waves.

The largest peak is because that excitation wave frequency is close to the damped natural heave frequency. The second increase close to 0 angular frequencies is due to the pitch and roll damped natural frequencies. The damped natural frequencies will be discussed in further sections.

Figure 5.4 and Figure 5.5 shows that the RAO moments respect the sway direction, the moments are very similar between the original and new CSC. The differences are below 1% even considering that the semi-submersible centre of gravity is shifted which means that the wave forces combined with it respective level arms are producing similar moments.

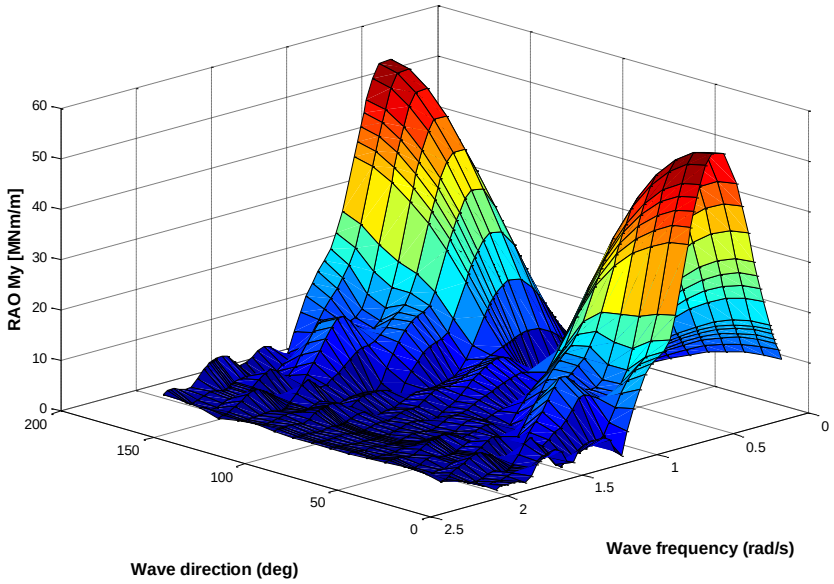

Figure 5.4 RAO Moment in the sway direction for the CSC.

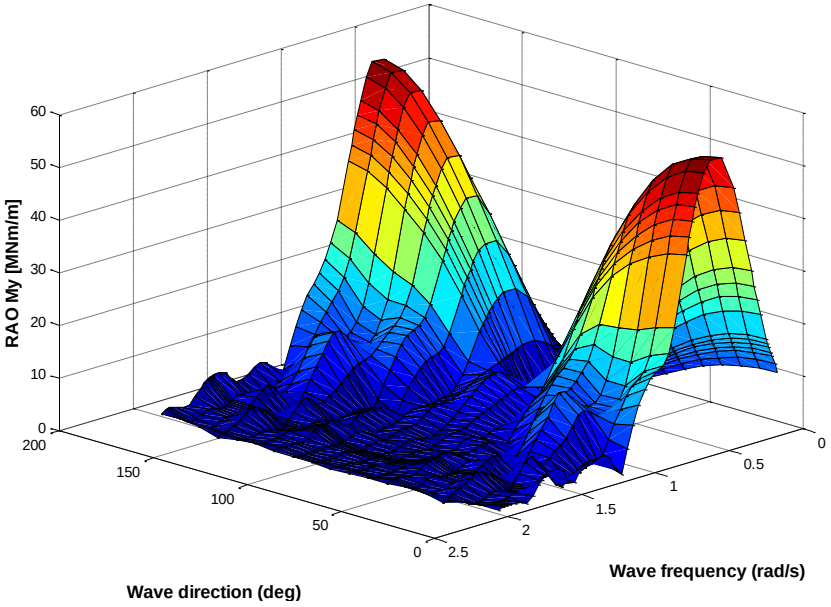

Figure 5.5 RAO Moment in the sway direction for the new CSC.

In these cases both figures show that the moment is dependent of the wave direction but the moment pattern is symmetric respect the wave direction of 90°. The largest RAO moment occur when waves hit the floater exactly between the pontoons at 0° and at 180° where the wave hit directly the pontoon end. The minimum RAO moment occurs for beam waves where the wave hits one pontoon with a difference in angles of 30° and the other pontoon is totally at beam waves.

From these results the new CSC is subjected to the same magnitudes of wave forces. This analysis is important in order to check the influence of the new mass and inertial properties of the CSC, in this case there were not significant variations on the external loads. In the Appendix A Figure A 3 to Figure A 6 shows are the rest of the RAO wave forces curves respects the centre of gravity for both CSC.

5.3. RAO motion

The motion of the platform is always a parameter of interest because is expected that the platform do not realize large amplitude of motion during operation. Figure 5.6 RAO for heave motion.

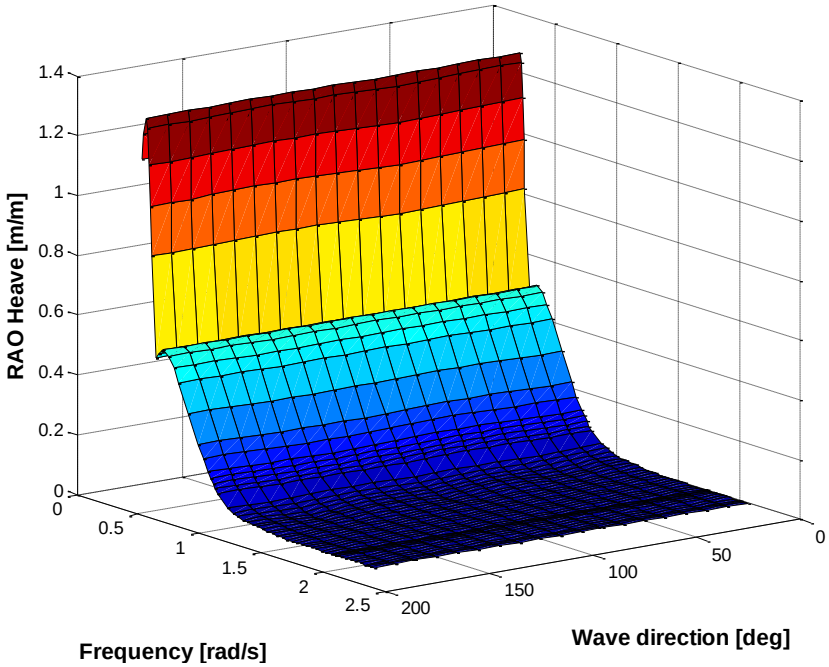

Figure 5.6 RAO heave motion for the new CSC

Figure 5.6 shows that the heave motion is independent from the excitation wave direction as was seen for the RAO "z" force as well. For the original CSC design there is no difference in this RAO. The RAO peak of the motion occurs at 0.215rad/s. From Table 5.1 the heave natural frequency is 0.25 rad/s using equation 5.1 is possible to obtain an approximation of the damping ratio that is $\xi = 0.3$.

$$\omega_{peak} = \omega_0\sqrt{(1-2\xi^2)} \qquad \textbf{(5.1)}$$

This can be considered as large damping ratio (Borg & Collu, 2015) but it is only relevant for values around the natural frequency far from it the contribution from the damping force is negligible on the solution. The damping term is composed by the potential damping and the Morison term which is the responsible for this large damping ratio.

In the case of RAO pitch there are significant differences on the motion amplitudes. The new CSC Figure 5.7 b) shows a reduction of amplitudes, the differences are due to the reduction on the inertia and restoring coefficients respect the original CSC Figure 5.7 a).

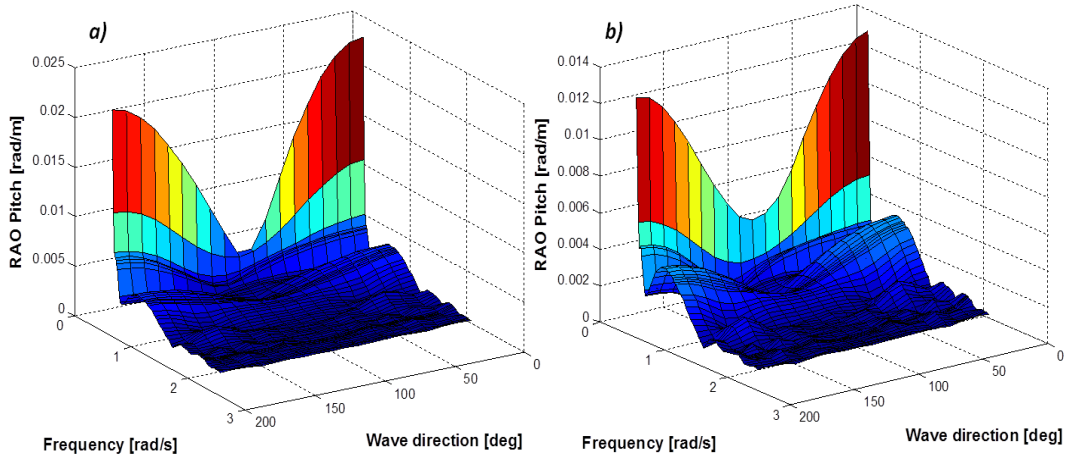

Figure 5.7 RAO pitch motion for the a) original and b) new CSC.

For both cases the maxima amplitude of pitch motion occurs close to the pitch natural frequency (CSC 0.18rad/s and new CSC 0.16rad/s). The pitch motion of the floater inside the wave range spectrum (0.251 – 1.256 rad/s) is inertia dominated as the excitation frequency are larger than it natural frequency. It motion amplitude is below than its static pitch deflection. The RAO heave motion is also inertia dominated as it natural frequency is close on the limit of the wave sea spectrum (0.251 rad/s).

The RAO roll motion exhibits the same behavior and magnitudes than RAO pitch thanks to the symmetry of the floater both the motion are out of phase 90°. When the CSC experiment maxima pitch motion the floater practically has non roll motion. Figure 5.8 shows the RAO roll motion for both CSC. Following the approximation of equation 5.1 the damping ratio for roll and pitch is $\xi = 0.11$.

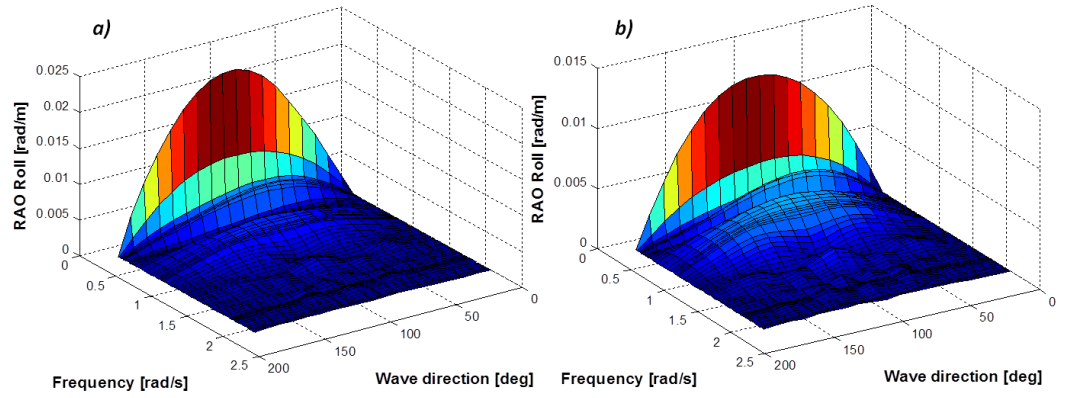

Figure 5.8 RAO roll motion for the a) original and b) new CSC.

The RAO for surge, sway and yaw are presented in the Appendix A from Figure A 7 to Figure A 9 just for information purposes because all of them are inertia dominated motions as does not have restoring term from a mooring system.

From the hydrodynamic motions and loads the new CSC maintains the same hydrodynamic characteristics than it previous design. It is expected that the upper beams

reduces significantly the stresses on the pontoon contributing to the structural strength of the CSC.

5.3.1. Response spectrum for heeling motion

The RAO or transfer functions of motion can be used in combination with a wave spectrum based on JONSWAP model in order to obtain the response spectrum as it was explained in section 2 (eq. 2.12). The wave spectrum parameters as the significant wave height (H_S) and the wave peak period (T_P) are presented in the Appendix B Table B 3. These were obtained for design extreme condition having a 50 year recurrence time period and are grouped in pairs as design load case. This extreme sea state is appropriate for an ultimate design where can be checked the structure strength or the maximum motion amplitudes.

Each load case (27) represents a extreme sea wave spectrum and shall be combined with each transfer function in order to obtain the response function. In this case the combination of the RAO pitch motion for 19 wave direction with all the 27 sea state shall results in 513 response curves. In order to simplify the analysis it's possible to characterize each curve through the standard deviation of the pitch response ($\sqrt{m_{0Pitch}}$), according equation 5.2.

$$STD = \sqrt{m_{0Pitch}} = \sqrt{\int \boldsymbol{R}_j(\omega_e) \cdot d\omega_e} \tag{5.2}$$

The standard deviation (STD) is proportional to the significant amplitude from a frequency spectrum and it is the mean value of the highest one-third part of the amplitudes. In this case Figure 5.9 presents the STD for pitch.

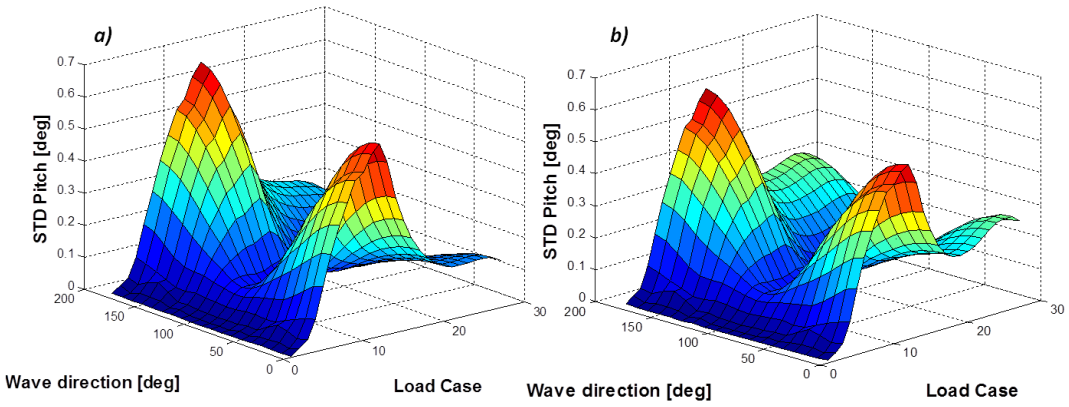

Figure 5.9 STD Pitch for a) CSC new and b) CSC under ULS

The pitch results present that the excitation waves produces as maxima heeling angle values below 1deg for both CSC for severe sea state condition. These results can be considered as acceptable as the total heeling motion is the combination of wave and wind loads. The wind loads are the responsible for the major amplitude of motion as it produces larger moment on the floater as was observed in the static analysis.

This pitch standard deviation is a measure of the dispersion of the motion around the equilibrium position that for this study occurs when the whole FOWT has 0° heeling, the turbine is fully vertically.

5.4. RAO cross section load

Through DNV HydroD is possible to obtain the cross sectional hydrodynamic loads on the pontoons from the frequency domain analysis using the panel method. This dynamic loads are composed by an inertial term (I), a restoring force (R) (just for heave, pitch and roll), the excitation wave force (E) and a hydrodynamics (D) (added mass and damping) term as its shows in equation 5.3.

$$q_j^{RAO}(x_b) = I_{j(\ddot{x}_j,m)} + R_{j(c_{i,j},x_j)} + E_{j,waves} + D_{j(\ddot{x}_j,\dot{x}_j,m_a,b_{i,j})} \quad \textbf{(5.3)}$$

These loads are given for a referential point (x_b) that contains a local coordinate system that is parallel to the global one showed in Figure 4.1.

These cross sectional loads are integrated across a specified cross section following the equation 5.4 for the shear and axial forces $(j = 1,2,3)$ and 5.5 for the torsion and bending moment $(j = 4,5,6)$.

$$Q_j(x) = \int_{stern}^{x} q_j(x_b) \cdot dx_b \quad \textbf{(5.4)}$$

$$M_j(x) = \int_{stern}^{x} q_j(x_b) \cdot \overline{Dis}(x_b) \cdot dx_b \quad \textbf{(5.5)}$$

The variable $\overline{Dis}(x_b)$ represents the moment level arm and is a distance between the cross section reference point and the center of gravity of the floater. These sectional loads allow to calculate the local stress on the pontoons by using the Euler Bernoulli beam theory.

Considering performing a further stress analysis using Euler-Bernoulli beam theory the sectional loads are obtained for the CSC at the pontoon cross section centre. Instead for the new CSC the reference point is located at the cross sectional centre of gravity of the upper beam and the pontoon as it was show in Figure 2.6. The strength analysis is going to be performed on the pontoon that is orientated along the "x" axis on Figure 5.1 for both CSC's units. The loads and stresses are suppose to be the same for the others pontoons du tot symmetry reason taking into account the equivalent incidence wave direction.

Figure 5.10 and Figure 5.11 a) presents the RAO Fx force in the "x" direction at a cross section 1 that is at 4m from the floater centre, for the original and new CSC respectively.

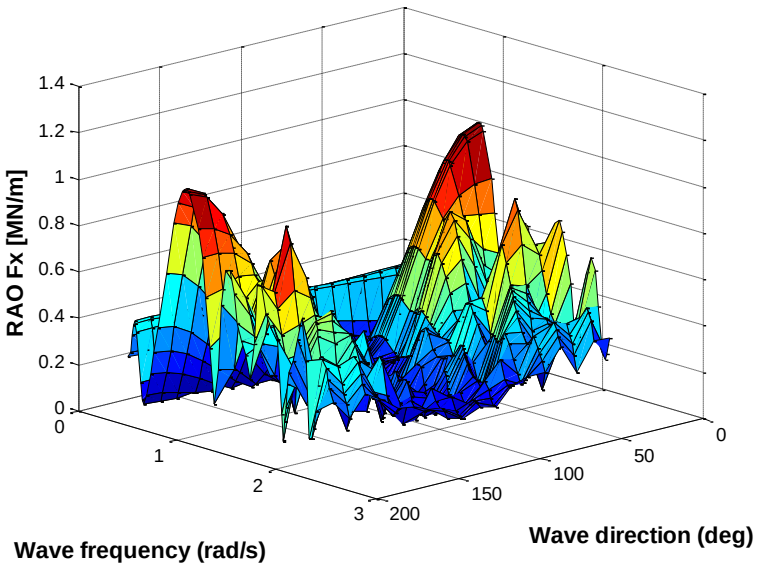

Figure 5.10 RAO "x" force on section 1 at 4m from the centre of the CSC.

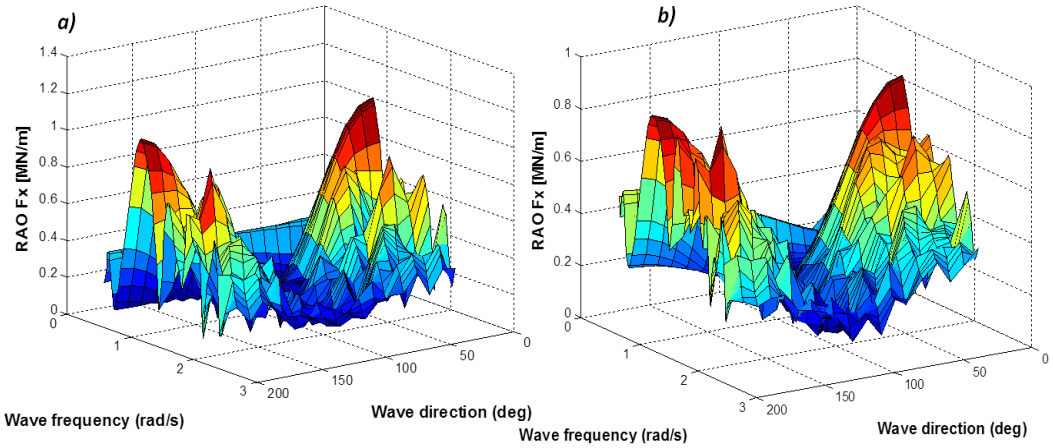

Figure 5.11 RAO "x" force on new CSC at a) section 1 and b) section 5 at 37m from the unit centre.

The force magnitude and behavior respect the wave direction and frequencies are maintained for both units. The RAO “x” force surface tend to decrease along the pontoon as can be seen on Figure 5.11 a) and b). At the peak value at 0° there is a reduction of 18% between the RAO Fx forces. This reduction is also presented along the pontoon in the original CSC.

For the cross sectional RAO “z” moment the magnitudes and behavior are the same between both CSC designs as can be observed in Figure 5.12 a) and b). The variation in longitudinal mass produced by the upper beam on the new CSC do not generates a significant variance in the loads, taking into consideration that the inertia term on equation 5.3 depends of the longitudinal mass distribution.

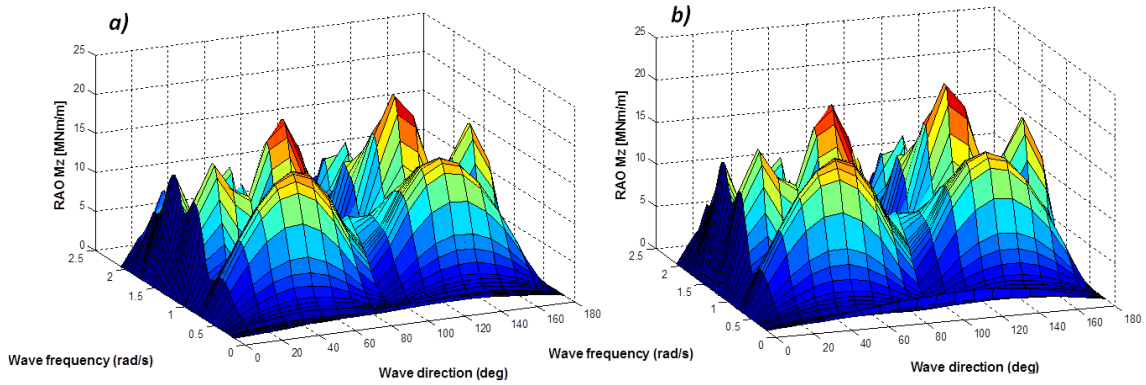

Figure 5.12 RAO "z" moment at section 1 on a) CSC and b) new CSC.

For the selected pontoon the wave direction of 0° and 180° does not produce any "z" moment and the maximum load occur at 60° and 120°, for the first angle is when the waves hits the other pontoon at its end. Meanwhile for 120° is when the wave hit exactly in between the pontoons. The RAO Mz decreases along the pontoon length, as occurred for the RAO Fx for both CSC.

However, for the RAO "y" moment the magnitudes are different. In Figure 5.13 a) and b) is possible to observe that the moment for the new CSC is lower. The mainly reason for this is because the level arm $\left(\overline{Dis}(x_b)\right)$ for the new CSC is smaller than the original floater design due to the reference point location is at -18.41m (brace-pontoon neutral axis) instead -27m.

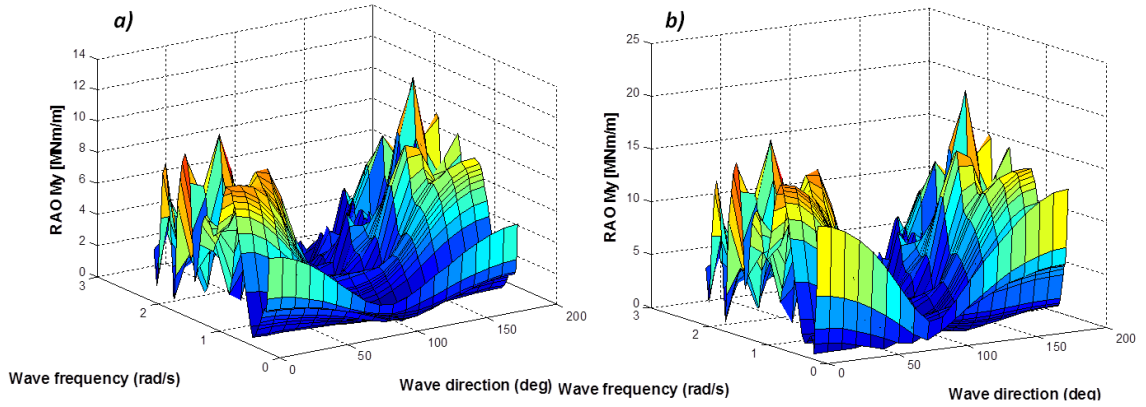

Figure 5.13 RAO "y" moment at section 1 on a) new CSC and b) CSC.

In the case of the RAO My, the moment magnitude decrease along the pontoon for both CSC as it s showed in Figure 5.14 for the 120° wave direction. Instead for the RAO Mz (Figure 5.15) is possible to notice that the force decrease is more significantly for the same wave direction. This load magnitude behavior along the pontoons cross sections occurs for all wave directions.

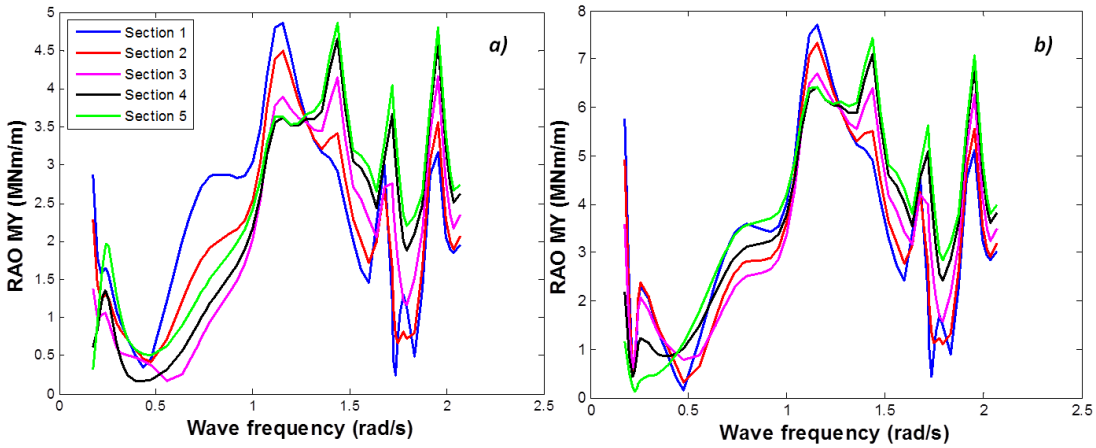

Figure 5.14 RAO My for 60° of wave incidence for a) new CSC and b) CSC

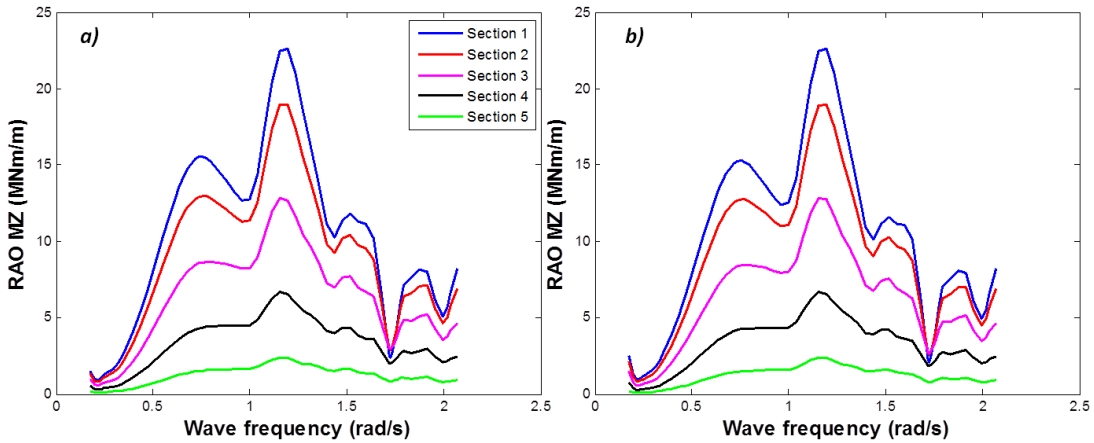

Figure 5.15 RAO Mz for 120° of wave incidence for a) new CSC and b) CSC

These integrated loads around the pontoons are going to be employed in the stress estimation following the Euler-Bernoulli beam theory. Previous studies from (Luan, Gao, & Moan, 2015) showed that axial stresses on the pontoon were until 80% larger than shear stresses, thus this analysis is going to be focused just on normal or axial stresses. Because this the hydrodynamic loads Fy, Fz and Mx are not relevant for further projects stages. In the Appendix A Figure A 10 to Figure A 15 are presented the Fx, Mz and My per cross section for both CSC units.

CHAPTER 6 STRESS ANALYSIS

After obtaining the sectional hydrodynamics loads, Chapter 6 shows the estimated axial stress at different cross section along the pontoon, based on Euler-Bernoulli beam theory for both CSC. These results are compared against the stresses obtained through Finite Element Method using beams and shell elements. Finally, the solutions are analyzed quantifying the stress reduction on the pontoon between the base and new CSC design.

6.1. Euler-Bernoulli stress

In order to apply the beam theory stress equation (eq. 2.16) the cross sectional loads obtained in the last chapter are employed.

From section 2.4 and Figure 2.6 the RAO axial stresses are calculated for points $P2, P4, P6\ and\ P8$ for the CSC and these are going to be compared respectively with $P2, P3, P4\ and\ P5$ from the new CSC. Figure 6.1 presents the axial stress for both CSC at cross section 1.

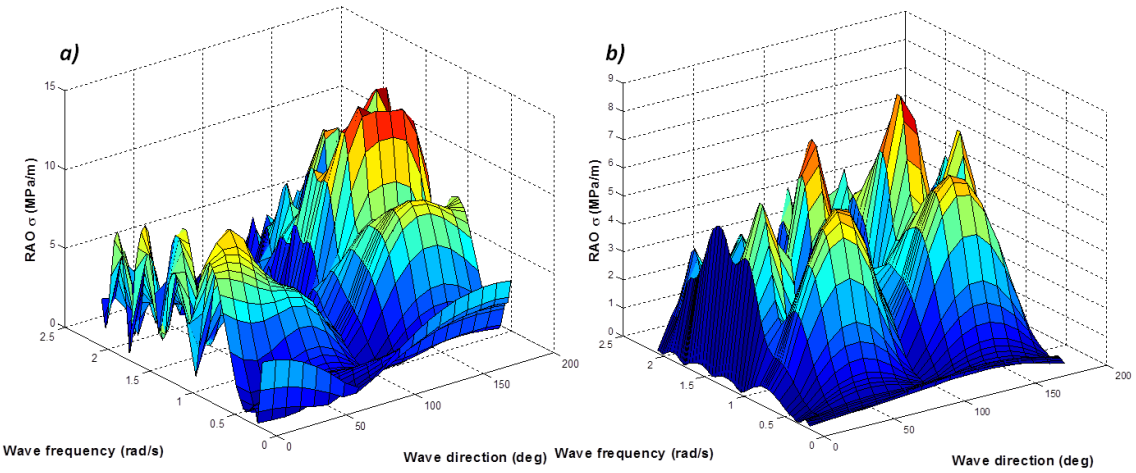

Figure 6.1 RAO axial stress at point P2 from cross section 1 for a) CSC and b) new CSC

Cross section 1 is located at 4m from the CSC center for both semi-submersibles. Immediately, is possible to observe that the new CSC Figure 6.1 b) has it largest RAO stress 34% lower than the largest RAO stress for the original CSC. Additionally, the upper connection produces on the pontoon a structural behavior symmetric respect the wave incidence about 90°. Instead for the CSC there is a clear higher stresses from the wave direction larger than 90°. This is because the wave hits directly the pontoon between 90° and 180°, for wave incidence lower than 90° the wave are not directly affecting it.

A more clear way to observe this is considering the wave loads involved. The total axial stress is composed by an axial force F_x, and two moments M_y and M_z. Due to the new CSC has a larger inertia respect the "y" axis of the cross section the axial stress exerted by M_y is going to be reduced significantly. As was showed in Chapter 5 the wave loads are similar between both units and therefore for the new CSC the total axial stress is going to follow the stress exerted by M_z and F_x mainly.

There are not considerable differences between RAO stresses between the pontoon points of the same cross section. This can be checked in the Appendix A from Figure A 16 until Figure A 21 for both CSC's.

For the CSC the RAO axial stress shows a decrease rate along the pontoon but for the new CSC the RAO stress decrease at a larger rate. Figure 6.2 presents the axial stress at section 5 that is at 37.5m from the FOWT centre.

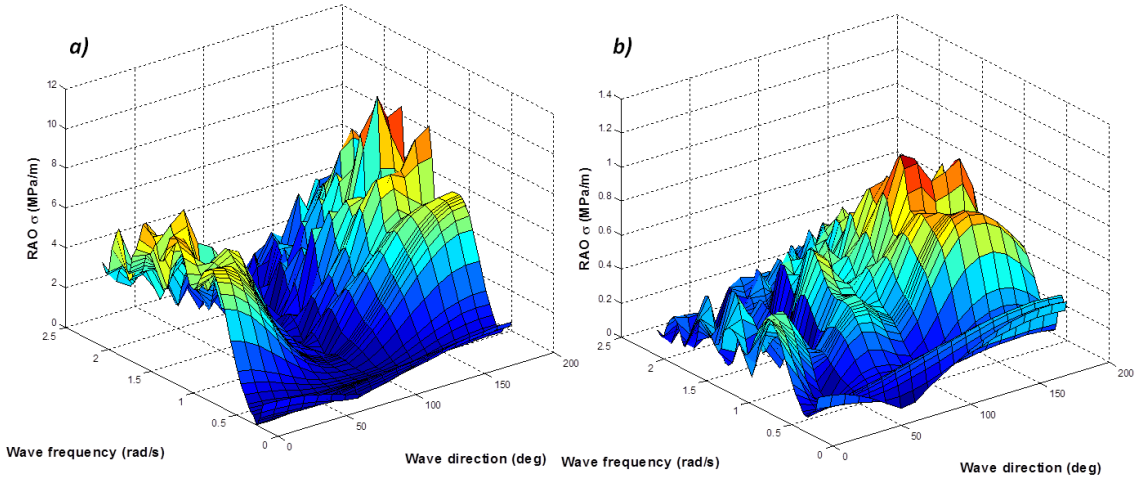

Figure 6.2 RAO axial stress at point P2 from cross section 5 for a) CSC and b) new CSC

For the new CSC the stress reduction along the pontoon is significantly if it is compared with the original design. This is because the new CSC is following the axial stress of M_z that decrease significantly along the pontoon cross section as can be seen in Figure 5.15 and in the Appendix A Figure A 12. In the original CSC M_y is the dominant force that maintains large stresses along the pontoon. This result remark the importance of the structural connection implementation in order to increase the structural strength of the FOWT by reducing the effect of the most significant stress on the CSC.

Figure 6.3 shows the stress decomposition at section 1 for both CSC's. As it was mentioned the wave loads are the same and the axial stress done by each load should be the same for the two units. However, due to the large bending inertia ($I_y = 528.9m^4$) of the new upper brace-pontoon cross section, the stress by My is reduced as it is shows in Figure 6.3 b) if its compared with the original CSC ($I_y = 5.85m^4$).

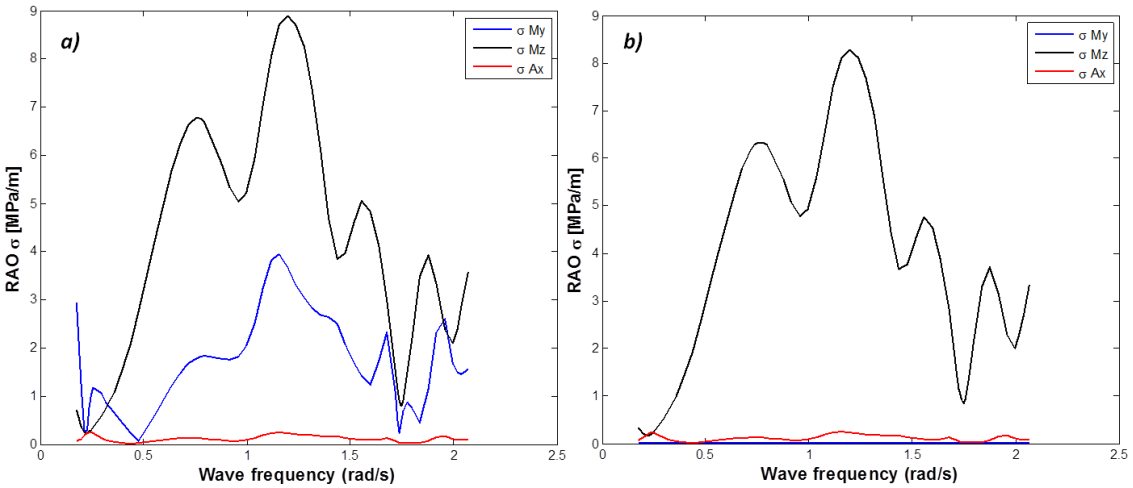

Figure 6.3 Stress decomposition for P2at section 1, wave direction 60° for a) CSC and b) new CSC

It is possible to compare amplitudes of the RAO axial stresses between both CSC designs but this are transfer functions and just indicates a relative behavior between an input excitation and the response. To best way to quantify the dynamic stress reduction between the old and new CSC design is to use the design wave spectra from Table B 3 in the Appendix B and obtain the standard deviation of the dynamic stresses per each FOWT.

Following the same calculus procedure explained in section 5.3.1 the ultimate dynamic stress is obtained for both CSC just considering the stresses on the cross section 1 close to the central column, at P2. Figure 6.4 and Figure 6.5 presents the standard deviation of the axial stress.

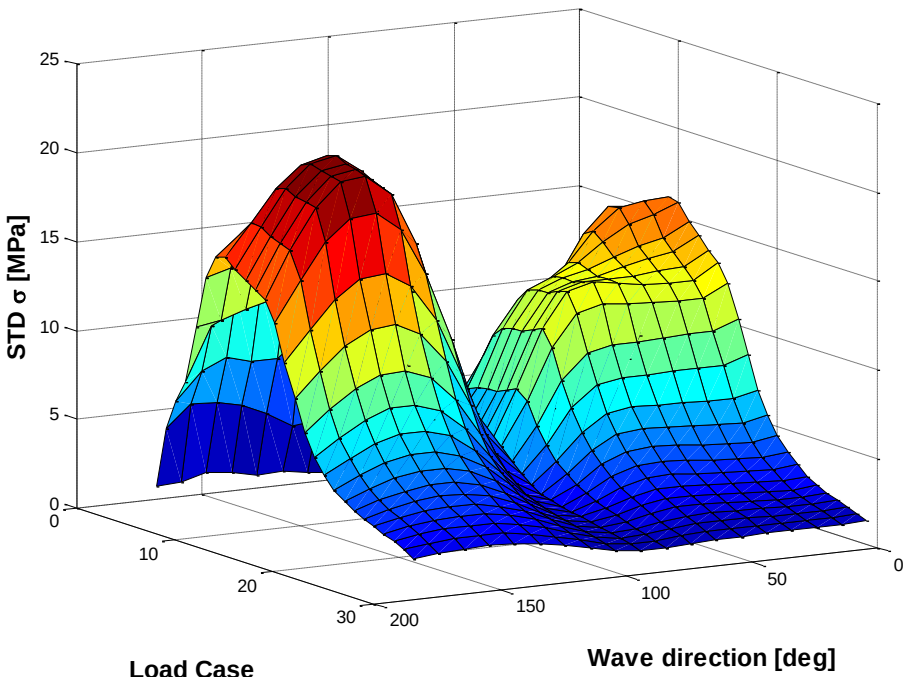

Figure 6.4 STD of axial stress at section 1, P2 for CSC as a function of the wave direction and design load case

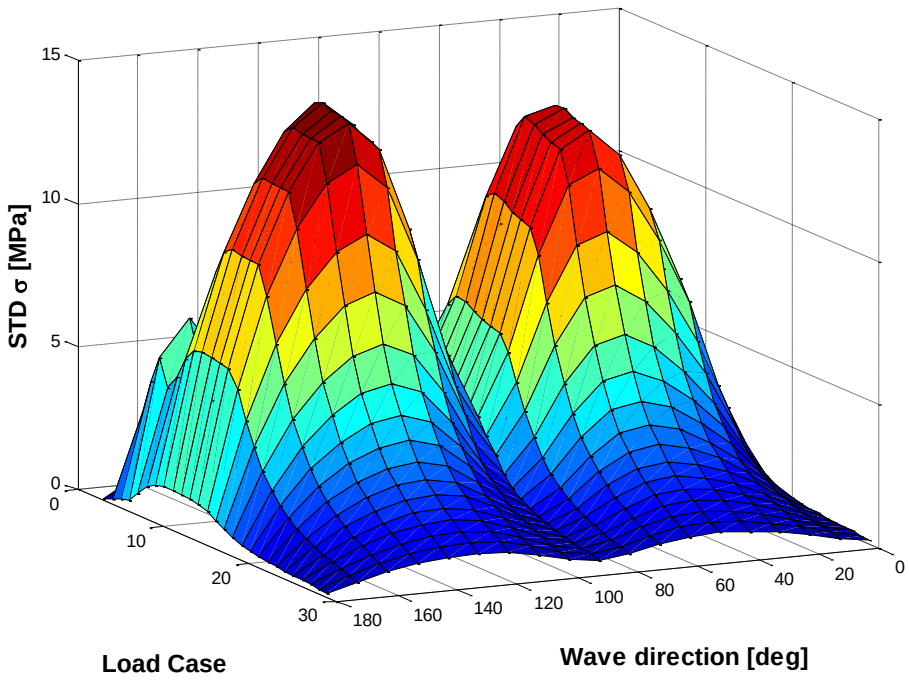

Figure 6.5 STD of axial stress at section 1, P2 for new CSC as a function of the wave direction and design load case

The load case that produce the largest dynamic load on the original CSC occur at 140° of wave incidence and for the new CSC occurs at 130°. From Figure 6.5 is possible to notice that the FOWT has a stress response almost symmetric respect 90° of wave incidence because the total stress follows Mz. For the original CSC design this is not observed as the My stress is dominating.

Table 6.1 presents the reduction of the dynamic axial stress on the CSC pontoon for the most critical sea states according the Euler-Bernoulli beam theory. It is observed that there is a significant reduction around 30% for the ultimate dynamic stresses. This reduction can be even more important for a fatigue analysis where these dynamic loads amplitudes are accounted for the stress range and are responsible of structural failure.

Table 6.1 Dynamic stress reduction respect the original CSC based on E-B for P2

TP	130° [%]	140° [%]
8	28	35
9	27	34
10	27	34
11	26	34
12	26	33
13	26	33

The next stage of the research is check that the stresses obtained by beam theory are correct using Finite Element Method. In the case of the original design of the CSC is expected that the numeric results would be close to the analytically estimated. However, in the case of the new CSC the behavior of the pontoon together with the upper brace may not follow the assumption behind beam theory leading to a different stress prediction.

The FEM analysis requires more computational resource and time to be obtained. For this reason the only wave direction to be considered are 130° and 140°.

Due to this study is only a numeric the finite element method is going to be computed using two types of element, beams and shells in order to be able to compare that the solutions are converging into a valid solution. The first step into the FEM analysis is to check that the numeric set-up is well defined through a comparison procedure.

6.2. Finite Element Method check

For the comparison procedure, the incidence wave of 0° is going to be employed because represents a simplified load case where there is not RAO Mz produced on the floater. First, the beam elements results are going to be analyzed and then the results based on shell elements.

The FEM analysis is going to be carried out in DNV Sestra, which allows taking the hydrodynamic loads from HydroD, transferring it to the structure and obtain finally the internal loads.

6.2.1. FEM beam check

The FEM study based on beam elements represent the simple numeric approach to observe the stresses on the pontoon considering deformations and in the case of the new CSC it is possible to observe the effect of the wave on the pontoon separately from the upper brace.

The FOWT model is converted to a beam model where each section of the unit is transformed into a segment with two nodes and mechanicals properties related to the cross section inertia, elasticity modulus of the material and the length of the segment as can be seen in Figure 6.6. For the pontoon the mass of the cross section is representative of the steel mass of the pontoon plus the mass of the water ballast, this was also applied for the respective outer column section near the pontoon. The turbine tower FEM model is not relevant for the stress analysis therefore it is not going to be discretized.

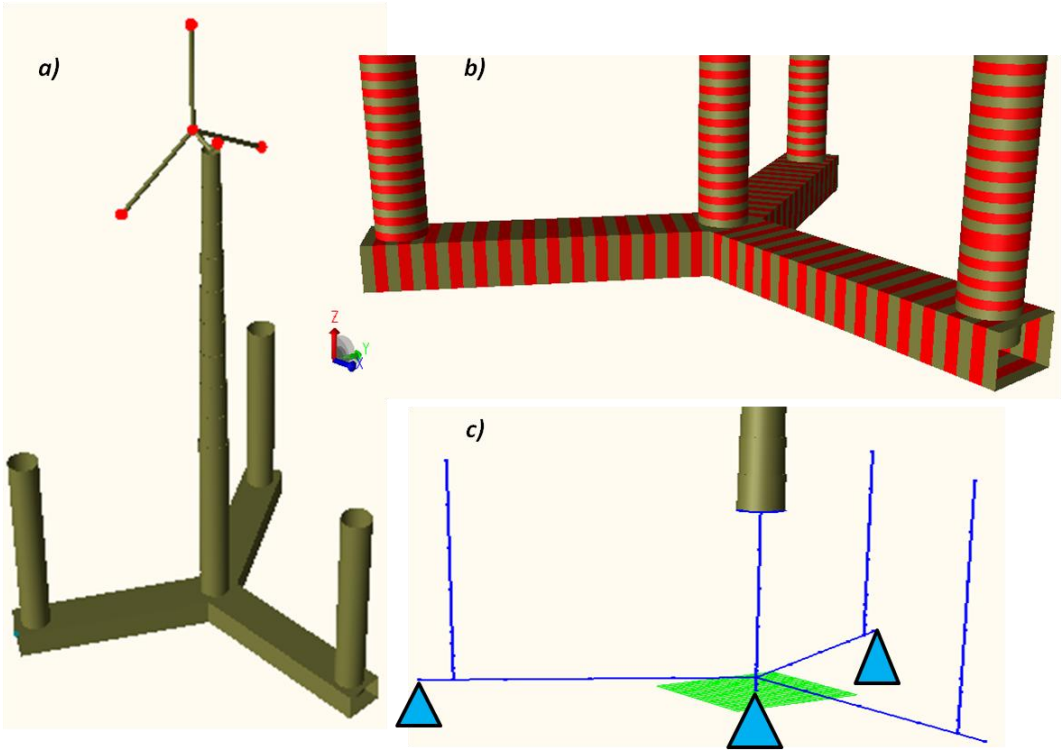

Figure 6.6 a) Beam model for the CSC design. b) The segment lengths on the pontoons are 1,5m and for the columns is 1m. c) Simplified beam structure of the CSC floater with the location of the support.

As was mentioned in Chapter 2 the FEM study is based on the solution of a set of differential equations that after the discretization becomes into a linear system of equations. In order to solve the system it is required to impose some boundary conditions.

The boundary conditions are the support located on the CSC as can be seen on Figure 6.6 c). This supports all together shall provide constrain to the floater to avoid translation or rotation due to dynamic loads, it main purpose is to fulfill the mathematical condition and therefore the support should not transmit reaction forces on the model that may be comparable with the external forces. It is suppose that the hydrodynamic loads shall be balanced with the hydrostatic forces like the mass of the structure.

The FEM-beam model should be good enough to represent the structural behaviors on the pontoon but not on other parts like the central column base where the pontoons are connected because it has a more complex interaction between the pontoons walls, for the current FEM-beam model there is just a node that connect all the pontoons and central column as can be observed in Figure 6.6.

The first parameter to compare is the sectional loads. Figure 6.7 presents that the internal loads from the FEM-beam models are the same respect the hydrodynamic loads integrated for a cross section from the HydroD module. This indicates that the external and internal loads are balanced.

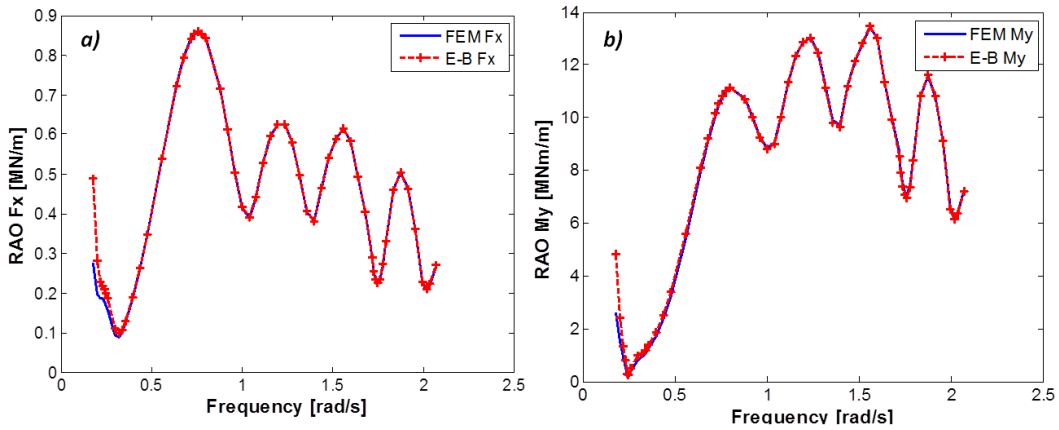

Figure 6.7 a) RAO Fx and b) RAO My obtained from HydroD (E-B) and Sestra (FEM) for the CSC for 0° wave direction at section 4.

Another parameter to check is the reaction force on the supports. Figure shows that the reaction forces on the vertical direction "z" are small and therefore do not influence the force balance between the waves and the CSC mass.

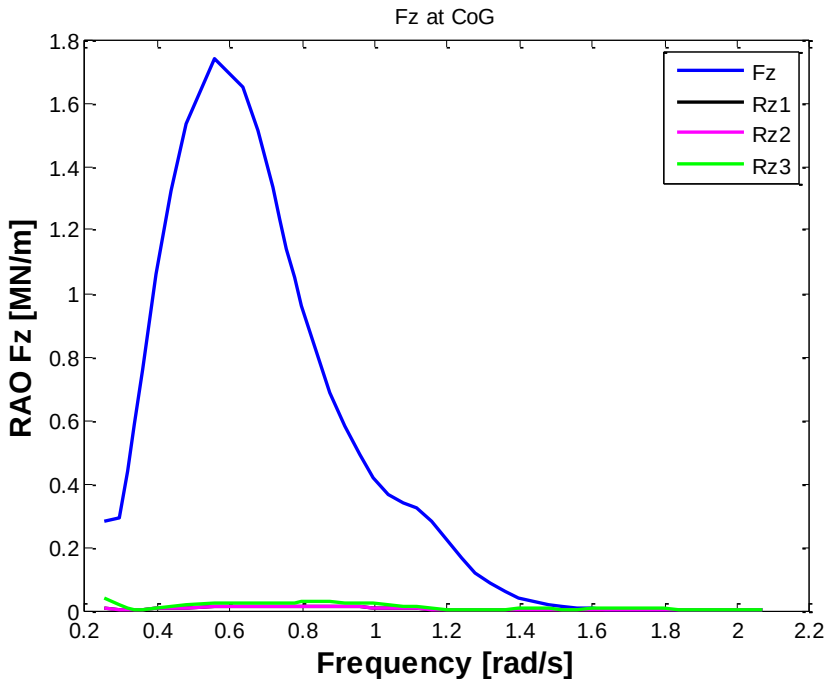

Figure 6.8 Force comparison between the total RAO Fz on the center of gravity and the vertical component of the support reactions.

Figure 6.9 show that also the "x" component of the reaction forces does not influence the internal loads on the floater. The relative difference between the forces is below 2% as its presented on the Figure 6.9. This indicates that there is not numeric influence on the solution.

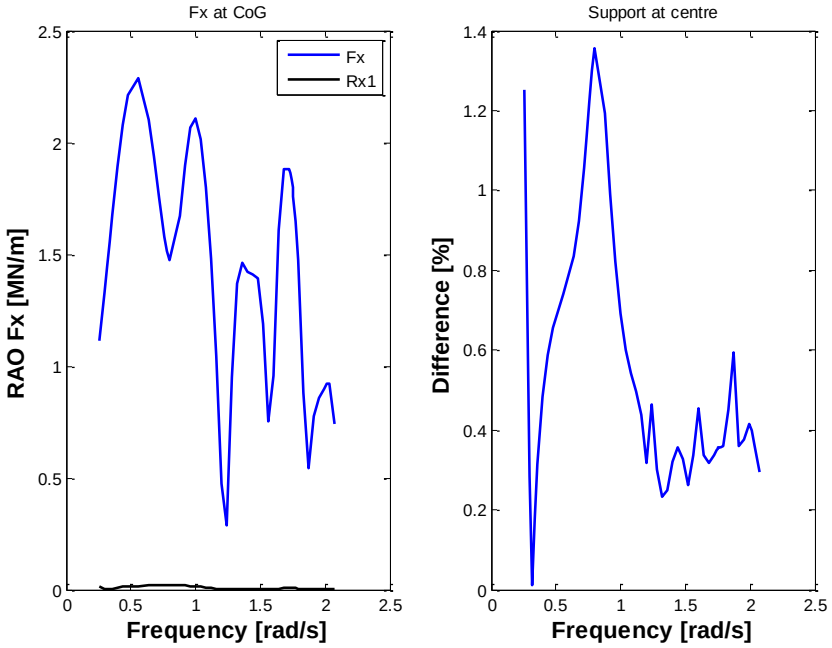

Figure 6.9 Force comparison in "x" direction and relative difference between the FOWT force and the reaction.

Due that the reaction forces and sectional forces are in agreement it is possible to analyze the cross sectional stress on the pontoon. Figure 6.10 present the stress comparison between the beam theory results and the FEM with beam element, for the equivalent points P2-P2 and P4-P3 at the pontoon semi-submersible designs, check Figure 2.6.

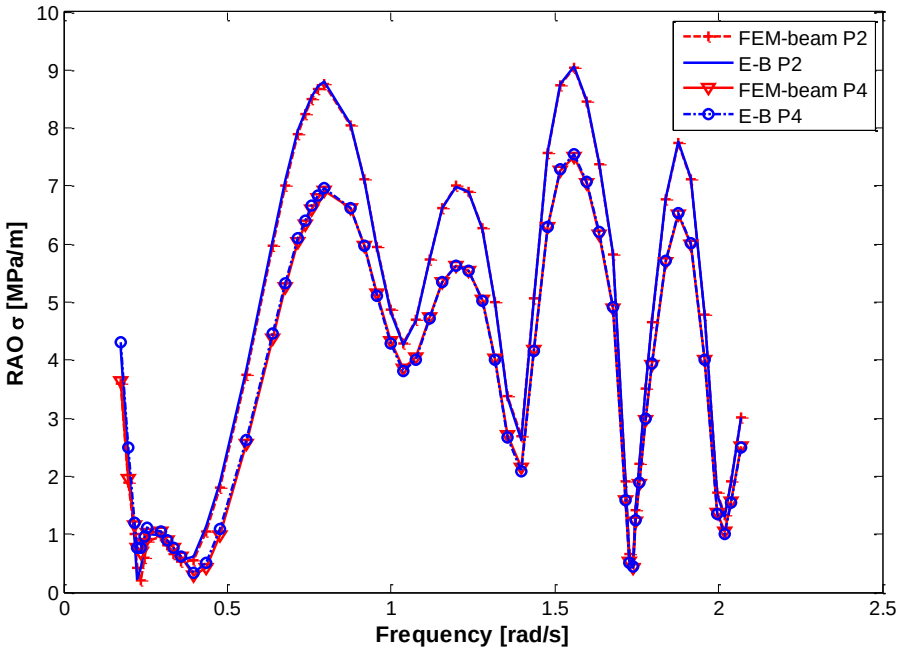

Figure 6.10 RAO axial stress from E-B and FEM-beam at section 1 for the CSC design

The numeric results are in agreement with the analytical solution from beam theory. This means also that the stress is just composed by an axial force F_x and a moment M_y as expected. In the Appendix A Figure A 22 are presented the RAO axial stresses per section,

where is possible to check the agreement between the numeric and the analytical results along the pontoon.

For the CSC new design the same procedure is going to be follow. Figure 6.11 shows that the moment and axial force at the entire cross section 4 of the FEM-beam model is the same that beam theory. For this the moment and forces from the FEM simulation were extracted from the pontoon and brace, then it is computed apart in order to translate them into the neutral axis according equation 6.1 and be able to compare with the beam theory solutions.

$$M_y^{Neutral\ axis} = M_y^{Pontoon} + r_{P\ NA} \times F_x^{Pontoon} + M_y^{Brace} + r_{B\ NA} \times F_x^{Brace} \quad \textbf{(6.1)}$$

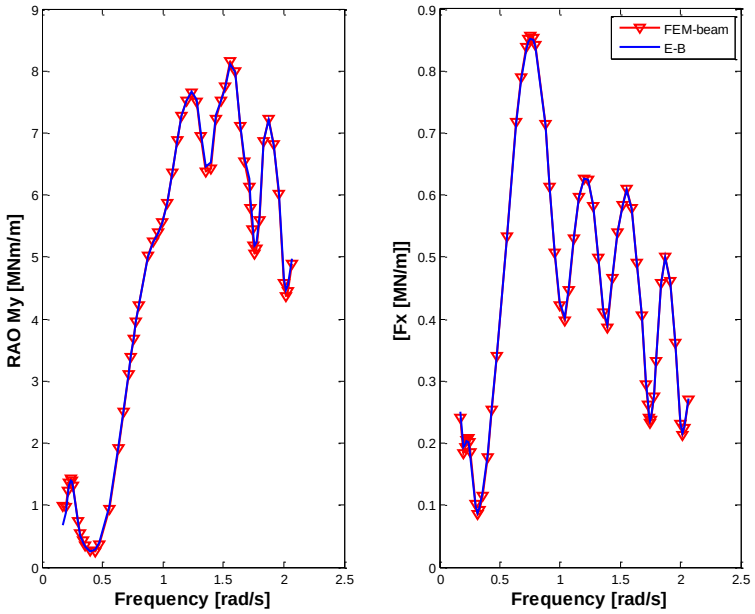

Figure 6.11 Cross section My and Fx at section 4 for 0° at new CSC

The support reaction difference presented in Figure 6.12 shows that there is not numeric alteration in the solution; the difference for the whole frequency range is below 1% also for F_z (Figure A 25 in the Appendix A).

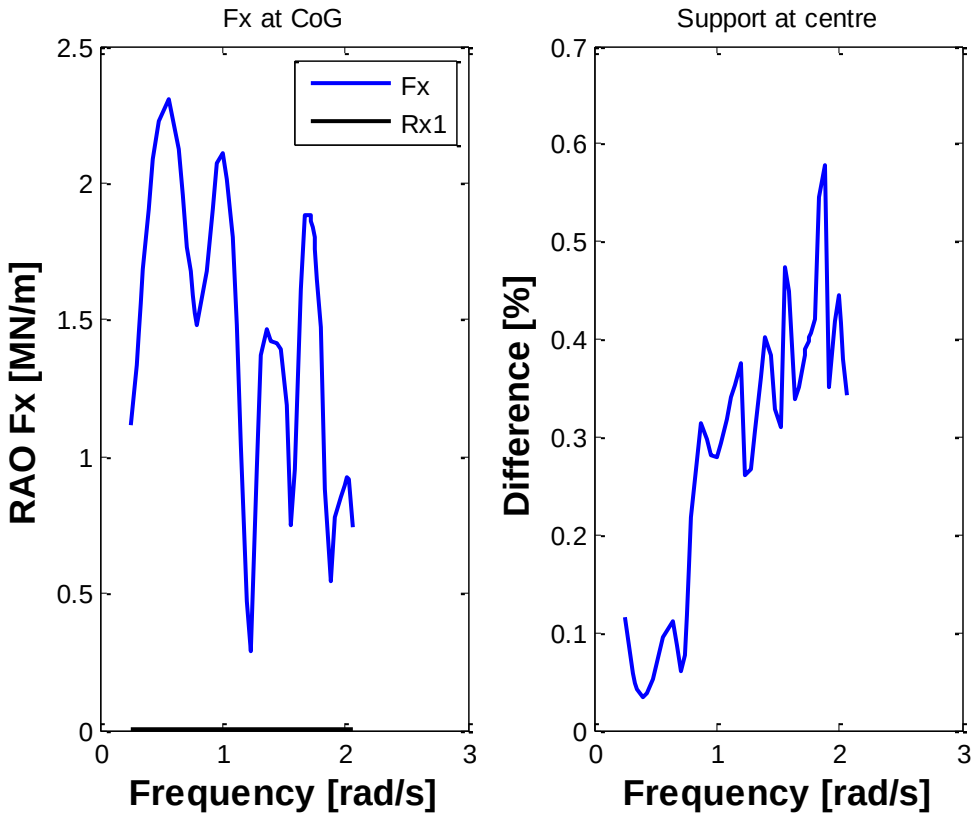

Figure 6.12 Difference between the magnitude of the reaction force in x direction respect the external Fx load on the new CSC

Figure 6.13 shows the RAO axial stress at section 4. It shows that the FEM results with beam elements are different from the solution of beam theory. Appendix A Figure A 24 shows that the solutions are different for all sections.

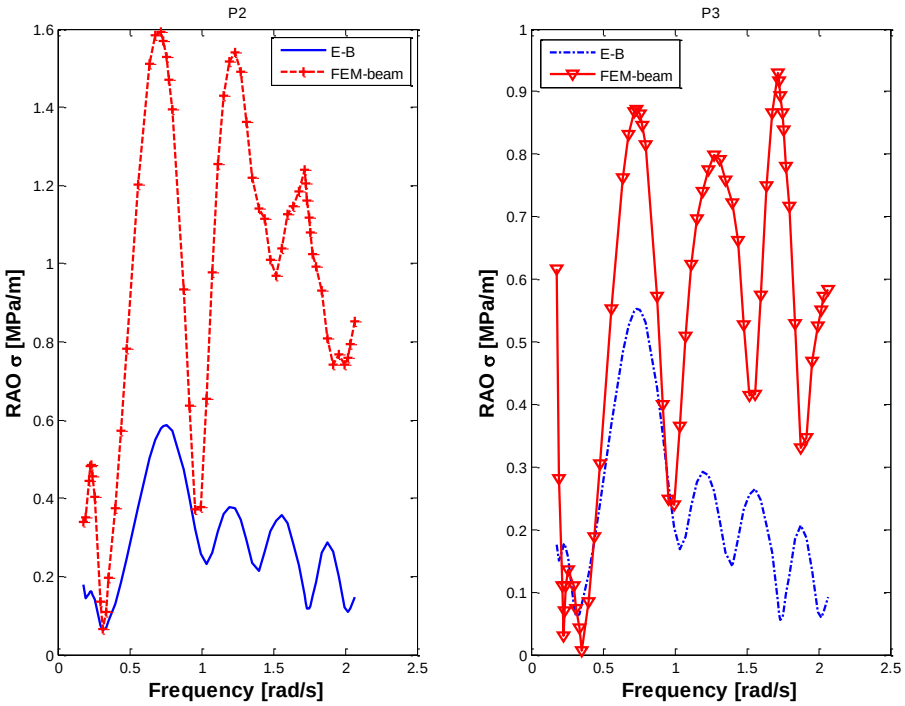

Figure 6.13 RAO axial stress from E-B and FEM-beam at section 4 for the new CSC

The RAO axial stress from beam theory solution is just taking the effect of the axial loads as the moment respect "y" is significantly reduced.

The stresses distribution on the pontoon is different as it is presented in Figure 6.14 between the analytic and numeric approach. The stress results are presented in a decomposed manner in order to remark that the My from FEM produces a more significant load than the estimated by beam theory. The axial stress on the pontoon can be considered in agreement between Fem-beam and the analytic estimation.

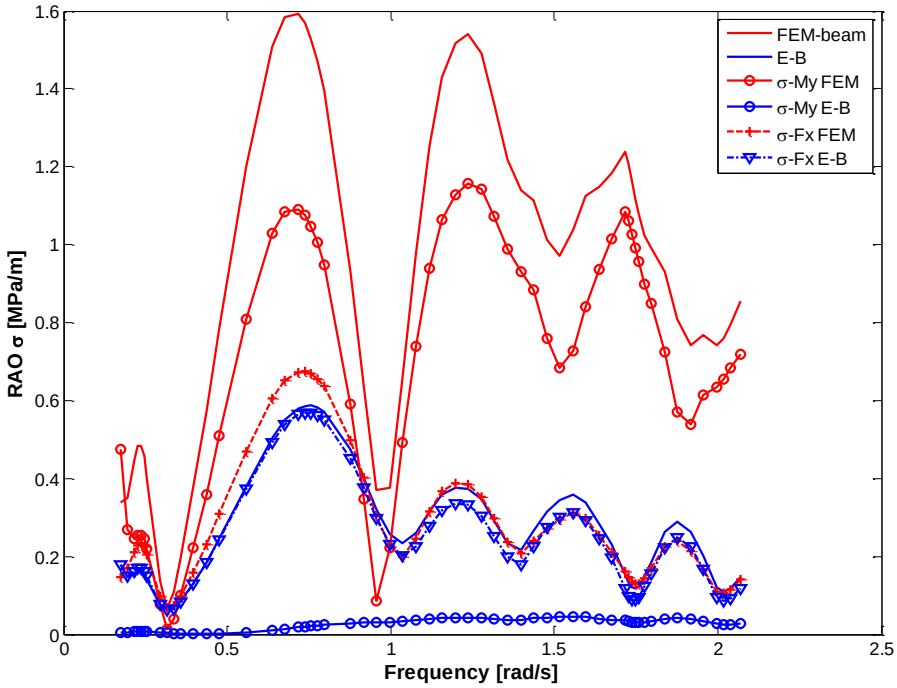

Figure 6.14 RAO axial stress contribution from Fx and My to the total stress at section 4 for P2 at the pontoon of the new CSC

It is important remark that the solutions presented in Figure 6.14 are amplitude of a complex number and there are phase angles that have to be taken into account where the stresses are added up into the total axial stress.

The validation study of the beam elements showed that the numerical set up followed into the DNV Sestra to obtain the RAO axial stress are satisfactory and do not introduce numerical deviation. The CSC design represents a simple case and allows checking that numerical solution is acceptable. The FEM model of the CSC pontoon follows the beam theory assumptions. Instead for the new CSC the FEM solution indicates that the pontoon and upper beam have a different stress distribution than the estimated with E-B analytical solution. The stress from FEM on the new CSC pontoon is larger than expected but still offering a reduction respect the original CSC design.

6.2.2. FEM shell check

The following section reveals the stress results using shell elements. This elements offer a more detailed model of the original structure. However, the mesh generation is important on order to achieve good solutions and therefore the FEM-shell model requires more numerical treatment than FEM-beam model.

Figure 6.15 show the FEM-shell model for the CSC, on it is possible to observe the structured mesh on the pontoon. This is important in order to obtain the correct axial stress at the element or nodes. The supports for this model are located below the central column.

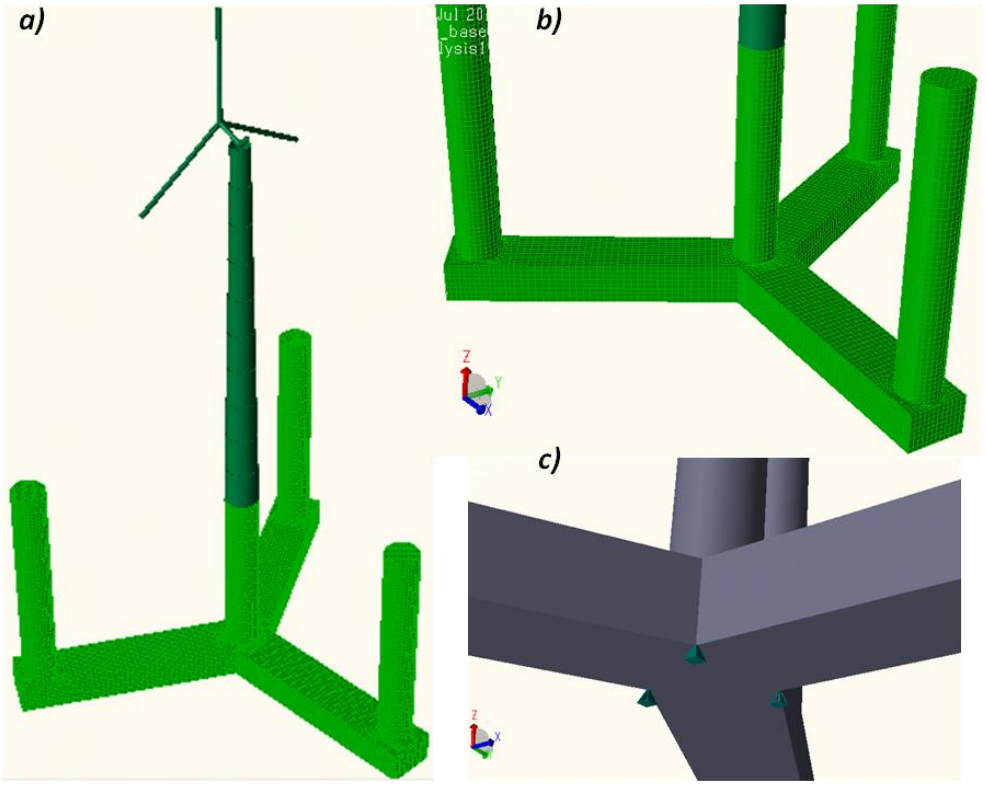

Figure 6.15 a) FEM shell model of the CSC. b) Close up at the structured mesh on the pontoon. c) Support location

Again the 0° wave incidence is employed and the reaction forces presented in Figure 6.16 are considerable large. The differences can reach 16% that means that the structural results for section 1and 2 can be influenced.

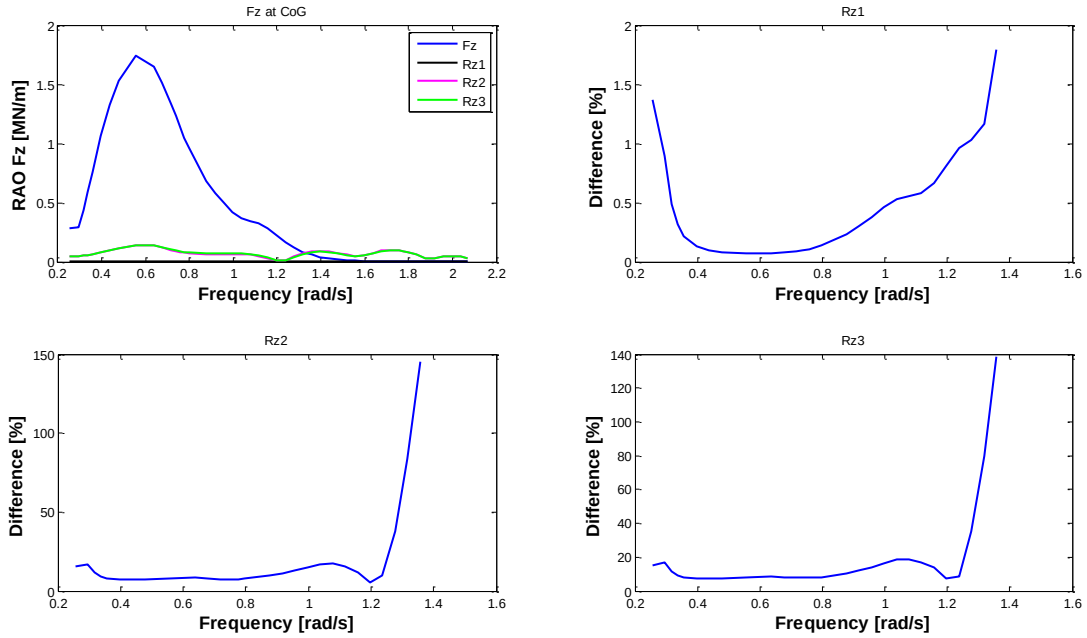

Figure 6.16 Support reaction forces and relative differences respect the Fz of the FOWT for the FEM shell CSC

A refinement process of the mesh on the pontoons was done in order to observe if the solution is mesh-sensitive. But only the sections 1 and 2 results are influenced as it is showed in Figure 6.17 where the solution tend to diverge, the other section present the same solution as the beam theory showing that the mesh do not influence the results.

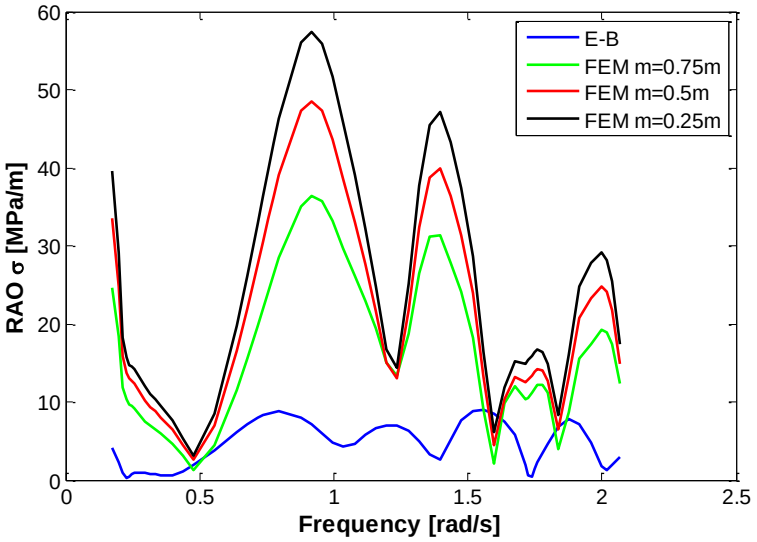

Figure 6.17 RAO axial stress for different mesh size at section 1 of the CSC

Figure 6.18 shows the axial stress for the CSC for different cross sections along the pontoon. The FEM solution shows that close to the central and outer column the RAO axial stress is not following beam theory. This can be related with additional structural effects generated by the columns. For sections 3 and 4 the FEM solution shows that the pontoon behaves structurally like a beam.

From the stress results of the CSC through FEM-shell is possible to state that the cross sectional forces (Fx, My) at least for section 4 and 3 are the same between the HydroD estimation (for E-B calcualtions) and the Sestra module.

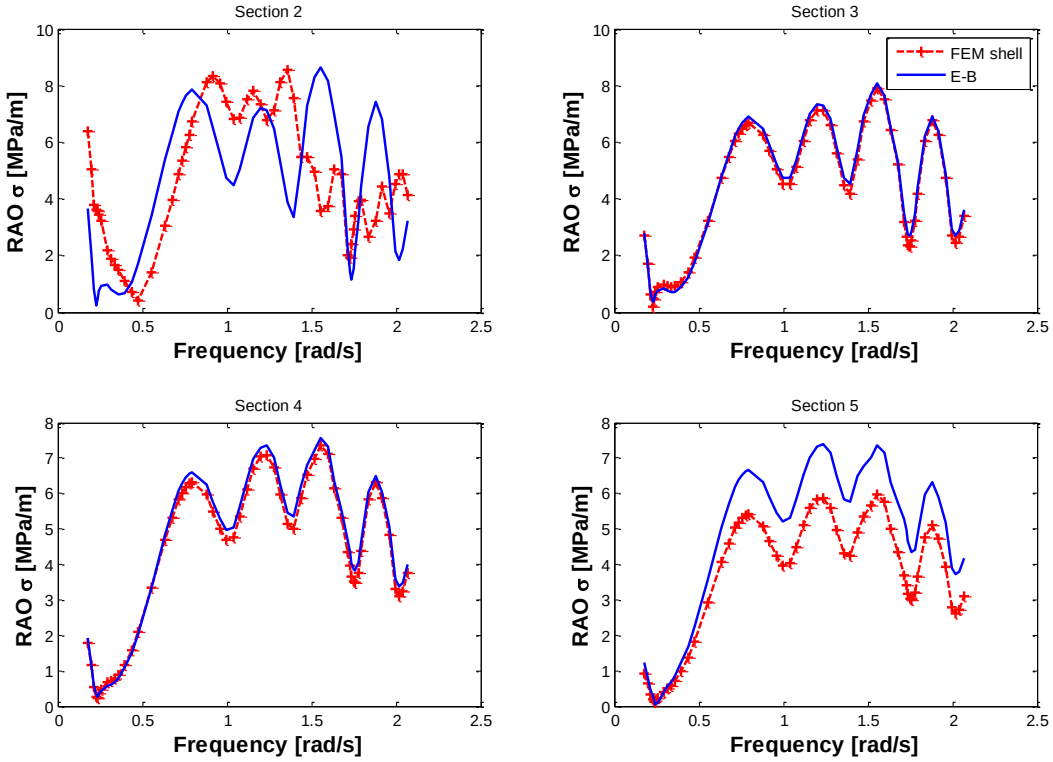

Figure 6.18 RAO axial stress from FEM shell for the CSC design at P2

The results of FEM simulation with shell elements can offer acceptable results at section 3 and 4 where the CSC pontoon follows structurally the Euler-Bernoulli assumptions. Close to the center the FEM-shell solution may be showing more structural behaviors or may be influenced by numeric deviation like force imbalance as was presented in Figure 6.17.

Figure 6.19 present the force imbalance for the FEM-shell of the new CSC design where the force imbalances can be considered large as it reach 20% as presented in Figure 6.19 and can lead to artificial stress estimation in the sections close to the center where the support are located.

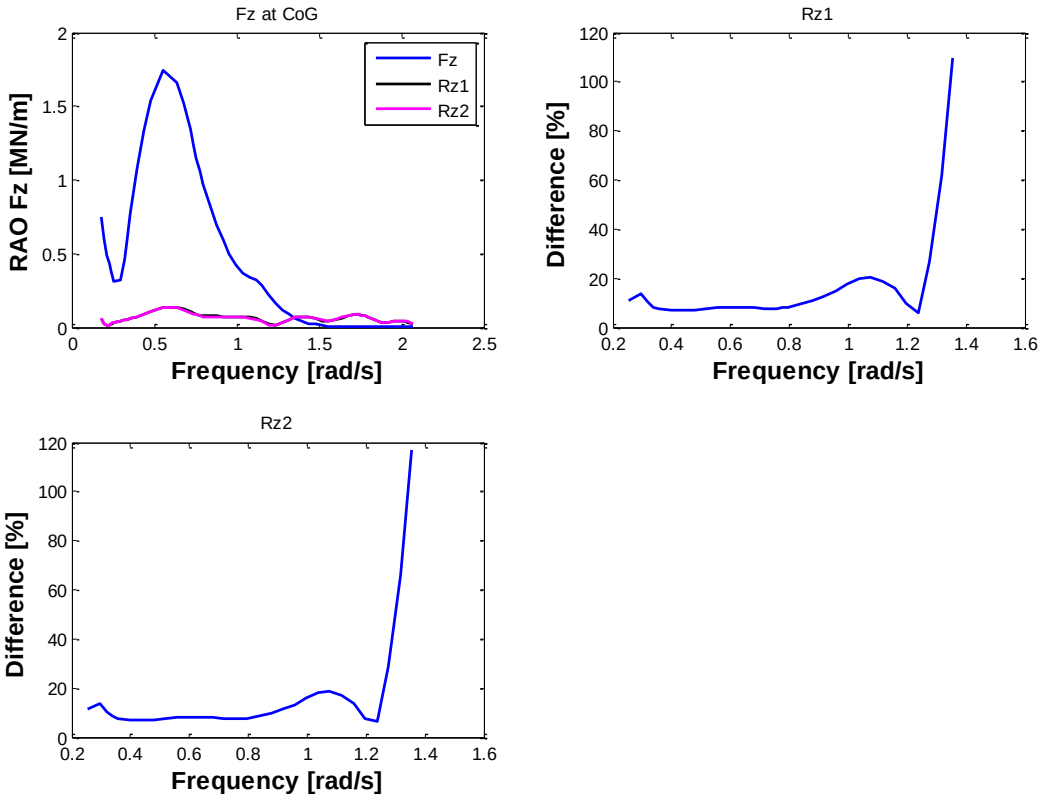

Figure 6.19 Support reaction force difference in "z" direction respect the total Fz force on the CoG of the new CSC

Figure 6.20 presents the RAO axial stress of FEM shell for the new CSC at section 4 of the pontoon. Figure A 26 in the Appendix A presents the RAO axial stresses along the sections on the pontoon for P3 where it is possible to observe that the E-B results predict lower stresses than the numeric method.

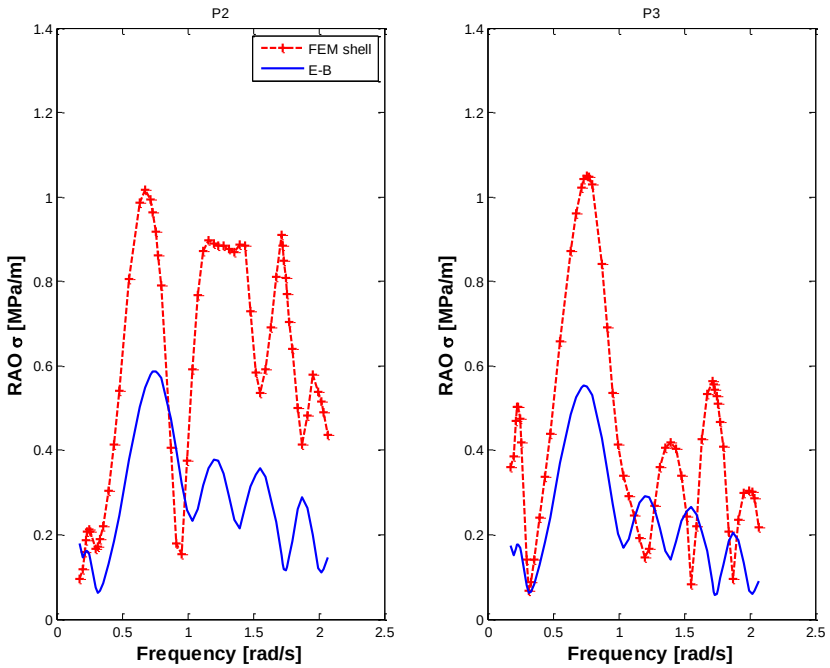

Figure 6.20 RAO axial stress from FEM shell at section 4 for new CSC design

Once again the FEM shell results differ from the analytical solution as was seen on the original CSC design. The reason is based on the underestimation of Euler-Bernoulli equation of the stress contribution from My as it is shown in Figure 6.21.

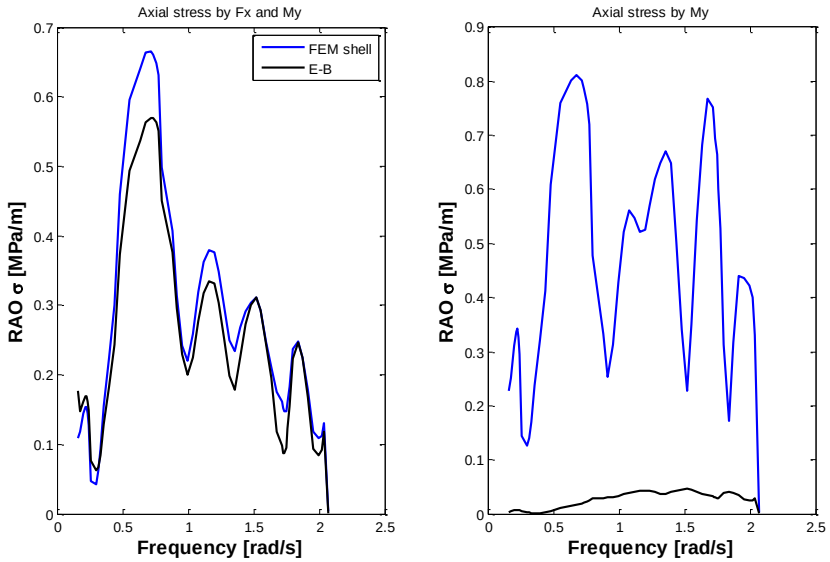

Figure 6.21 RAO axial stress decomposition by forces at section 4 on P2 at the pontoon of the new CSC

The stress component generated by the axial force and part of bending at the pontoon is similar to the stress estimated by beam theory. But the stress done just by bending forces My on FEM-shell indicates that the pontoon is under considerable bending forces that contribute in similar magnitude together the axial forces to the total stress. Additionally, this stress distribution is indicating at least that the axial force on the pontoon from FEM-shell is similar to the axial forces obtained from the HydroD integration.

The FEM shell validation shows that this elements are more sensitive to the simulation set up as was seen that the support reaction forces do modify the axial stress on the pontoons sections 1 and 2. The numeric results were in agreement with beam theory solution for the CSC design but for the new CSC the solution if different.

Beam theory (E-B) is not able to predict the total axial stress on the pontoon. The stress done by axial load Fx can be satisfactory predicted by the numeric model but the stress by My is usually underestimated.

At the end, FEM beams and shell elements reproduces according with beam theory the stresses on the pontoon for section 3 and 4 (Figure 6.22) of the original CSC design. In the case of the new CSC design the total axial stresses predicted by FEM were larger than the stress obtained by the analytical solution, as expected because the non-uniform load condition between the pontoon and the upper brace would lead to a different structural behavior respect the prediction by Euler-Bernoulli assumption.

The checking procedure at 0° degree of wave incidence for all FEM elements showed that the upper brace induce a significantly stress reduction by the wave loads as can be appreciated in Figure 6.22. The analytical solution tends to underestimate the stresses on

the pontoon of the new CSC design. The simulations with shell elements have larger forces at the support locations; this may induce significantly deviation of the stress values at location close to central column of the FOWT. For further analysis the just section 4 is going to be simulated with FEM.

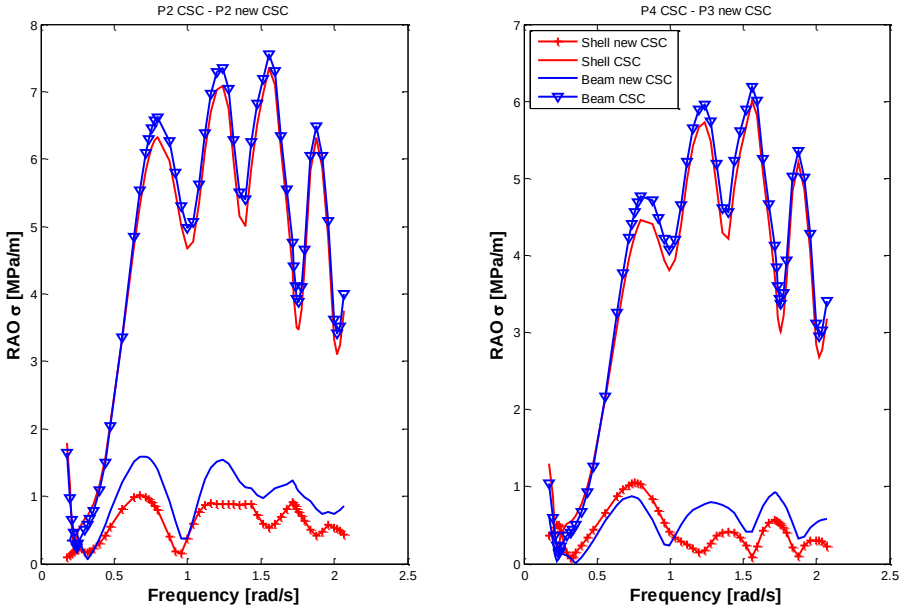

Figure 6.22 RAO axial stress comparison between FEM results at section 4 of the pontoon

For the most critical wave direction obtained from section 6.1 the stress analysis will focus just on section 4 which is at 30m from the center of both CSC. The FEM analysis will help to quantify with more accuracy the stress on the pontoon of the new CSC design as it is capable to obtain a more acceptable stress distribution by the wave forces.

6.3. FEM on critical wave incidence

For the CSC design the most critical wave direction from the ultimate limit state based on beam theory estimation was 140° and for the new design was 130°.The following analysis will review the stress estimation offering more accurately solutions, especially for the new CSC design.

6.3.1. FEM beam

Maintaining the same numerical set up of the previous FEM beam simulations, the case for 130° wave incidence is presented in Figure 6.23 for the CSC and new CSC. The stress prediction for the CSC presents good agreement between the numeric method and beam theory. For the new CSC the FEM-beam solution have similar behavior respect the frequency but in general the E-B solution tend to underpredict the axial stress.

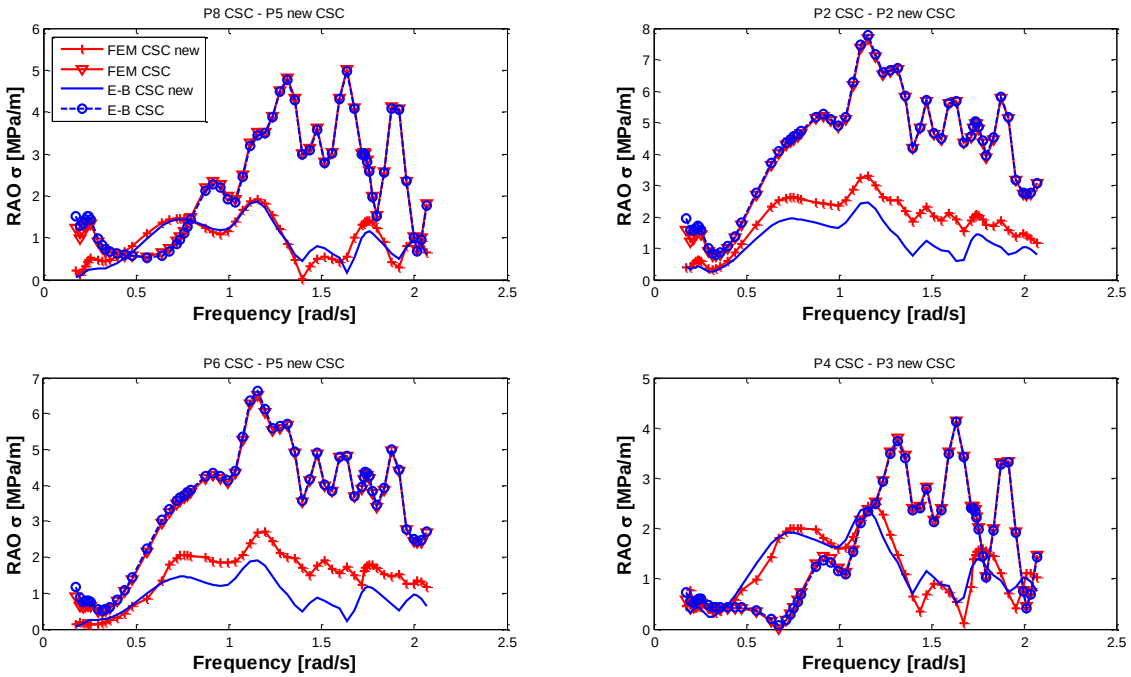

Figure 6.23 RAO axial stress at section 4 for 130°, using FEM beams for both semi-submersibles

The close solution between FEM and E-B solutions indicates that the stress on the pontoon is not dependant of the moment respect "y" axis. Considering the wave incidence respect the pontoon orientation the wave loading is producing more Mz than My. Therefore the difference presented between the FEM solution and the analytical one is due the relative small presence of My stress.

By separating the stress contribution of the total axial stress in Figure 6.24 for the new CSC at section 4 is possible to observe that the contribution from My is the cause of difference in the stress estimation.

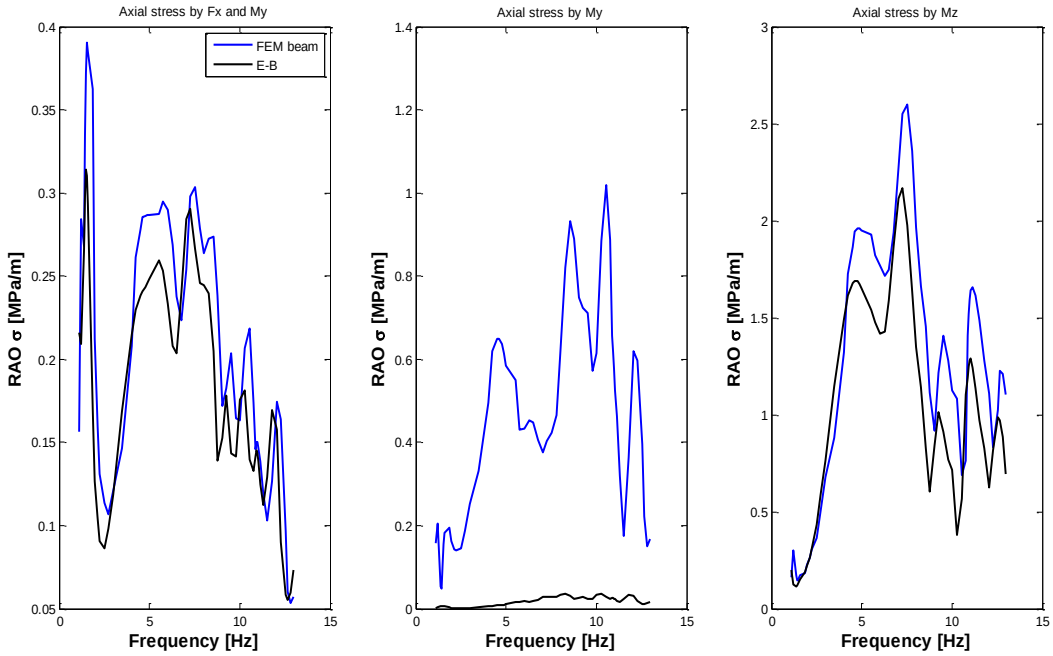

Figure 6.24 Stress decomposition for new CSC at section 4

The E-B solution tends to be lower than the numeric solution by finite element method. For the wave direction of 140° Figure 6.25 shows that the beam theory can offer an acceptable estimation of the stress on the pontoon at section 4 as the solution for the CSC are practically the same respect the numerical and for the new CSC the differences for some wave frequency can reach 100% of the E-B results but for the rest of the wave spectrum the FEM-beam is presenting the same behavior.

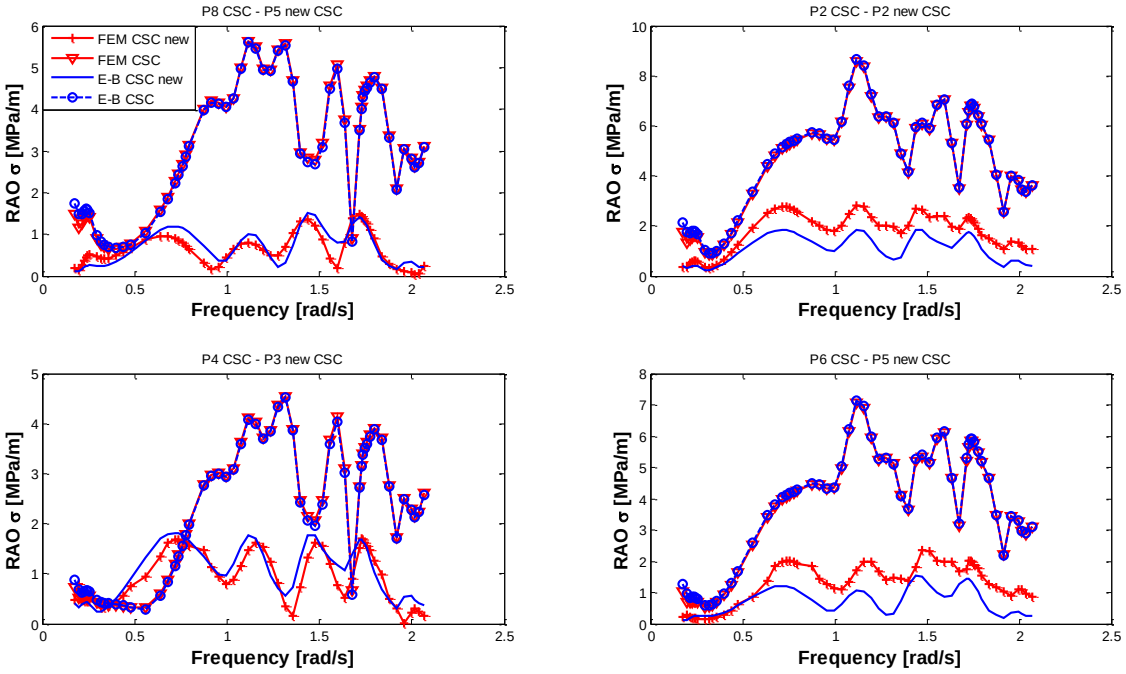

Figure 6.25 RAO axial stress at section 4 for 140°, using FEM beams

As it was seen during the verification of the beam results the FEM analysis gives a higher stress estimation as the My is larger than predicted on beam theory.

In order to obtain the ultimate limit state of the RAO stresses from the last results the FEM with shell elements is going to be obtained and compared with E-B solution in the same way as it was done before.

6.3.2. FEM shell

According the results on Figure 6.26 the FEM shell solution differs totally respect the beam theory. The stresses predicted along the pontoon for the original CSC design are one order of magnitude larger than the analytical solution. Even for the new CSC the approach offer different structural behaviors respect the frequency spectrum.

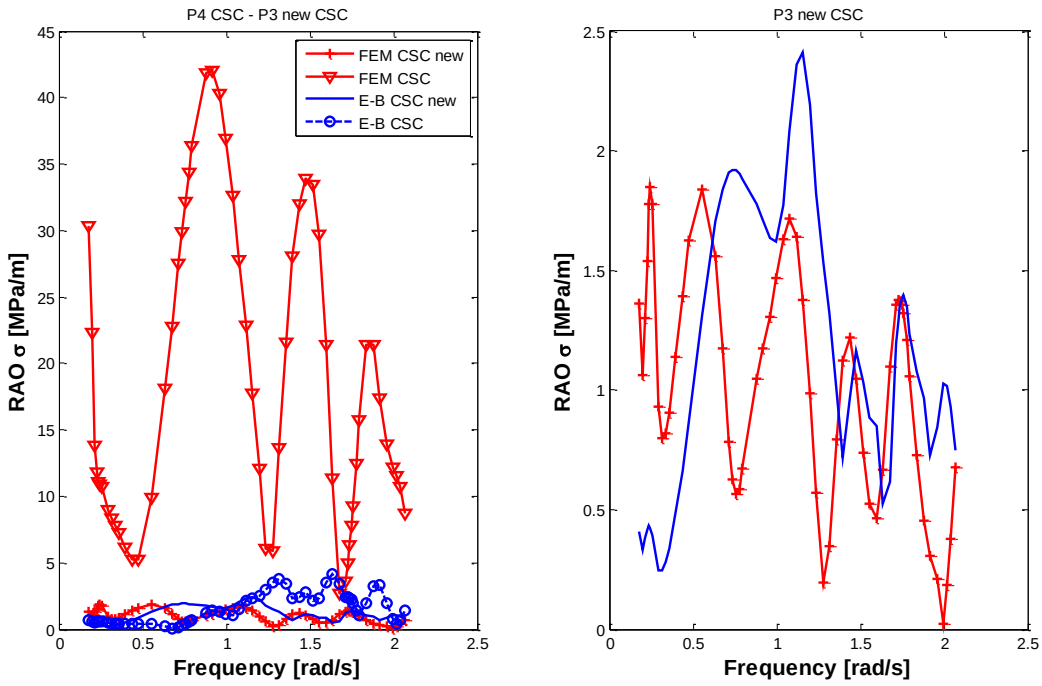

Figure 6.26 RAO axial stress at section 4, wave direction 130°, using FEM shell elements

Checking the forces on the support reactions on Figure 6.27 it is possible to notice that the forces on the model are imbalanced through the large percentage values. The FOWT is relying totally on the artificial support in order to face the wave loads instead of its own restoring capacities for some wave frequencies.

It is expected that if the hydrodynamics loads decrease the reaction forces on the support would decrease accordingly. This is an indication that the numeric set up for shell elements is not appropriate for the stress simulation for the wave incidence of 130° on the CSC design.

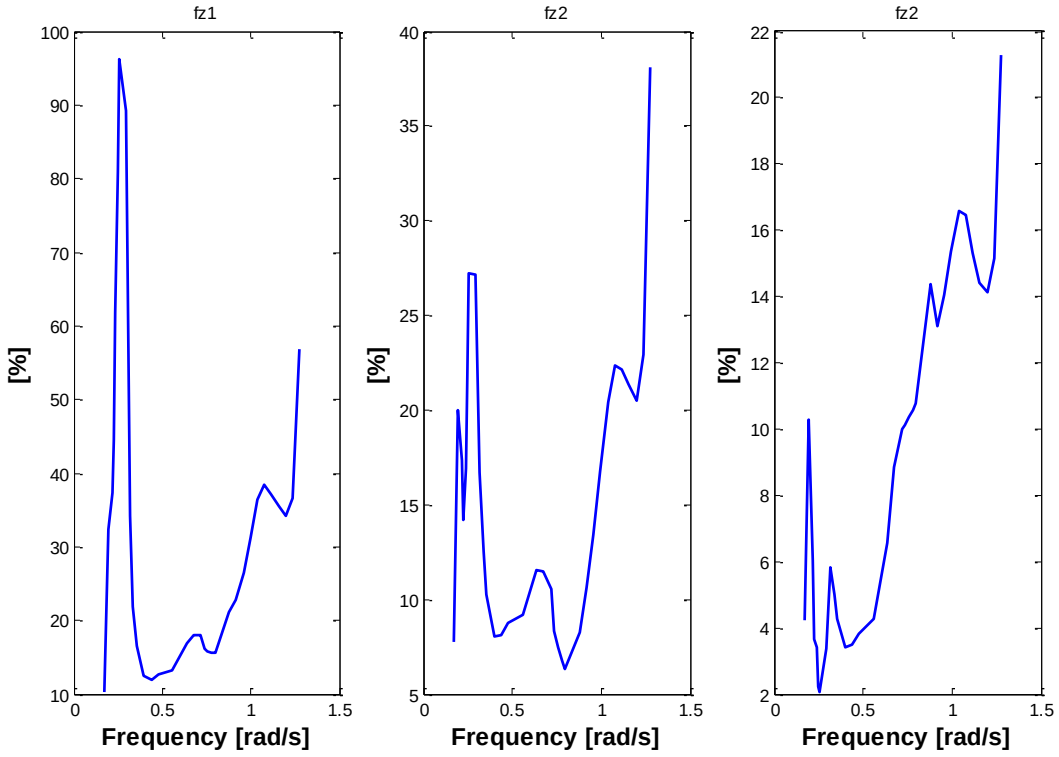

Figure 6.27 Differences between the reaction forces respect the total force in "z" direction at the CSC center of gravity

This problem is also present on the FEM-shell result for 140° wave incidence as can be seen on Figure 6.28 where the stresses on the CSC are again one order of magnitude larger than the predicted by analytical equations. The solution based on shell elements for the CSC and new CSC requires more numerical checks in order to produce satisfactory results. This may lead to check the numerical resolution scheme and the stiffness matrix.

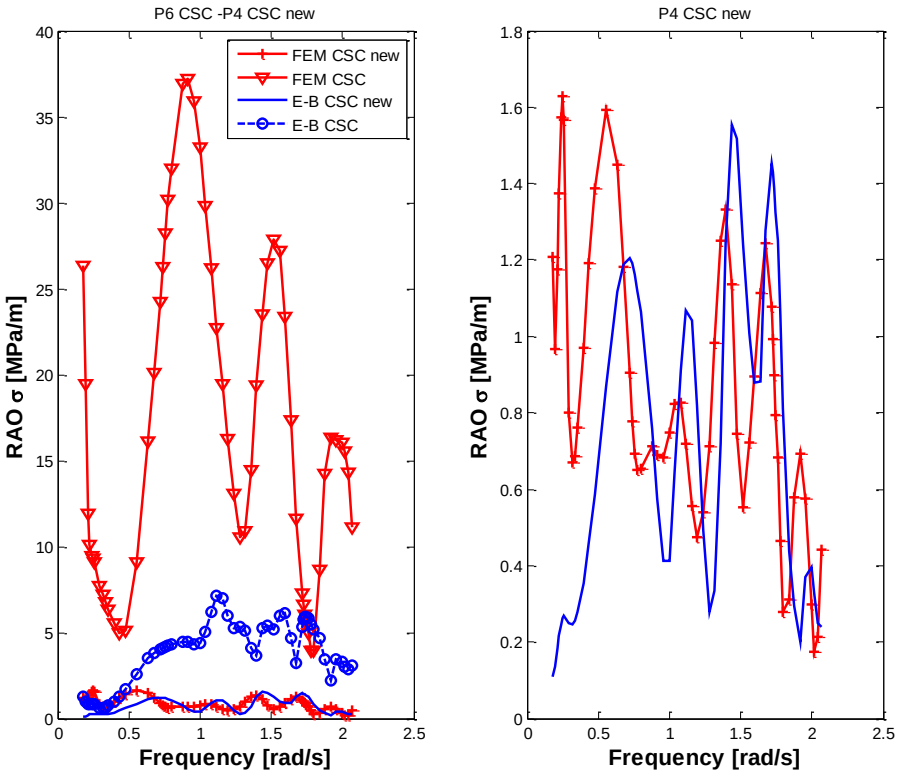

Figure 6.28 RAO axial stress at section 4, wave direction 140°, using FEM shell elements

Finally, for the ULS check the only results that are going to be employed are the FEM beam results as the FEM shell should require numerical treatment related with the mesh generation, node locations or even solution method as it could not transfer the hydrodynamic loads into the structural models as it was successfully done by the FEM with beams.

6.3.3. Ultimate Limit State

In order to compute the dynamic stress on the pontoon using the FEM-beam solutions, the load cases from Appendix B Table B 3 is applied on the transfer function (RAO) for 130° and 140° following the same procedure for beam theory. Figure 6.29 and Figure 6.30 presents the ULS solutions.

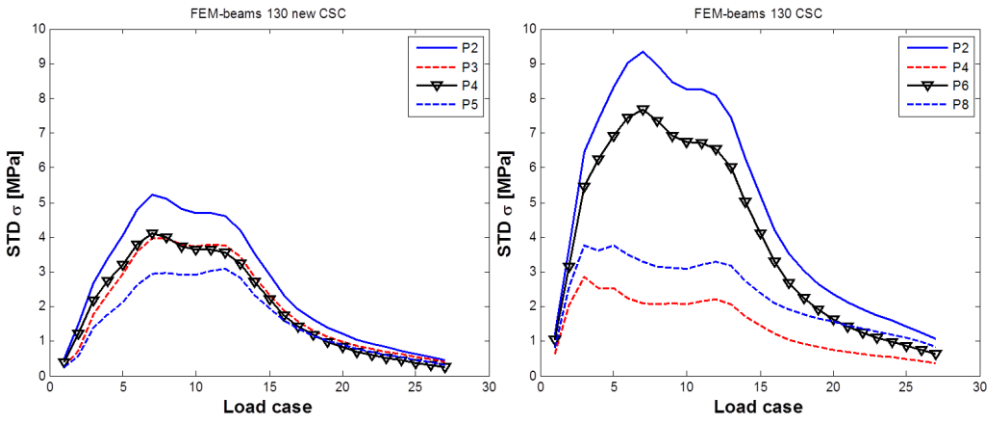

Figure 6.29 STD axial dynamic stress on the pontoon for the new and original CSC at section 4 for 130°.

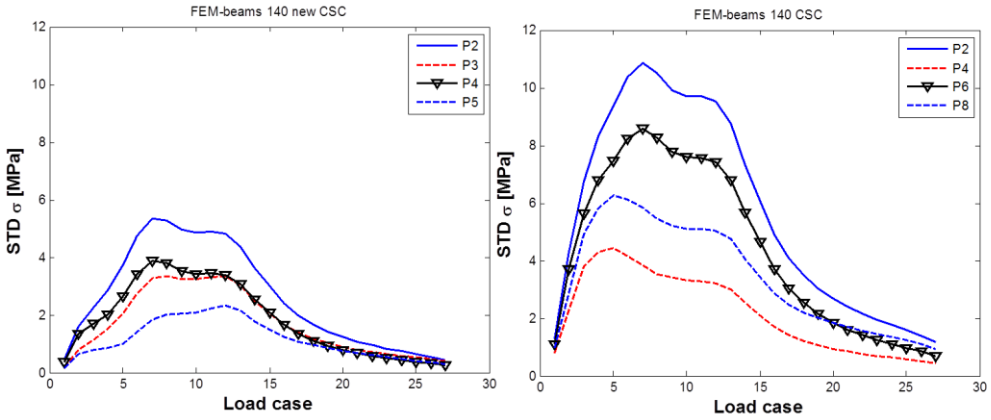

Figure 6.30 STD axial dynamic stress on the pontoon for the new and original CSC at section 4 for 140°.

The ULS results shows that the new CSC pontoon has lower dynamic stress on its cross section respect the original CSC for the most critical load cases. As the upper beam constrains the motion of the pontoon the stress on the cross section is changed respect the wave incidence. For the original CSC P4 and P8 had the largest stresses but for the new CSC P2 and P4 are the most affected by the wave loading.

Table 6.2 present the stress reduction between semi-submersibles at the equivalent points P8 and P5. The addition of an upper beams help to reduce more than 60% the dynamic effect on the pontoon, allowing on this way to make a stronger FOWT against wave loading and probably with more endurance to withstand the fatigue damage.

Table 6.2 Dynamic stress reduction between original and new CSC from FEM-beams for P8-P5

LC	130° [%]	140° [%]
8	67	81
9	66	79
10	65	79
11	63	77
12	62	76
13	62	76

The final results show that the FEM beam model for the new CSC has larger axial stress than predicted by analytical estimation. The assumption that the pontoon and brace would behave as a whole beam is not totally true because the wave loads is just acting on the pontoon and the structure cannot behave entirely as a rigid body. The upper brace actually contribute to constrain the pontoon deformation but cannot deform with the same proportions as the pontoon, neither follow the same deformation mode.

CHAPTER 7 CONCLUSIONS

This project was about the numerical structural assessment of the pontoons of the conceptual floating offshore wind turbine CSC developed at the Centre of Ship and Offshore Structure at NTNU. A new version of the CSC design was developed by adding some heavy beams above still water line connecting its outer column with the central column. This connection was designed to maintain the braceless concept applied that lead to a structure with fewer connections and therefore with less number of sensitive fatigue spots.

The new CSC model present a higher center of gravity that increase its static heeling angle respect the turbine moment at rated speed. The hydrodynamic analysis was execute in frequency domain using DNV SESAM software, the natural period for heave, pitch and roll remains practically unaltered, outside the sea wave frequency.

The motion amplitude for heave, roll and pitch also remain very similar to the original CSC as the hull design was unaltered, however modifications on the mass distribution leads to minors changes in the transfer functions amplitudes.

The damping ratio modeled through the Morison equation lead to a high value if it is compared with others offshore applications. However, as the floating structures for offshore wind turbine applications are still under development there is limited data available and the only option to improve or check the damping ratio is through model test on basins.

For the original CSC design the stress estimation thought the analytical equation from Euler-Bernoulli can give acceptable results when are compared with the numeric solution form finite element method using beams or shell element.

For the new CSC the pontoon and brace do not follow beam theory assumptions as a whole structure. From the hydrodynamic analysis the sectional loads should be obtained separately for the pontoon and brace. Later, it is possible to calculate the stresses using E-B the stresses on each structure independently.

The DNV SESAM software is a reliable tool for the hydrodynamic analysis but the options for obtaining the sectional loads are limited as it cannot be applied on particular cross sections of the floater but it uses numeric infinites planes that would cover parts that are not of interest.

The FEM-shell simulation offered good result for the original CSC design during the validation case but for a more complex case force and for the improved CSC the simulation leads to very high stress solution and numeric imbalances.

The results from FEM-beam simulation shows that the new CSC design has more structural strength as the pontoons are subjected under lower dynamic streses. The upper

beam helps to give a better support to the pontoon through the columns resulting in a closed structural loop.

These results contribute into the design development of the CSC and will lead to further works, from the project results some recommendations are given into the following section.

7.1. Recommendations

The dynamic loads were obtained from a frequency domain simulation, therefore just wave loads were considered for the stress analysis. In order to take into account the wind load simultaneously with waves a time domain simulation will be required. This numeric approach would lead to a more complete dynamic stress assessment of the pontoon as the wind loads usually produces larger moment on the semi-submersible. Also, the time domain simulation can give a better idea about the motion of the FOWT under a design sea state because it offers directly the motion as a function of time.

The time domain simulation may offer the advantage of taking into consideration the relative motion between the floaters respect the waves and wind allowing to observe a realistic motion amplitude and it mean position.

This project presented the advantage of a structural reinforcement from the ultimate strength resistant point of view. However, for offshore structures the fatigue assessment is also important to achieve a complete structural design. Thus, the stress history of a time domain simulation can be employed to the calculation of fatigue damage and check if the structure can offer a work time period of at least 20 years.

With the fatigue results and the ultimate state stresses is possible to check in detail if the heavy beams dimensions can be reduced in order to optimize it design and balance it between increase the FOWT strength and reduce it mass. This would lead to increase the air gap between the still water line and the lower part of the upper beam.

During the analysis was observed large stress values at the connection between the floater and the tower at the central column top on the new CSC. This section should be analyzed in detail because it’s going to be the first place of the unit on receive the wind loads and probably would induce large stress on the upper beams as well.

The FEM shell simulations should be carried on further design stage with a more detailed structural design of the floater that includes stiffeners and bulkhead. For early design stage the FEM study with beams can offer the global loads and results needed for complete a conceptual design. The shell elements required a more detailed mesh design and numerical set up in order to achieve acceptable results.

REFERENCES

Arapogianni, A., Moccia, J., Williams, D., & Phillips, J. (2011, November). *Wind in our Sails. The coming of Europe's offshore wind energy industry.* Retrieved from European Wind Energy Association: http://www.ewea.org/publications/reports/wind-in-our-sails/

Benitz, M., Lackner, M., & Schmidt, D. (2015). Hydrodynamics of offshore structures with specific focus on wind energy applications. *Renewable and Sustainable Energy Reviews, 44*, 692-716.

Borg, M., & Collu, M. (2015). Offshore floating vertical axis wind turbines, dynamics modelling state of the art. Part III: Hydrodynamics and coupled modelling approaches. *Renewable and Sustainable Energy Reviews, 46*, 296–310.

Bulder, B. H., Henderson, A., Huijsmans, R. H., Peeringa, J. M., Pierik, J. T., Snijders, E. J., . . . Wolf, M. J. (2003). *Floating Off ShoreWind Turbines for Shallow waters.* Obtenido de Energy research Centre of the Netherlands (ECN): www.ecn.nl/docs/library/report/2003/rx03039.pdf

Butterfield, S., Musial, W., Jonkman, J., Sclavounos, P., & Wayman, L. (2005). *Engineering Challenges for Floating Offshore Wind Turbines.* Obtenido de National Renewable Energy Laboratory (NREL): http://wind.nrel.gov/public/SeaCon/Proceedings/Copenhagen.Offshore.Wind.2005/documents/papers/Future_innovative_solutions/S.Butterfield_Engineering_Challenges_for_Floating.pdf

Clauss, G., Lehmann, E., & Östergaard, C. (2012). *Offshore Structures: Volume I: Conceptual Design and Hydromechanics.* London: Springer London.

DET NORSKE VERITAS AS. (June de 2013). Design of Floating Wind Turbine Structures. *OFFSHORE STANDARD DNV-OS-J103*, 37.

DNV. (2010). *SESAM User Manual Sestra.* Høvik: DET NORSKE VERITAS.

Dr.techn. Olav Olsen AS. (01 de 06 de 2015). *Renewable Energy*. Recuperado el 01 de 06 de 2015, de Dr.techn. Olav Olsen AS - Structural Engineering: http://www.olavolsen.no/en

Fukushima Offshore Wind Consortium. (s.f.). *Research Floating Wind Turbine Technology*. Recuperado el 01 de 06 de 2015, de Fukushima Offshore Wind Consortium: http://www.fukushima-forward.jp/english/index.html

Horns Rev 1. (s.f.). *Horns Rev 1*. Recuperado el 1 de June de 2015, de Vattenfall, Dong Energy: http://www.hornsrev.dk/en

Huijs, F., de Bruijn, R., & Savenije, F. (2014). Concept design verification of a semi-submersible floating wind turbine using coupled simulations. *Energy Procedia, 53*, 2-12.

Huijs, F., de Ridder, E.-J., & Savenije, F. (2014). COMPARISON OF MODEL TESTS AND COUPLED SIMULATIONS FOR A SEMI-SUBMERSIBLE FLOATING WIND TURBINE. *ASME 2014 33rd International Conference on Ocean, Offshore and Arctic Engineering OMAE2014.* San Francisco: ASME.

Huijs, F., Mikx, J., Savenije, F., & de Ridder, E.-J. (2013). Integrated design of floater, mooring and control system for a semi-submersible flaoting wind turbine. *EWEA Offshore 2013 Vienna.* Vienna: EWEA.

Jonkman, J. (2006). *NREL Offshore Baseline 5MW.* Golden: National Renewable Energy Laboratory (NREL).

Jonkman, J., Butterfield, S., Musial, W., & Scott, G. (2009). *Definition of a 5-MW Reference Wind Turbine for Offshore System Development.* Golden: National Renewable Energy Laboratory.

Journée, J. M., & Massie, W. W. (2001). *Offshore Hydromechancis.* Delft: Delft University of Technology.

Karimirad, M., & Moan, T. (2012). Feasibility of the Application of a Spar-type Wind Turbine at a Moderate Water Depth. *Energy Procedia, 24*, 340-350.

Langen, I., & Sigbjörnsson, R. (2014). Dynamisk Analyse av Konstruksjoner. En *Dynamic Response of Marine Structures.* Trondheim: NTNU.

Lefebvre, S., & Collu, M. (2012). Preliminary design of a floating support structure for a 5 MW offhore wind turbine. *Ocean Engineering*, 15-26.

Luan, C., Gao, Z., & Moan, T. (2015). Criteria and procedure for concept design of the hulls of semi-submersible wind turbine. *Draft work to be published*.

Musial, W., & Ram, B. (September de 2010). *National Renewable Energy Laboratory.* (N. R. (NREL), Ed.) Recuperado el March de 2015, de Wind Research Publications: http://www.nrel.gov/wind/publications.html

Ramachandran, G., Bredmose, H., Sorensen, J., & Jensen, J. (2014). Fully Coupled Three-Dimensional Dynamic Response of a Tension-Leg Platform Floating Wind Turbine in Waves and Wind. (ASME, Ed.) *Journal of Offshore Mechanics and Arctic Engineering, 136*.

Roddier, D., Cermelli, C., Aubault, A., & Weinstein, A. (2010). WindFloat: A floating foundation for offshore wind turbine. *Journal of Renewable and Sustainable Energy 2*.

Statoil. (2015). *Hywind Demo*. Obtenido de Statoil: http://www.statoil.com/en/TechnologyInnovation/NewEnergy/RenewablePowerProduction/Offshore/Hywind/Pages/HywindPuttingWindPowerToTheTest.aspx

Viselli, A., Goupee, A., & Dagher, H. (2014). Model test of a 1:8 scale floating wind turbine offhore in the gulf of Maine. *33rd International Conference on Ocean, Offshore and Arctic Engineering.* San Francisco: ASME.

WAMIT, Inc. (s.f.). *wamit.* Obtenido de www.wamit.com

APPENDIX A

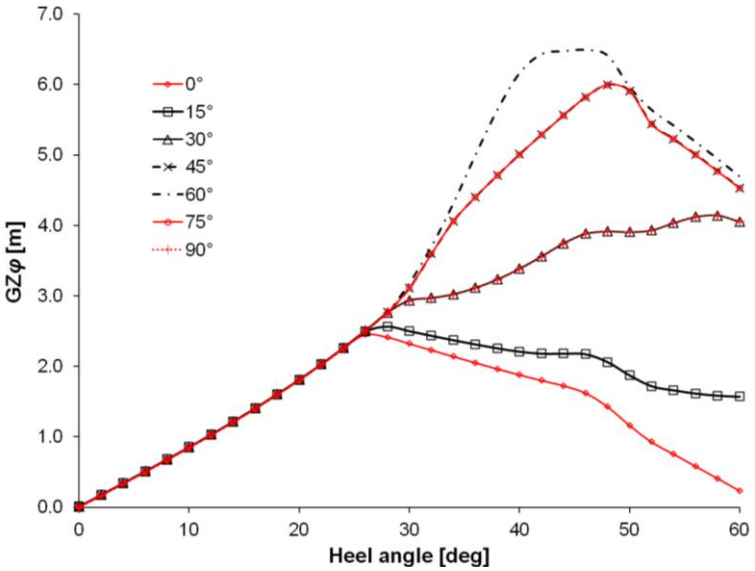

Figure A 1 Righting arm curve for CSC.

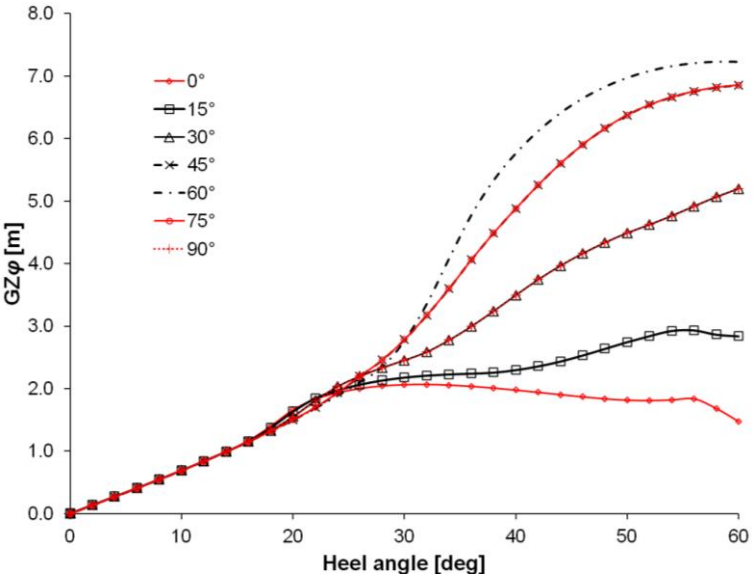

Figure A 2 Righting arm curve for new CSC.

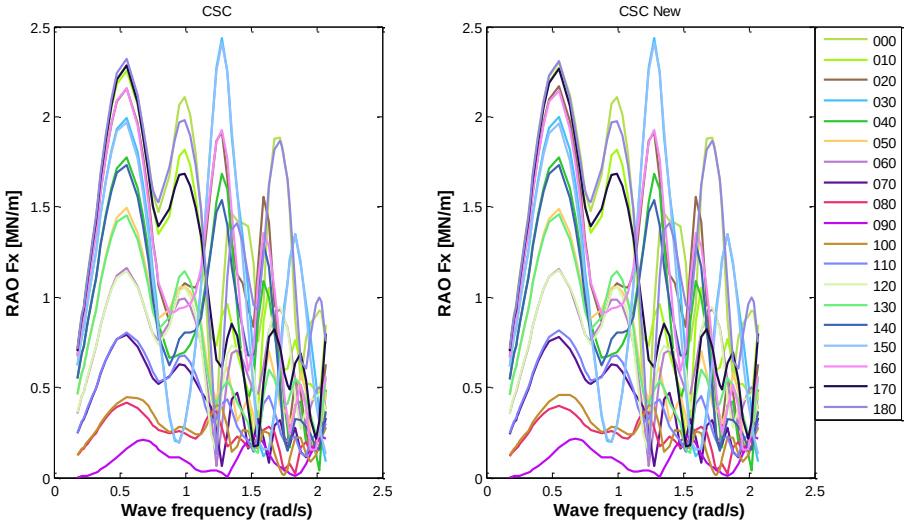

Figure A 3 RAO force in surge direction for both CSC

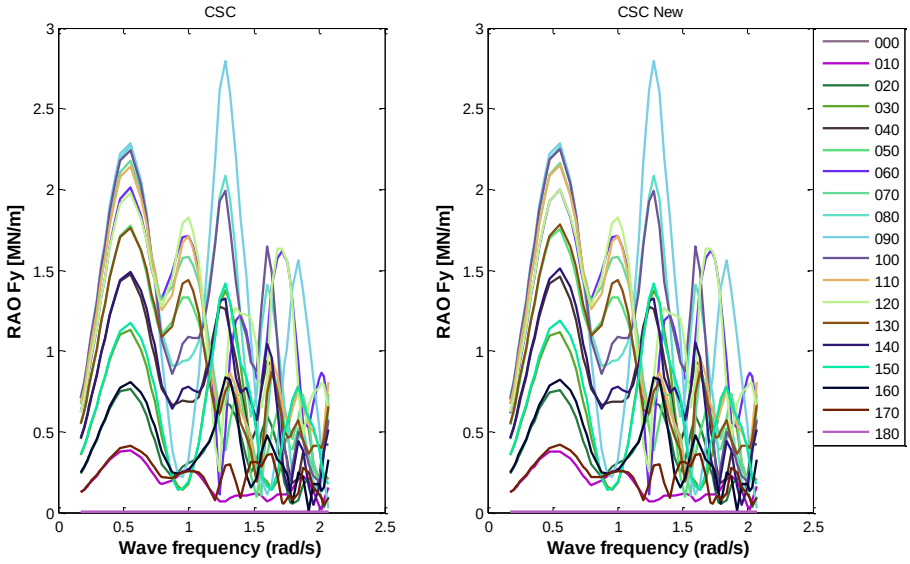

Figure A 4 RAO force in sway direction for both CSC

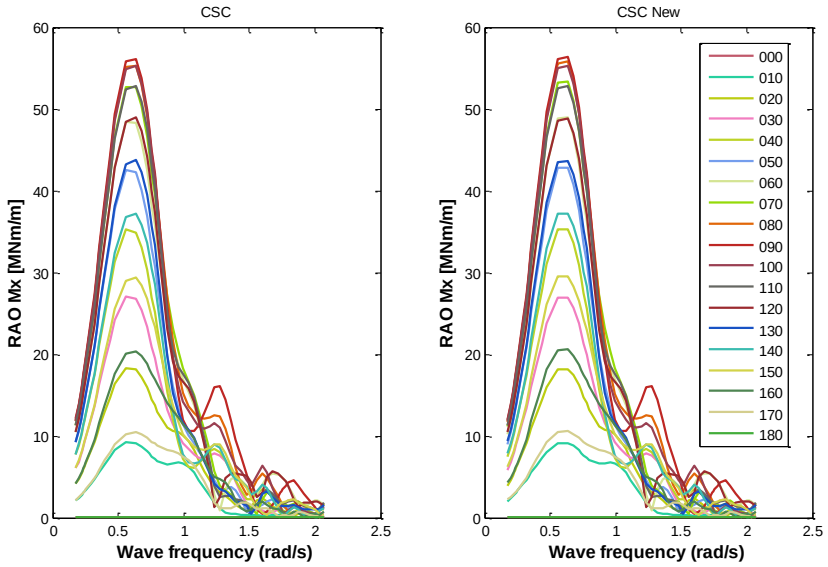

Figure A 5 RAO moment in surge direction for both CSC

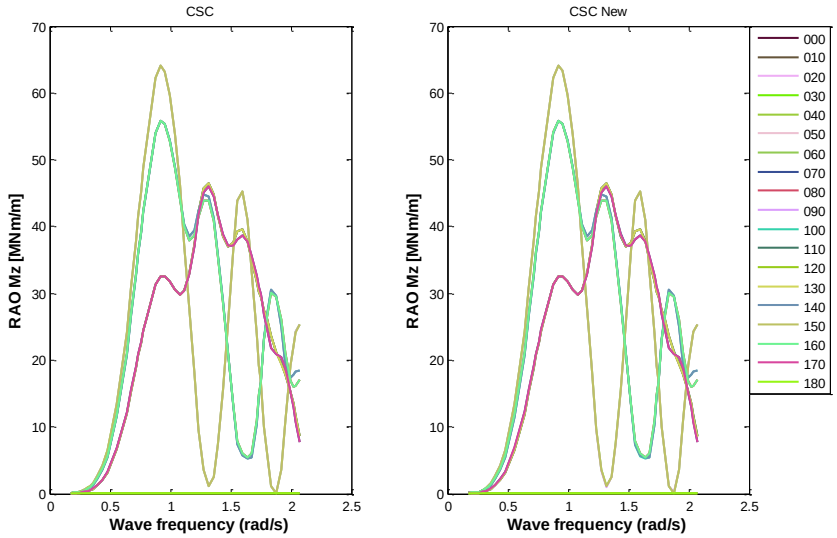

Figure A 6 RAO moment in heave direction for both CSC

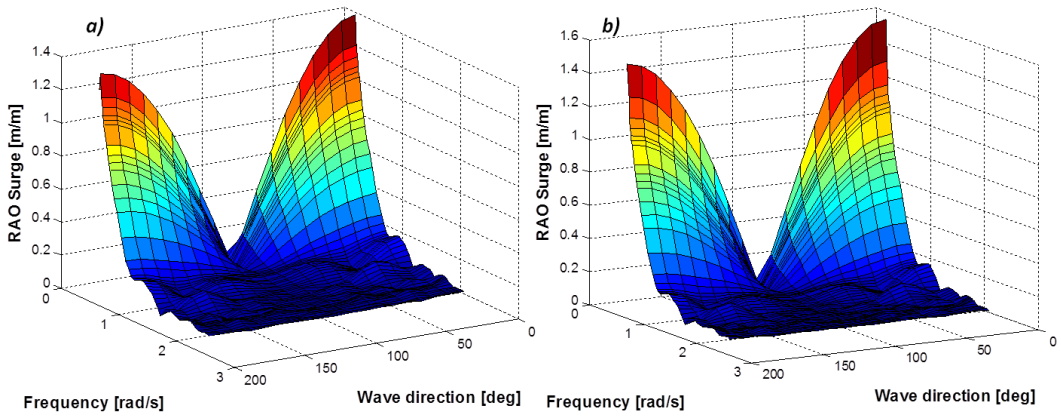

Figure A 7 RAO surge motion for the a) original and b) new CSC.

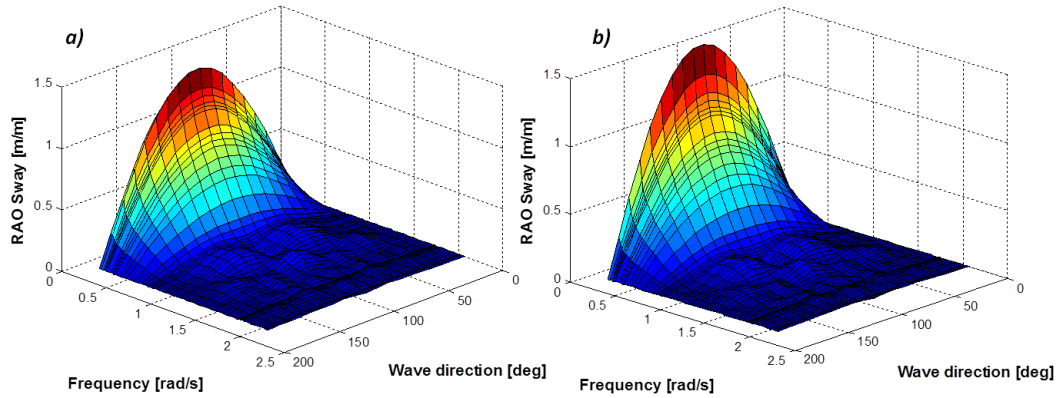

Figure A 8 RAO sway motion for the a) original and b) new CSC.

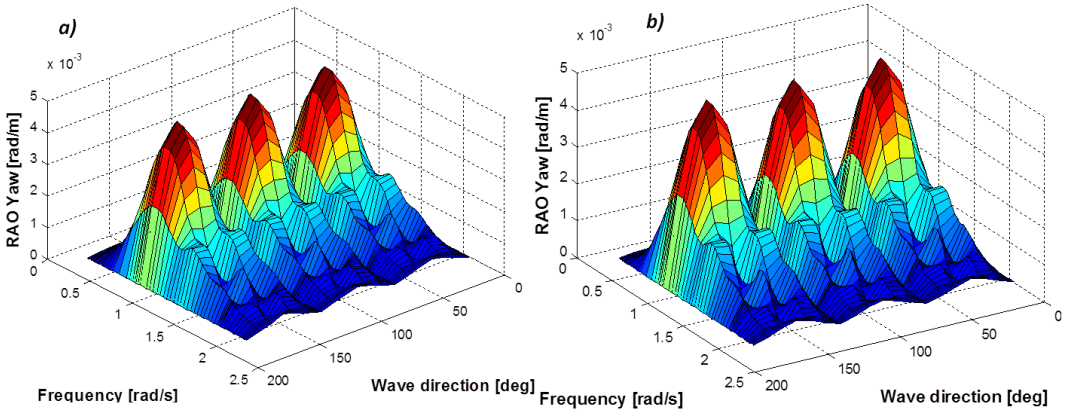

Figure A 9 RAO yaw motion for the a) original and b) new CSC.

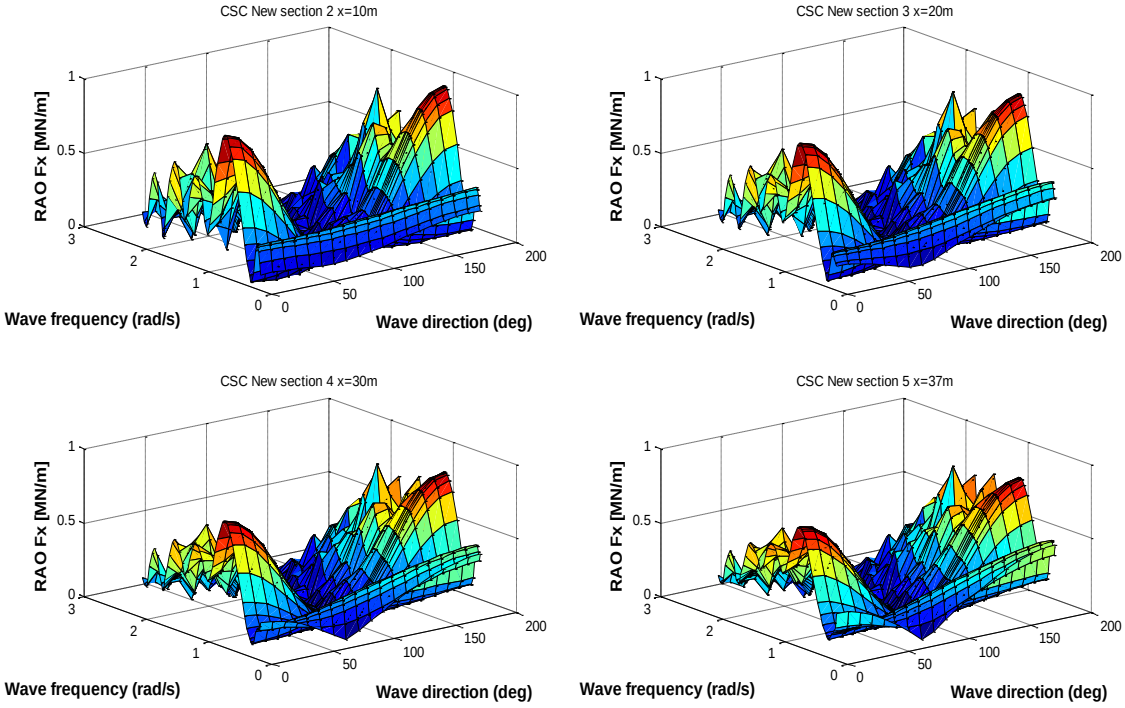

Figure A 10 RAO Fx for the new CSC.

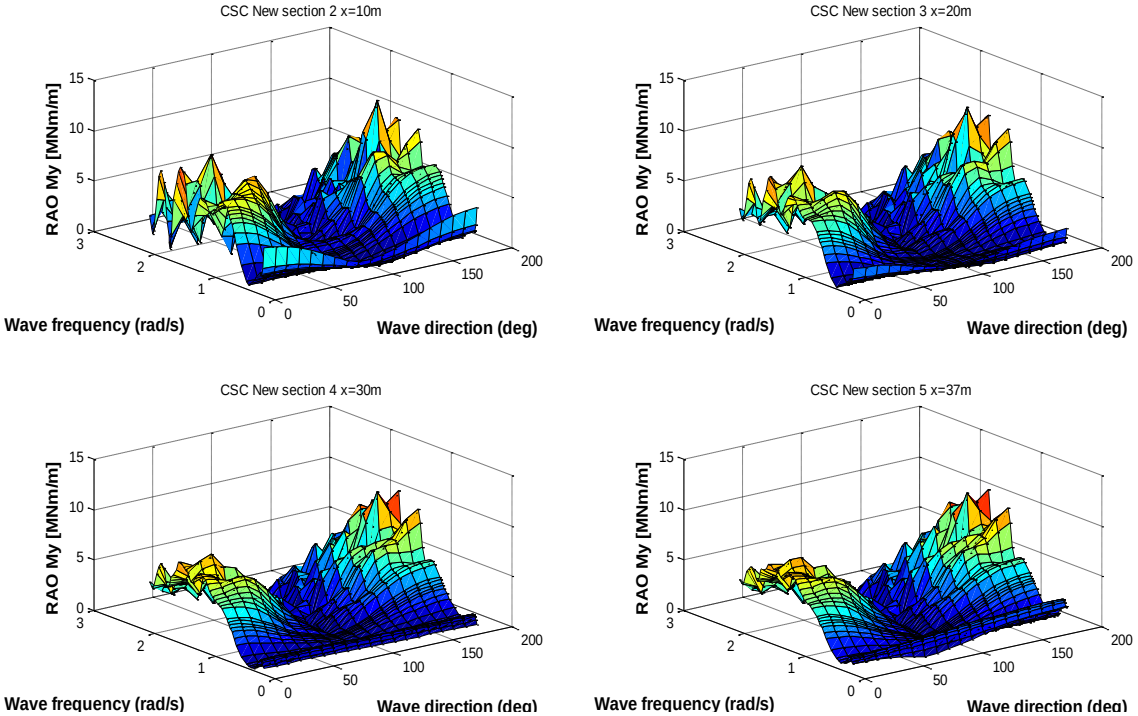

Figure A 11 RAO My for the new CSC.

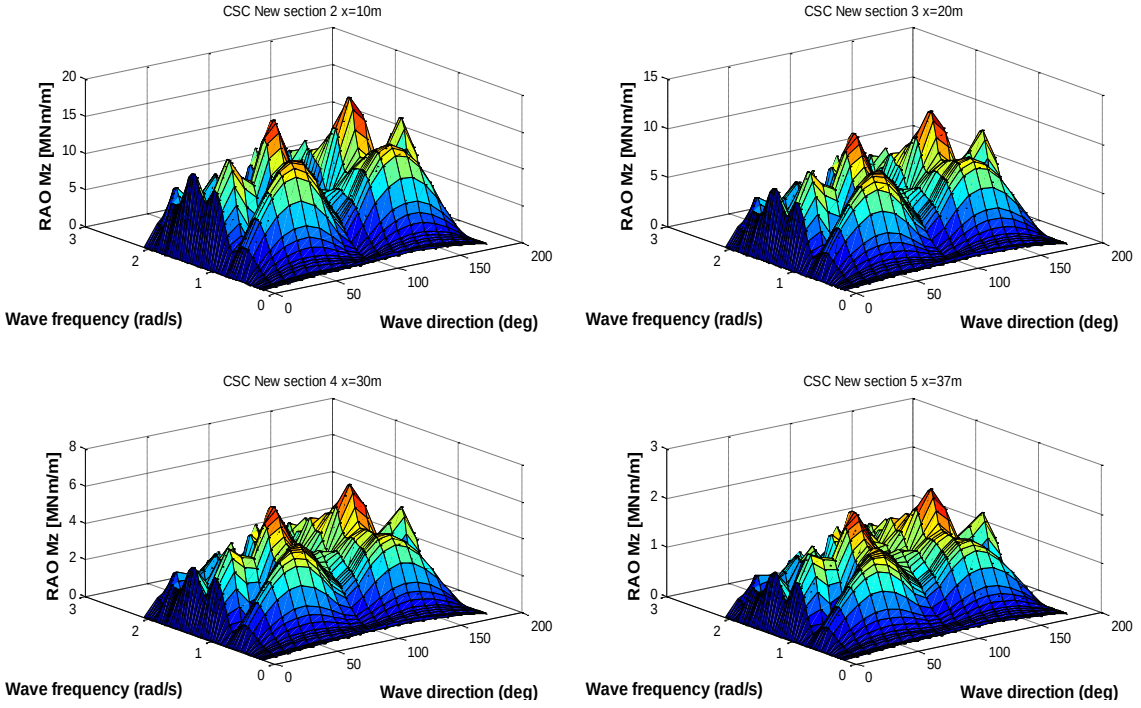

Figure A 12 RAO Mz for the new CSC.

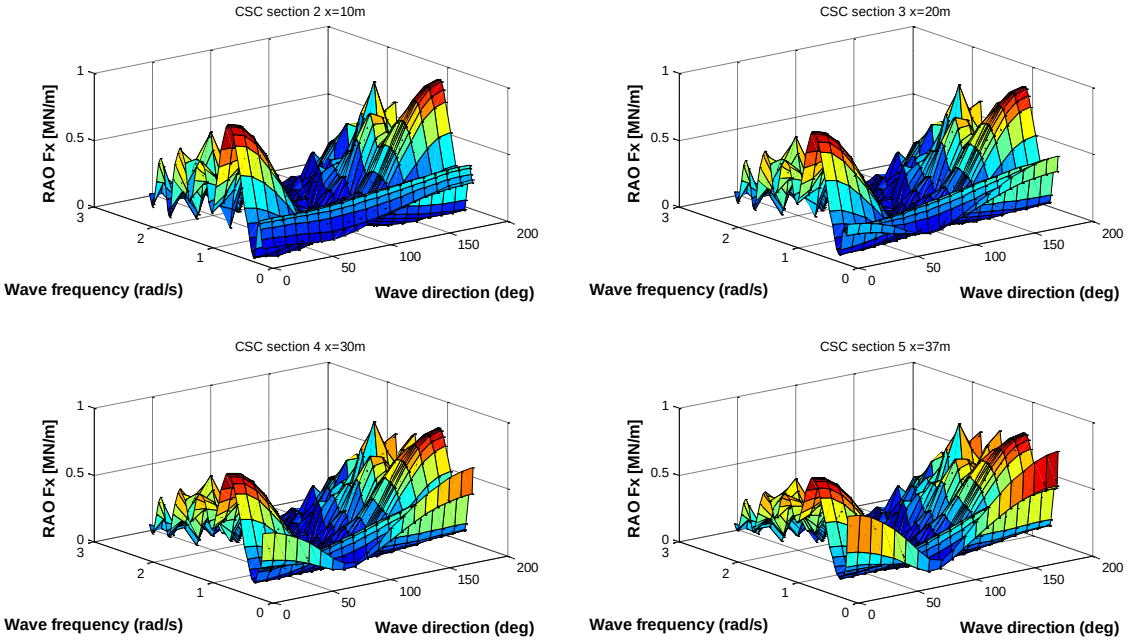

Figure A 13 RAO Fx for the CSC.

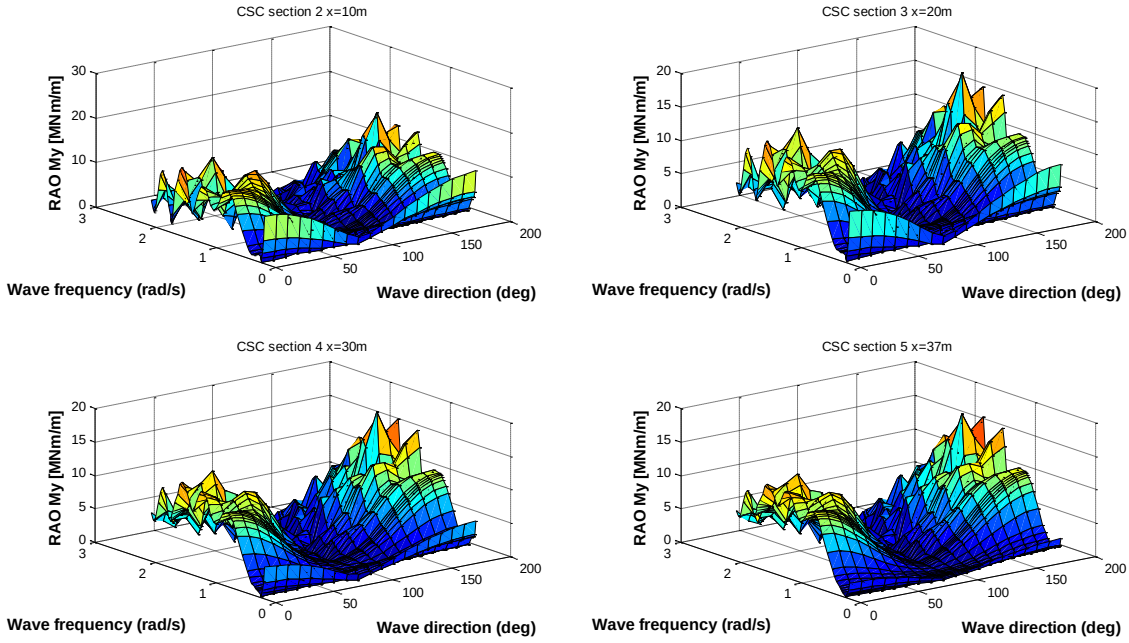

Figure A 14 RAO My for the CSC.

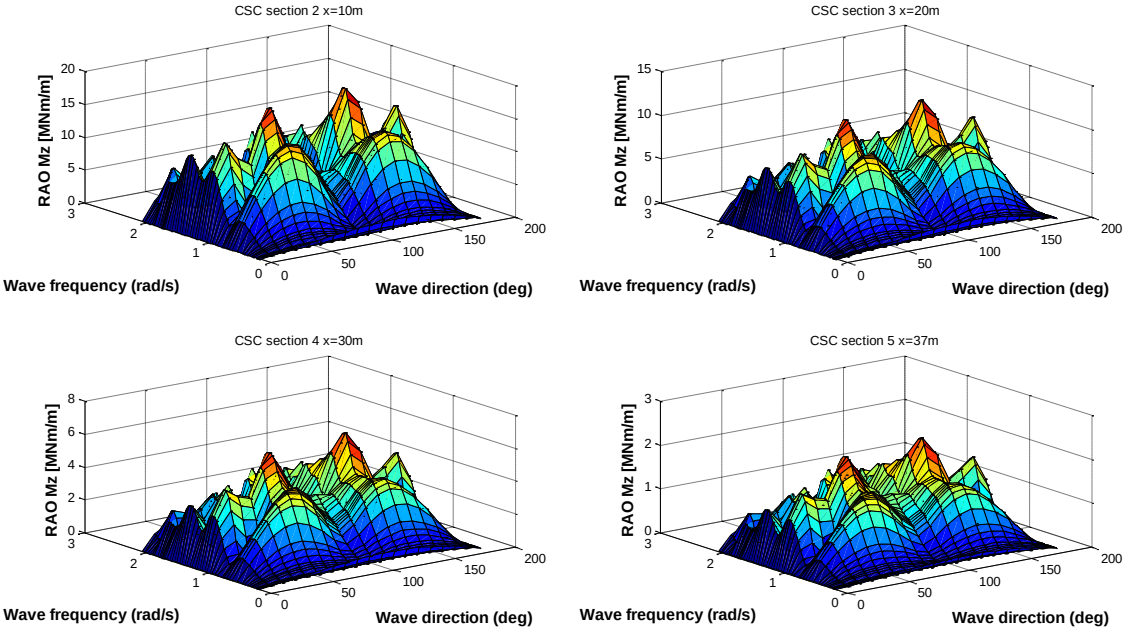

Figure A 15 RAO Mz for the new CSC.

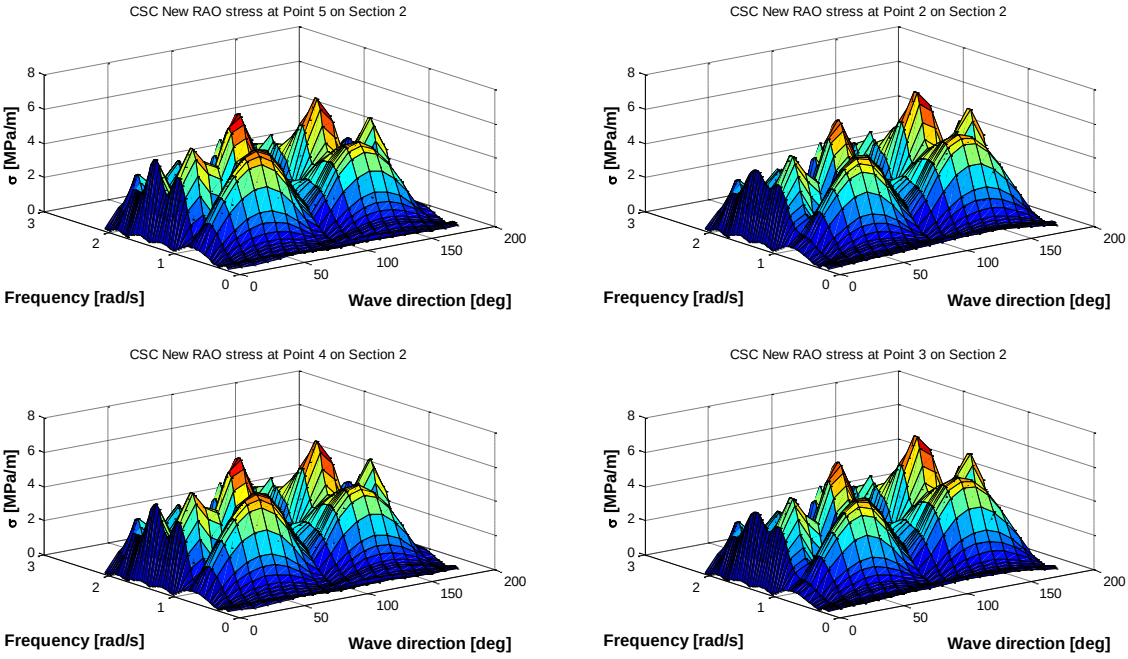

Figure A 16 RAO stress for the new CSC at cross section 2

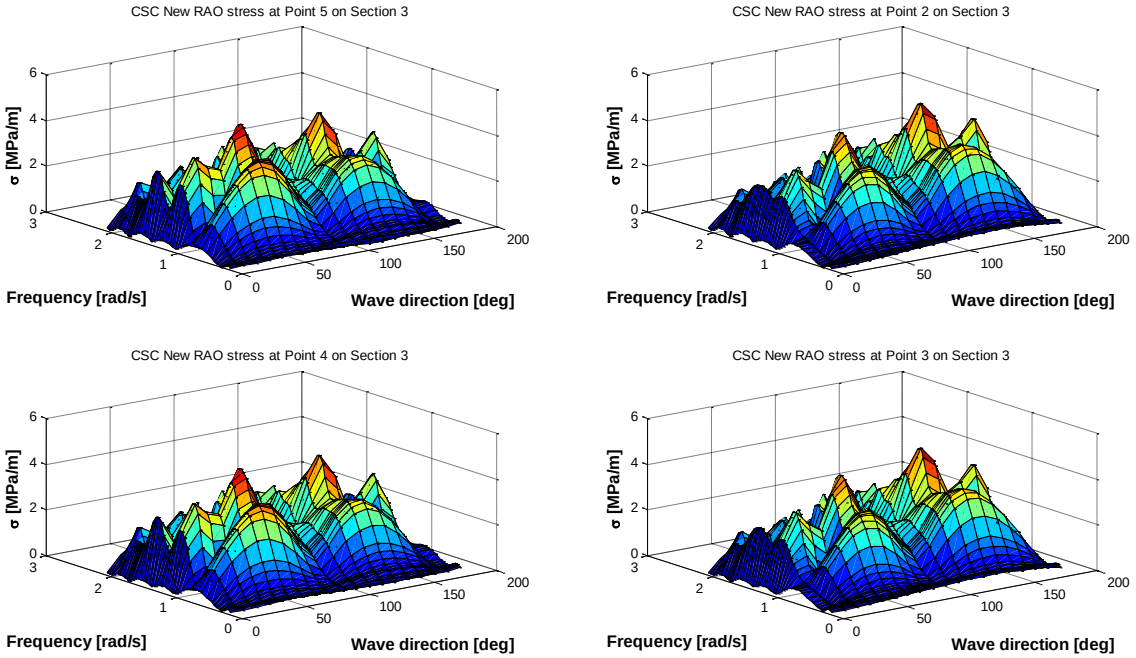

Figure A 17 RAO stress for the new CSC at cross section 3

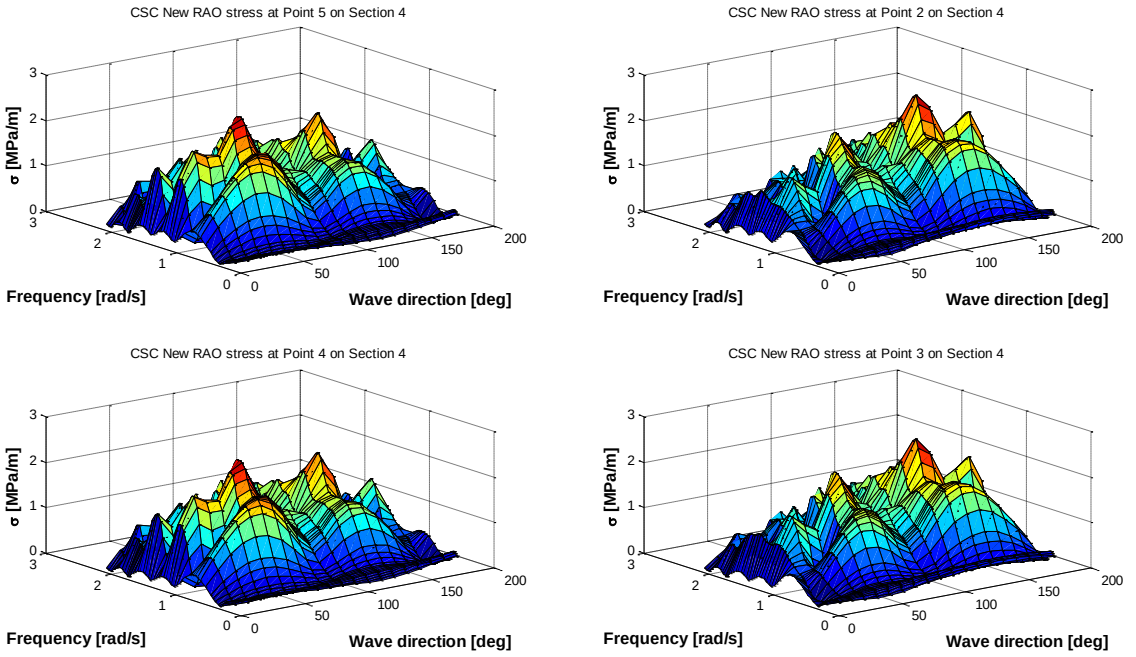

Figure A 18 RAO stress for the new CSC at cross section 4

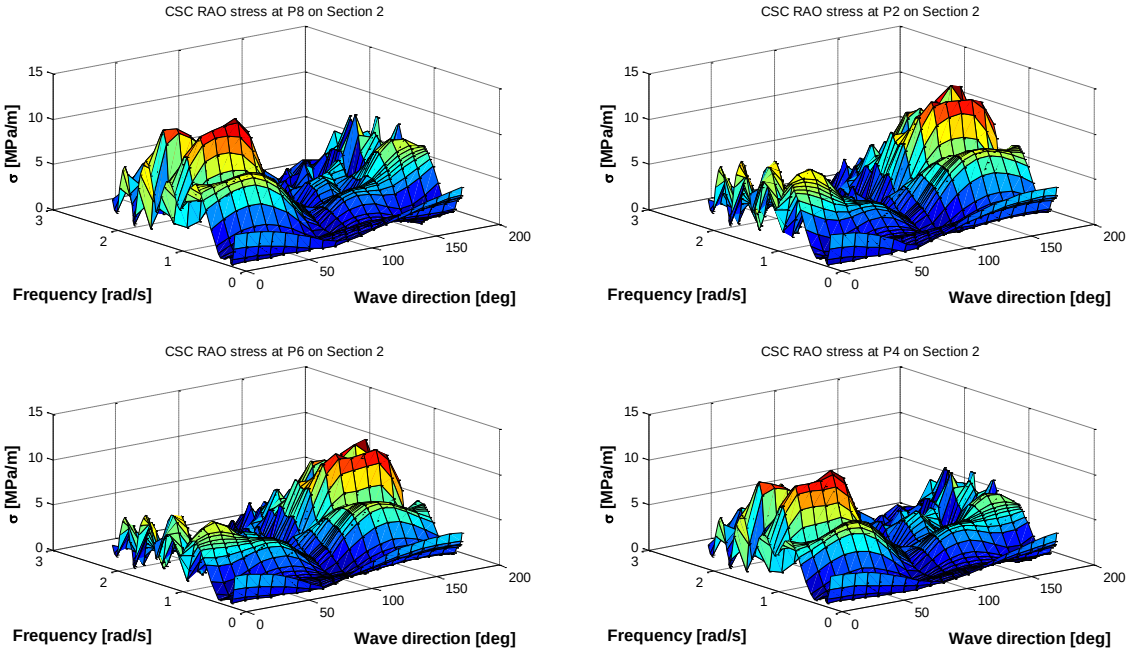

Figure A 19 RAO stress for the CSC at cross section 2

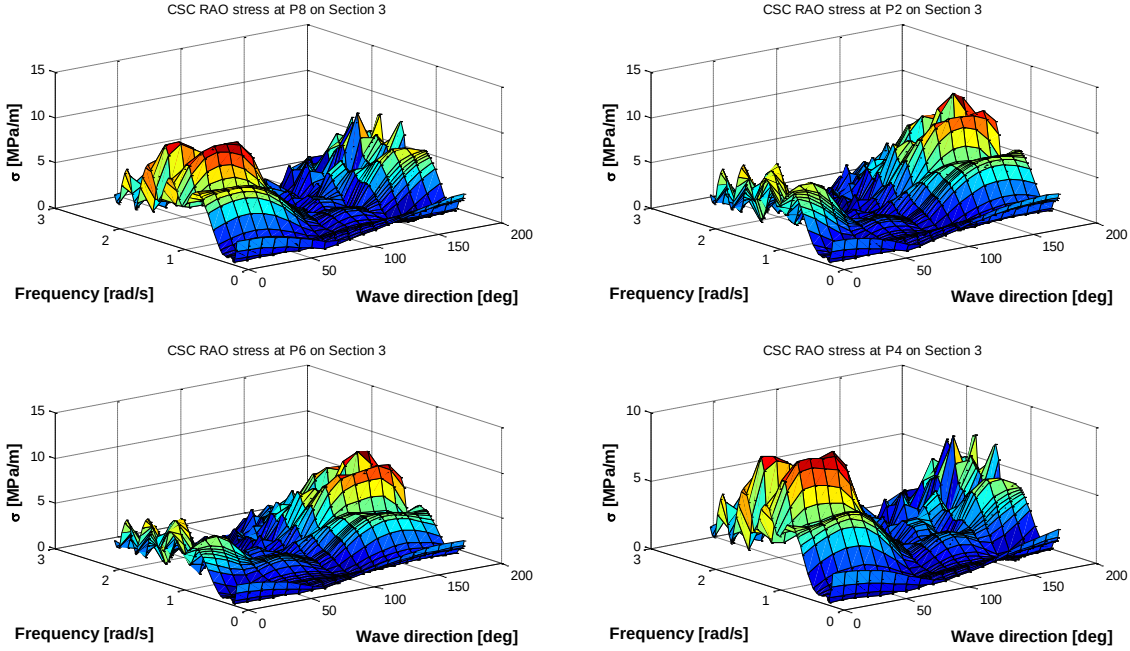

Figure A 20 RAO stress for the CSC at cross section 3

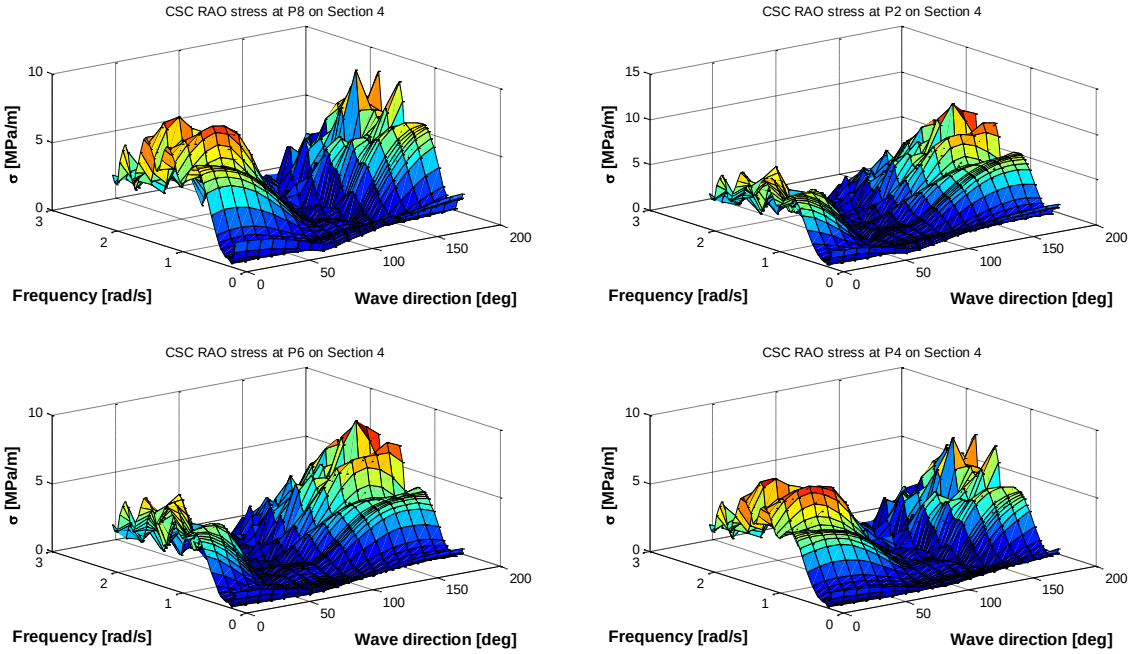

Figure A 21 RAO stress for the CSC at cross section 4

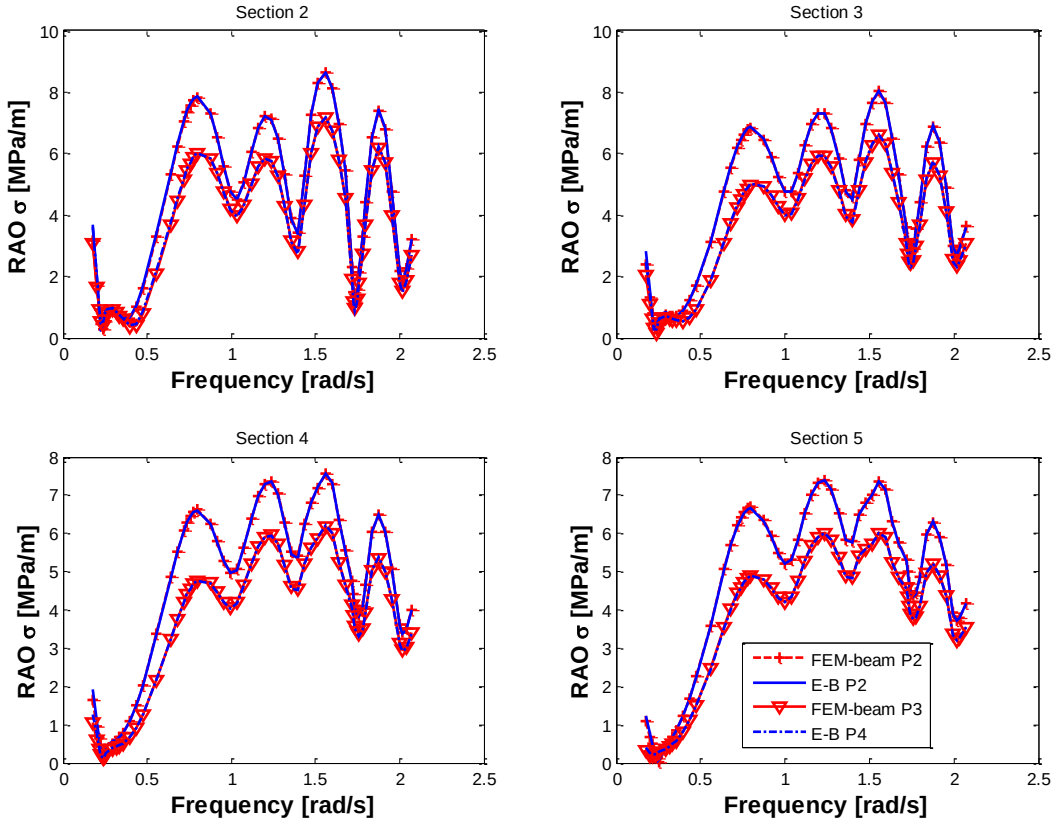

Figure A 22 RAO axial stress from E-B and FEM-beam for the CSC design

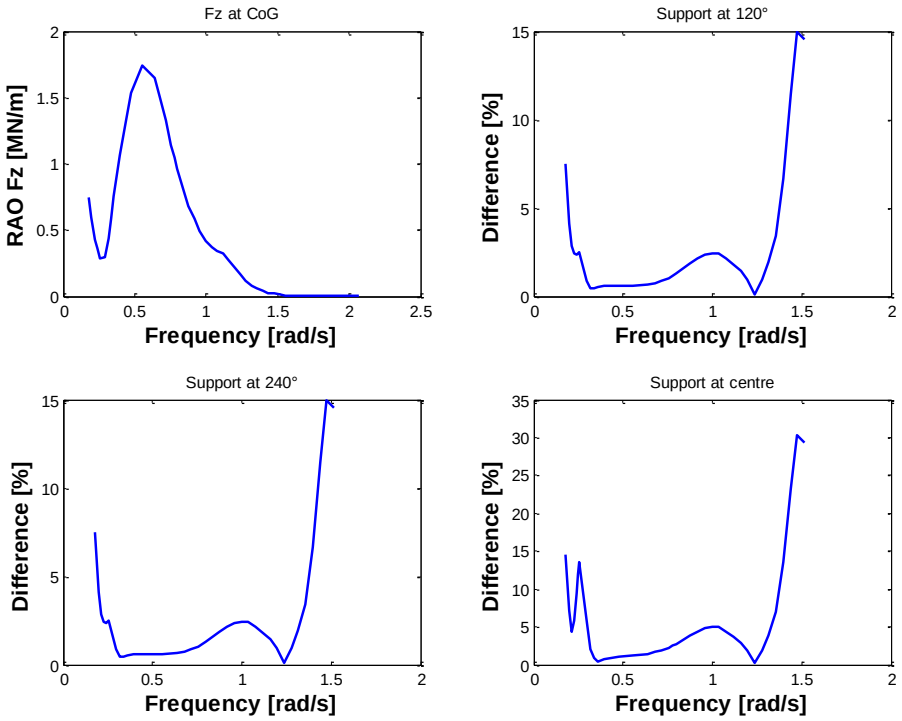

Figure A 23 Reaction force comparison for the CSC at 0° FEM beam

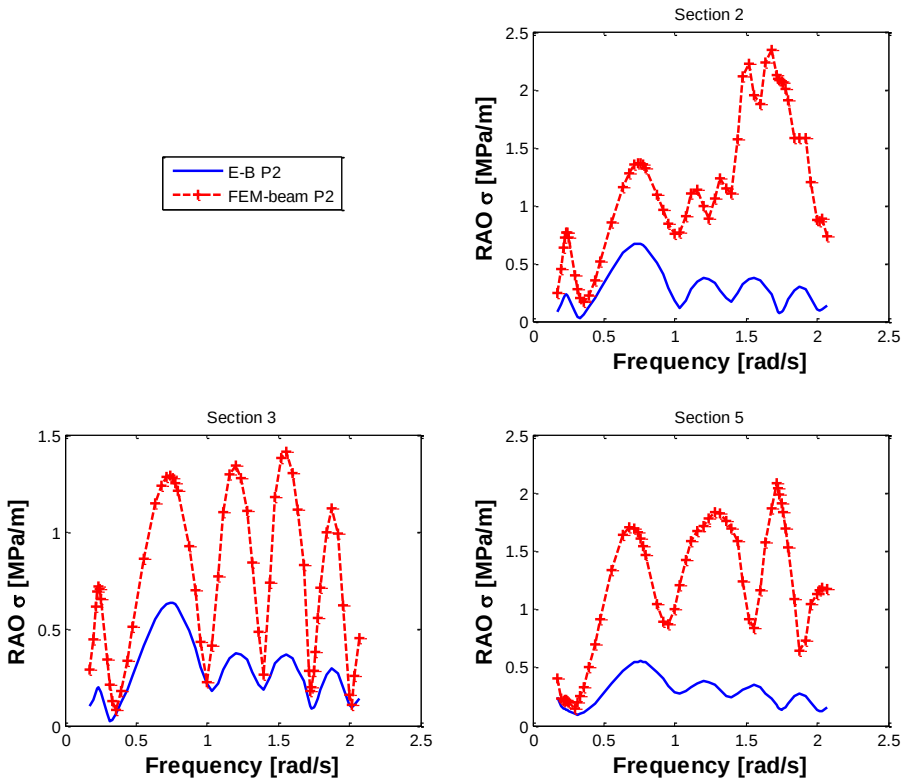

Figure A 24 RAO axial stress from E-B and FEM-beam for the new CSC design

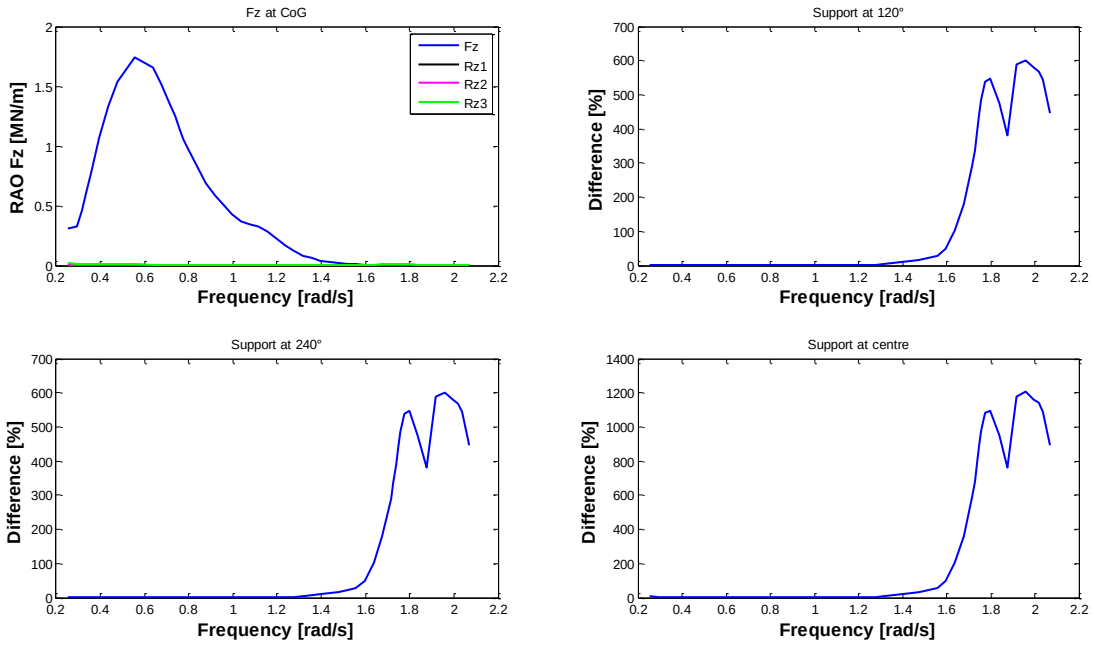

Figure A 25 Reaction force comparison for the new CSC at 0° FEM beam

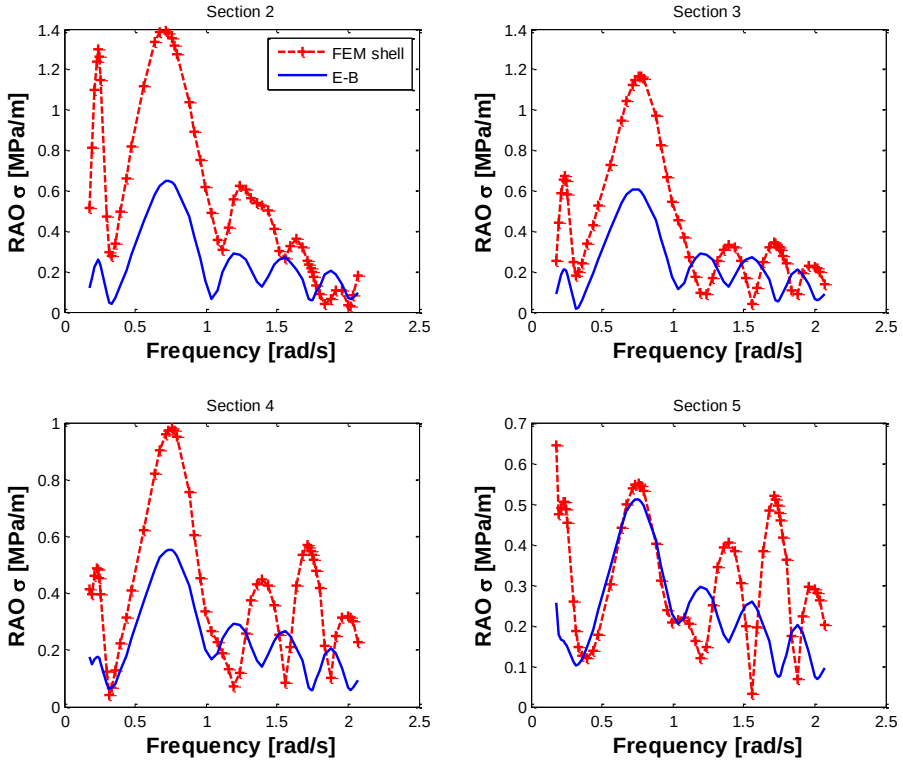

Figure A 26 RAO axial stress from FEM shell at P3 on the pontoon of the new CSC

APPENDIX B

Table B 1 Simulation range angular frequencies [rad/s]

0.157	0.557	1.157	1.727
0.175	0.637	1.197	1.737
0.197	0.677	1.237	1.747
0.215	0.717	1.277	1.757
0.226	0.737	1.317	1.777
0.237	0.757	1.357	1.797
0.246	0.777	1.397	1.837
0.255	0.797	1.437	1.877
0.296	0.877	1.477	1.917
0.317	0.917	1.517	1.957
0.336	0.957	1.557	1.997
0.357	0.997	1.597	2.017
0.397	1.037	1.637	2.037
0.437	1.077	1.677	2.069
0.477	1.117	1.717	

Table B 2 Drag coefficient C_D

Central column	Outer column	Pontoon
0.80	0.64	1.41

Table B 3 Sea state parameters for JONSWAP spectra based on recurrence period of 50 years

Load case	Hs (m)	Tp (s)
1	2.06	3
2	3.18	4
3	4.29	5
4	5.39	6
5	6.49	7
6	7.61	8
7	8.77	9
8	9.99	10
9	11.28	11
10	12.66	12
11	14.09	13
12	15.31	14
13	15.02	15
14	12.34	16
15	10.4	17
16	9.06	18
17	8.05	19
18	7.25	20
19	6.58	21
20	6	22
21	5.5	23
22	5.06	24
23	4.67	25
24	4.28	26
25	3.87	27
26	3.44	28
27	2.92	29